Exploring Topological Transitions and Majorana fermions using Kwant

Aman Sharma

A dissertation submitted in the partial fulfilment of
BS-MS dual degree in science

Indian Institute of Science Education and Research Mohali
April, 2021

Certificate of Examination

This is to certify that the dissertation titled "Investigations of Topological Phase Transitions using Kwant and Majorana fermions in semiconductor-superconductor heterostructures" submitted by Mr. Aman Sharma (Reg. No. MS16012) for the partial fulfilment of BS-MS dual degree program of the Institute, has been examined by the thesis committee duly appointed by the Institute. The committee finds the work done by the candidate satisfactory and recommends that the report be accepted.

Dr. Abhishek Chaudhuri

Dr. Yogesh Singh

Dr. Sanjeev Kumar
(Supervisor)

Dated: April 08, 2021

Declaration

The work presented in this dissertation has been carried out by me under the guidance of Dr. Sanjeev Kumar at the Indian Institute of Science Education and Research Mohali.

This work has not been submitted in part or in full for a degree, a diploma, or a fellowship to any other university or institute. Whenever contributions of others are involved, every effort is made to indicate this clearly, with due acknowledgement of collaborative research and discussions. This thesis is a bonafide record of original work done by me and all sources listed within have been detailed in the bibliography.

Aman Sharma
(Candidate)

Dated: April 29, 2021

In my capacity as the supervisor of the candidate's project work, I certify that the above statements by the candidate are true to the best of my knowledge.

Dr. Sanjeev Kumar
(Supervisor)

Acknowledgements

I would like to thank my supervisor Dr. Sanjeev Kumar whose constant support and suggestions throughout the project helped me to move in the right direction and perform my work in the best possible way.

List of Figures

Notation

$\vec{E}$	Electric Field
$\vec{B}$	Magnetic field
$\hbar$	Planck's Constant
t	time
$\vec{v}$	velocity of the particles
F	Force
L	Length of the lattice
W	Width of the lattice
a	lattice constant(kept a=1 at most places)
Δ	Superconducting gap
α	Rashba Spin Orbit coupling coefficient
t	Hopping Parameter(taken t=1 otherwise stated)
k_x, k_y, k_z	Wavevectors along x, y and z directions respectively
μ	Chemical potential
Q	Topological Invariant
$c, c^\dagger$	Creation and annihilation operators
γ_1, γ_2	Majorana Operators
MBS	Majorana Bound States
ABS	Andreev Bound States
Φ_0	Magnetic flux quantum
$\uparrow$	Up spin
$\downarrow$	Down Spin
E	Energy of the system

Contents

ABSTRACT

In this thesis, we study and derive the topologically robust edge states for the Quantum Hall Effect in a 2D electron gas. We then extend this model and try to derive a system which produces topologically robust edge states just like Quantum Hall Effect but without the application of a magnetic field which we call Quantum anomalous hall effect and the device we call Chern Insulator. We study the various symmetries possessed by graphene and break them one by one to create Quantum anomalous hall effect out of graphene. We combine a Chern insulator and its time reversed form and derive what we call Quantum spin hall insulator and study the robustness of its edge states from scattering. We extend the model for this Quantum spin hall insulator which is also called 2D topological insulator and derive a mathematical model for a 3D topological insulator by stacking together these 2D-topological insulators in three dimensions. We study the experimental imaging methods which can be used to study the surface states of a 3D topological insulator. We next study various methods which can be used to obtain Majorana fermions in topological systems including vortices of a p-wave superconductor, a quantum spin hall insulator, and a 3D topological insulator. Later we lay out a step by step procedure by which starting from a 1D kitaev chain model we derive a mathematical model for the realisation of Majorana fermions in semiconductor-superconductor heterostructures by applying an external magnetic field and having the Rashba spin orbit coupling in the system. After that we explain various developments that have taken place in the field since 2010 after the theoretical model for the experimental realisation of Majorana fermions in semiconductor-superconductor heterostructures was proposed. We also discuss the shortcomings which experiments face and why it has still not been possible to truly realise Majorana fermions in the experiments.

Chapter 1

Quantum Hall Effect

The pioneering work by Fowler, Fang, Howardand Stiles has shown that new quantum phenomena become visible if the electrons of a conductor are confined within a typical length of 10 nm. Their discoveries opened the field of two- dimensional electron systems which since 1975 is the subject of a conference series. It has been demonstrated that this field is important for the description of nearly all optical and electrical properties of microelectronic devices.—(Klaus von Klitzing)

1.1 Quantum Hall Effect

Hall effect discovered by Edwin Hall in 1879 while working on his doctoral degree at Johns Hopkins University is considered the mother of all the topolological effects. As he writes in his original paper[1] he was inspired to work upon the problem while reading Maxwell's theory of electromagnetism, as a motivation to understand better how magnetic field interacts with the electric current as it was little known at that time whether magnetic field interacts with conductor or the electric current itself. Hall performed his experiment at the room temperature. When the same experiment was repeated at low temperature it gave quantized plateaus of the hall conductance. The effect was first predicted theoretically by Ando et al[2], University of Tokyo researchers in 1975 and confirmed later experimentally by Wakabagashi and Kawaji[3] in 1978.

Quantum hall effect revealed a whole wealth of properties of solid state systems at low temperatures and inspired a generation of research, such as the integer hall effect in graphene at the temperatures as high as room temperature[4]. Klaus Von Klitzing in 1985 received Nobel Prize in Physics for discovering the quantization of Hall resistance in silicon based MOSFET samples[5].
As generally the norm is we start with discussing Classical Hall Effect and then move on to quantum hall effect and discuss its topological effects and edge states.

Classical hall effect goes as follows: We take a rectangular metallic sheet and apply a potential difference at the two opposite edges. The sheet is immersed in a perpendicular magnetic field. As the moving charges experience Lorentz force it is expected they will deflect towards one side of the sheet. This should lead to the development of potential difference between the other two edges. Equivalently, the deflection of current due to Lorentz force can be stopped by applying a potential difference with a battery in the opposite direction.

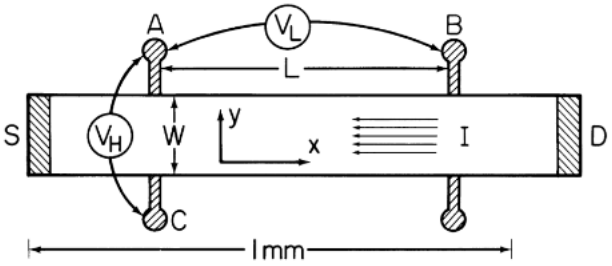

Figure 1.1: (Source:[6]) Quantum Hall Effect Schematic

Lorentz force acting on particles moving inside an electric and magnetic field is given by

$$\vec{F} = e(\vec{E} + \vec{v} \times \vec{B}) \tag{1.1}$$

In the steady state average force acting on the particles is zero, so putting $\vec{F} = 0$ we get,

$$\vec{v} \times \vec{B} = -\vec{E}$$

Crossing with $\vec{B}$ on both sides,

$$\vec{B} \times (\vec{v} \times \vec{B}) = -\vec{B} \times \vec{E}$$
$$\Rightarrow (\vec{B}.\vec{B})\vec{v} - (\vec{B}.\vec{v})\vec{B} = -(\vec{B} \times \vec{E})$$

$\vec{B}.\vec{v} = 0$, because $\vec{B}$ and $\vec{v}$ are perpendicular. Therefore,

$$\vec{v} = \frac{\vec{E} \times \vec{B}}{|B|^2} \tag{1.2}$$

Also, $\vec{B} = B\hat{z}$, which implies,

$$\vec{v} = \frac{(\vec{E} \times \hat{z})}{B} \tag{1.3}$$

This is the velocity of the particles moving in a direction perpendicular to electric field and line perpendicular to the rectangular plane of the sheet. We can use this expression to derive the hall current density which is given by $\vec{j} = ne\vec{v}$.

$$\vec{j} = \frac{ne}{B}\vec{E} \times \hat{z}$$
$$j = (\frac{ne}{B})E \tag{1.4}$$

In the above expression, current is perpendicular to the direction of applied electric field, so the factor accompanied with electric field on the right hand side, $\sigma_H = \frac{ne}{B}$ is hall conductance.
Hence, the expression for hall resistance in classical hall effect is $\frac{B}{ne}$. We can obtain now the expression for quantum hall conductance as a multiple of quantum of conductance, $\frac{e^2}{h}$, by making the replacement $\nu = \frac{nh}{eB}$ and obtain the expression for quantum hall effect as, $\sigma_H = \frac{\nu e^2}{h}$. An experimental plot for quantum hall effect looks like as in the figure:

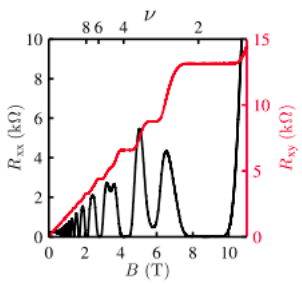

Figure 1.2: (Source:[7]) Quantum Hall Plateaus

As we have seen earlier, $\sigma_H = \frac{\nu e^2}{h}$. ν here can only take the integer values as 1,2,3... As we vary the magnetic field the system sweeps across various ν values and gives conductance values which are integer multiples of $\frac{e^2}{h}$. The plateaus observed are robust to disorder to the extent that the error in straight line of the plateaus is as low as 10^{-7}.

Now, we try to obtain a theoretical plot for the effect. It is possible to obtain the conductance vs magnetic field plot using the python based kwant package, which is very useful in making such plots using tight binding approximation.

Hamiltonian for the electrons in a 2D electron gas is given by:

$$H = -\frac{\hbar^2}{2m}(\partial_x^2 + \partial_y^2) \tag{1.5}$$

Suppose f is a two dimensional function written as $f(x, y)$. We wish to write its first and second derivatives in the discrete form, which is written as,

$$\frac{\partial f}{\partial x} = (\frac{\partial f}{\partial x})_m = \frac{f_{m+1} - f_{m-1}}{2\Delta x}$$

and,

$$\frac{\partial^2 f}{\partial x^2} = (\frac{\partial^2 f}{\partial x^2})_m = \frac{f_{m+1} + f_{m-1} - 2f_m}{\Delta x^2}$$

Coming back to our tight binding model each lattice site on the lattice is represented by the outer product, $|i, j\rangle\langle i, j|$. Hence, using the above formulae, ∂_x and ∂_x^2 can be written as,

$$(\frac{\partial}{\partial x})_{(i,j)} = \frac{|i+1, j\rangle\langle i, j| - |i, j\rangle\langle i+1, j|}{2a} \tag{1.6}$$

$$(\frac{\partial^2}{\partial x^2})_{(i,j)} = \frac{|i+1, j\rangle\langle i, j| + |i, j\rangle\langle i+1, j| - 2|i, j\rangle\langle i, j|}{a^2} \tag{1.7}$$

Similarly, writing the expressions for $(\frac{\partial}{\partial y})_m$ and $(\frac{\partial^2}{\partial y^2})_m$

$$(\frac{\partial}{\partial y})_{(i,j)} = \frac{|i, j+1\rangle\langle i, j| - |i, j\rangle\langle i, j+1|}{2a} \tag{1.8}$$

$$(\frac{\partial^2}{\partial y^2})_{(i,j)} = \frac{|i, j+1\rangle\langle i, j| + |i, j\rangle\langle i, j+1| - 2|i, j\rangle\langle i, j|}{a^2} \tag{1.9}$$

Taking the hermitian conjugate of an operator like $|i+1, j\rangle\langle j|$ gives $|j\rangle\langle i+1|$. Using this property one can clearly see from the above expressions that $(\iota\frac{\partial}{\partial x})_m$ or $(\iota\frac{\partial}{\partial y})_m$ and similarly $(\frac{\partial^2}{\partial x^2})_m$ or $(\frac{\partial^2}{\partial y^2})_m$ written in the quantized form are hermitian operators which is as expected.
Replacing the quantized forms of $\frac{\partial^2}{\partial x^2}$ and $\frac{\partial^2}{\partial y^2}$ which we just derived in the two dimensional hamiltonian we get,

$$H = -\frac{\hbar^2}{2m}\sum_{i,j}(\frac{|i+1, j\rangle\langle i, j| + |i, j\rangle\langle i+1, j| - 2|i, j\rangle\langle i, j|}{a^2} + \frac{|i, j+1\rangle\langle i, j| + |i, j\rangle\langle i, j+1| - 2|i, j\rangle\langle i, j|}{a^2})$$

$$\Rightarrow H = \sum_{i,j}(4t|i, j\rangle\langle i, j| - t(|i+1, j\rangle\langle i, j| + |i, j\rangle\langle i+1, j| + |i, j+1\rangle\langle i, j| + |i, j\rangle\langle i, j+1|)) \tag{1.10}$$

The term accompanying $|i, j\rangle\langle i, j|$, i.e. $4t$ is called onsite potential. It is interpreted as potential energy at each lattice site. The term accompanying the operators of the type, $|i+1, j\rangle\langle i, j|$ i.e -t is called hopping parameter.

In the quantum hall effect there is also a magnetic field applied perpendicular to the experimental material. How do we account for it in our model? We utilize a formalism given by Rudolf Peierls[8], by which an additional phase factor is multiplied to the hopping parameter after interpreting magnetic field applied to the material as magnetic potential.
The following transition happens in the hopping term:

$$t_{ij} \rightarrow t_{ij} exp(\iota \frac{e}{h} \int_{x_i}^{x_j} A(\vec{x}) d\vec{s}) \tag{1.11}$$

For a magnetic field applied in the z-direction we can choose our vector potential to be $\begin{bmatrix} -By \\ 0 \\ 0 \end{bmatrix}$.
We can check that this indeed gives us a magnetic field in the y-direction.

$$\vec{B} = \nabla \vec{\times} \vec{A}$$
$$= \begin{bmatrix} \hat{i} & \hat{j} & \hat{k} \\ \partial_x & \partial_y & \partial_z \\ -By & 0 & 0 \end{bmatrix} = \hat{k}B$$

Hence, we can use the above expression of vector potential to calculate the peirels phase. So,

$$t_{ij} \rightarrow t_{ij} exp(i \frac{e}{h} \frac{(y_i + y_j)(x_i - x_j)}{2}) \tag{1.12}$$

We use the following parameters to obtain the required plot:
a=lattice constant=1,t=hopping parameter=1,μ_{syst}=system chemical potential=0.6,μ_{lead} =lead chemical potential=0.6,L =Length of the sample=50,w=width of the sample=10,w_{lead} =width of the lead =10,B=magnetic field=0.55.

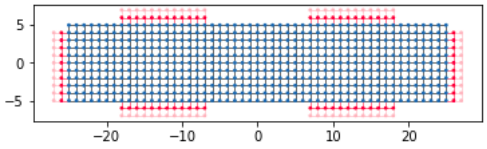

Figure 1.3: QHE Lattice

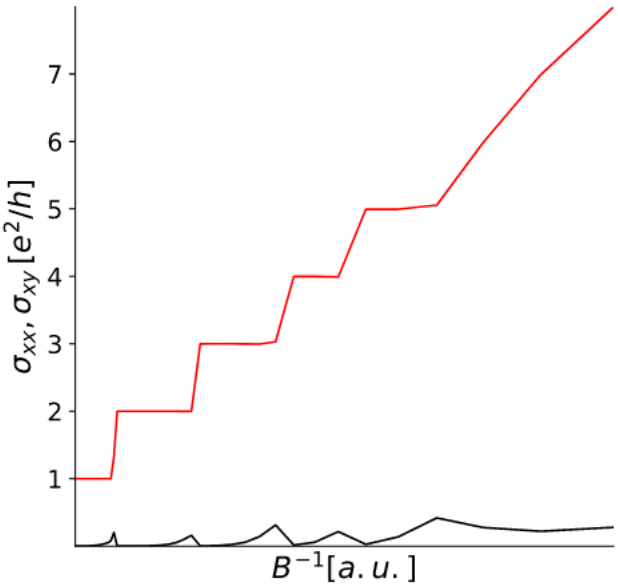

Figure 1.4: QHE Plateaus

1.2 Corbino disk geometry

A corbino disk geometry can be explained as follows: An annulus disk that is a disk with a hole at the centre is kept on a surface and a magnetic field is passed through the centre of the disk and out of the page. There may be an electric current passing from inner edge to outer edge of the disk. A circular electric field can be created around the disk by passing a time dependent electric flux through the centre.

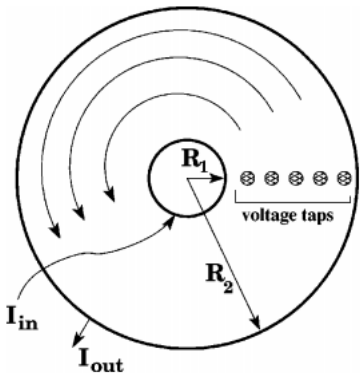

Figure 1.5: (source:[9]) Corbino disk geometry

Interestingly, corbino disk geometry can be used to study why Quantum Hall Effect(QHE) is robust. Laughlin was the one who came up with an argument for the robustness of QHE using corbino disk, and it is known as Lauglin's pumping argument.
It goes as follows. We take a corbino disk on a plane and immerse it in a magnetic field perpendicular to it. We pass a time dependent magnetic field through the centre of the disk which sets up a circular electric field around the disk. We can measure hall current generated as a result along radial direction of the disk. We show by an argument that when we change the flux in the centre of the disk by as amount $\Phi_0 = \frac{h}{e}$ the charge transfer from inner to outer edge is of an integer amount. It is this topological effect which causes the hall current to be quantized.
Suppose ΔQ charge is transferred from inner to outer edge in time ΔT, then the current is , $I = \Delta Q/\Delta T$.
Calculating the electric field around the loop due to changing magnetic flux using faraday's law,

$$\oint \vec{E}.d\vec{r} = \frac{\partial \Phi}{\partial t}$$

.
Assuming the electric field to be constant throughout the disk, $d\vec{r}$ and $\vec{E}$ are along the same direction, so we get,

$$E \oint dr = \frac{\partial \Phi}{\partial t}$$

$$\Rightarrow E = \frac{1}{2\pi R}\frac{\partial \Phi}{\partial t} \tag{1.13}$$

Radial current density, $j = \frac{I}{2\pi R}$.

$$j = \sigma_H E$$

$$\Rightarrow \sigma_H = \frac{I}{\frac{\partial \Phi}{\partial t}} \tag{1.14}$$

Now the argument goes as follows: as we change the magnetic flux in the centre of the disk by $\Phi_0 = \frac{h}{e}$ the electronic states at the edges come back to the original, that is when $\Phi = 0$, hence an amount of charge, which is integer multiple of the electronic charge, ne, is transferred between the edges.
So, $\Delta Q = I\Delta T = \sigma_H(\frac{\partial \Phi}{\partial t})\Delta T = \sigma_H(\Delta \Phi) = \sigma_H(\frac{h}{e}) = ne$.

$$\sigma_H = \frac{ne^2}{h} \tag{1.15}$$

Because an integer amount of charge must be transferred from one edge to the other upon a Φ_0 change in the flux at the centre the conductance is quantized. The condition that an integer amount of charge must be transferred is a topological condition and works as the topological invariant. The value of the integer depends upon the chemical potential of the disk.

1.3 Discrete Energy Levels due to quantized momenta

When a magnetic field is applied perpendicular to the plane of a 2D electron the electrons inside start revolving in circles with a certain momentum. Since, electrons are quantum mechanical particles and an electron exists as a wave so their angular momentum must be quantized. So, $L = n\hbar$ is the only possible angular momentum.
For an electron moving in a circle with velocity v in a magnetic field, its radius, known as cyclotron radius is given by $r_c = \frac{mv}{eB}$ and its angular momentum is given by $L = mvr_c$.

$$\Rightarrow L = mvr_c = eBr_c^2$$

This implies, for the quantized orbits,

$$n\hbar = eBr_c^2$$

$$r_c^2 = \frac{n\hbar}{eB} \tag{1.16}$$

Labelling, $l_B = \sqrt{\hbar/eB}$, we may write $r_n = \sqrt{n}l_B$. We call l_B magnetic length. Energy of the cyclotron orbits is given by, $L\omega_c = n\hbar\omega_c$. Energy levels are quantized as simple harmonic oscillator energy levels, so also including the zero point energy in the spectrum, the energy levels are given by $E_n = \hbar\omega_c(h + \frac{1}{2})$ and are called Landau levels.
We understand from the above analysis that larger the radius of cyclotron higher is the energy level. The electrons tend to arrange in energy levels due to nothing but quanization of their angular momenta which is due to their wave nature.

1.4 Understanding the formation of edge states

We have understood that on the application of a magnetic field perpendicular to a conducting sample at low temperature leads to the formation of cyclotron orbits of electrons. But, what happens when the orbit is close to the edge? So close that the distance from the edge is smaller than the radius of the orbit itself. The electron cannot bounce off and leave the material so it bounces back. This is the classical way of understanding the formation of edge states. The electronic states which are formed at the edges are called skipping orbits.
Quantum mechanically, the way of understanding the formation of skipping orbits is more refined. We assume there exists a potential inside the bulk whose value rises to infinity near the edges. It is plausible to assume such a potential because we know electrons cannot leave the edge so it is acceptable to put the potential infinite outside the material.
Due to added potential, however, landau levels no longer remain flat, they rather curve around and steep near the edges. Due to this deformation of Landau Levels, the filled levels can now cross at the fermi level and lead to the formation of conduction states. These newly formed states are called edge states or skipping orbits. These states have an even more interesting property. It is that the states at the opposite edges travel in opposite directions, a property due to which they are also referred as chiral edge states. On which edge the direction chiral edge state travels in which direction depends only on the orientation of magnetic field. Switching the direction of magnetic field also changes the direction of propagation of chiral states at the edges.
We can obtain the plot for bending landau levels and see how Landau levels cross the fermi level and give conducting states.

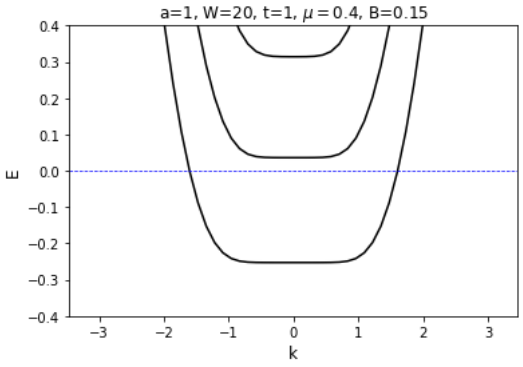

Figure 1.6: Bending Landau levels due to infinite potential barrier near the edges

By the new formalism we have a potential which steeps near the edges and is zero outside the material. The potential can be equivalently interpreted as having an electric field arrowing perpendicular to the edges inside the bulk. At the same time we have a magnetic field perpendicular to the plane of the material. These two fields will deflect the electrons moving along the edges unless the velocity takes a certain value and this value can be interpreted as drift velocity with,

$$v = \epsilon_y / B$$

There is one more interesting property of the edge states. Even for the shapes which are not rectangular, for example hexagon, formation of states along the edges is possible.
Edge states for a rectangular sample plotted using kwant can be seen in the figure.

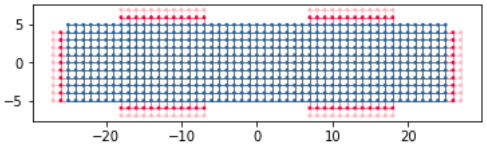

Figure 1.7: QHE bar lattice

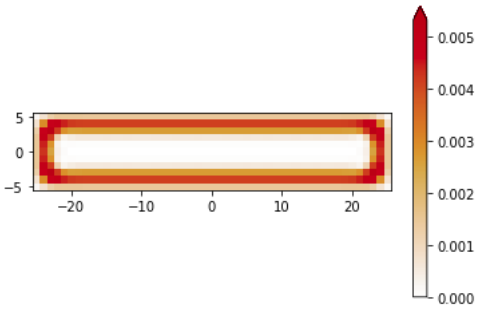

Figure 1.8: QHE Edge states. Parameters:B=0.55,μ=0.6

1.5 Laughlin pump in the newly developed formalism

What happens when we apply an electric field across the quantum hall effect bar? On applying the electric field electrons at the edge which are at the fermi level experience a force which is given by $\hbar \dot{k_F} = -eE$.
We know we can express the fermi momentum in terms of N due to periodicity of the lattice and it

goes as, $K_F = 2\pi N/L$. Using this we arrive at the expression,

$$\hbar \dot{k_F} = \hbar(\frac{2\pi \dot{N}}{L}) = eE$$

$$\dot{N} = \frac{eEL}{2\pi\hbar} = \frac{eEL}{h}$$

$$\dot{N} = \frac{EL}{\Phi_0} \tag{1.17}$$

It may seem from the above expression that the number of electrons at the edge is increasing and the charge is not conserved. But, actually the extra charge comes from the other edge, that means charge is being pumped from one edge to the other through the bulk.
This is a phenomenon which is not possible without the presence of bulk. Bulk in this case defines a property of the edge, and so it forms a classic example of bulk edge correspondence.
For a chiral state the charge is conserve, but in this case fermi surface starts moving on the application of electric field and charge starts increasing at the edge. However, the overall charge is conserved because extra charge come from the other edge, and the charge at the other edge is depleted. This phenomenon is called chiral anomaly. If we sum up the conclusion it tells us chiral edge states are not possible without the bulk.

1.6 Hall conductance in the new formalism

Earlier we gave an argument for the quantization of edge states using Lauglin pump when we said that an integer number of electrons must pass from the inside to the outside edge of the corbino disk which causes the hall conductance to be quantized. Now, we give an argument for the quantization of hall conductance with the help of edge states. We again take an annulus disk with a hole in the centre and immerse inside a perpendicular magnetic field. We pass through the centre a magnetic flux, changing which allows us to create a circulating electric field around the disk. The bulk of such a system is gapped and consists of electrons orbiting around magnetic flux lines while on edges there are chiral edge states.
Let us see how the edge states look like for a corbino disk when no flux is passing through the centre. The plot which is shown in the figure on the right and below have been prepared using kwant.

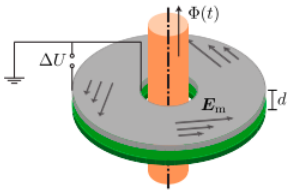

(a) (Source:(10))A corbino disk schematic with a time varying magnetic flux at the center

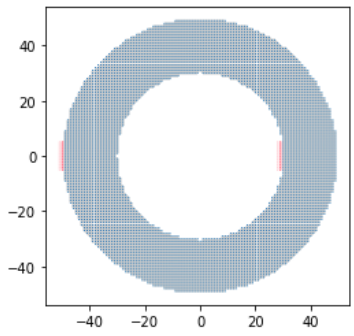

(b) Corbino disk lattice

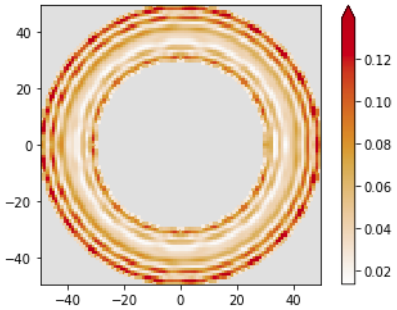

(c) Corbino disk edge states
(Parameters:r_{in}=30,r_{out}=50,μ=0.9,B=0.15)

Figure 1.9:

Note that no electric field has been applied across the disk, however, there is current flowing in clockwise and counterclockwise direction at the inner and outer edge due to edge states but the net current is zero.
Now, a battery is connected across the inner and outer edge. This battery causes the charge to build up at one of the edges which leads to an imbalance of currents flowing in the clockwise and counterclockwise direction, so there is a net current flowing in one of the directions depending upon the the polarity of the applied potential. It is notable that the net current is in a direction perpendicular to the externally applied electric field which happens to act in the radial direction. Since, electric field and current are in the perpendicular directions the current is hall current.
If there are N channels carrying the current along any of the edges, because the transport along the edge is ballistic, the conductance is Ne^2/h. If the number of edge states N_1 on the outer edge is greater than the number of edge states N_2 on the inner edge the current is given by,

$$I = (N_2 - N_1)\frac{e^2}{h}V$$

. $(N_2 - N_1)$ is an integer so,

$$I = n(\frac{e^2}{h})V \tag{1.18}$$

This is an equation which yields the hall conductance to be,

$$\sigma_H = (\frac{ne^2}{h}) \tag{1.19}$$

Chapter 2

Chern Insulator

This was a model for a "quantum Hall effect without Landau levels", now variously known as the "quantum anomalous Hall effect" or "Chern insulator". It just involves particles hopping on a lattice (that looks like graphene) with some complex phases that break time reversal symmetry. By removing the Landau level ingredient, replacing it with a more standard crystalline model the "topological insulators" were born.—(F. Duncan M. Haldane)

2.1 How to get chiral edge states without applying an external magnetic field

What we would like to do now is to find a lattice hamiltonian that describes the edge states in Quantum Hall Effect. What we have done so far is to take a material, apply a magnetic field to it and get circulating electrons and consequently get the edge states. What we would like to do currently is to directly write a hamiltonian which describes the edge states. For this, our plan is to start from the lower dimension and consequently build towards the higher dimensions. If we could write a hamiltonian for a one dimensional wire which hosts counter propagating modes part of our job would be done, because then we could stack together a large number of these one -dimensional wire to get a two-dimensional structure. And, the hamiltonian which we so write for this two-dimensional structure would be the one which we are seeking for. The counter propagating modes, when the 1D wires are stacked in a 2D structure, will all cancel each other except the ones which are at the edges. And these are the required edge modes.
Now the foremost objective that we have is to find a hamiltonian for 1D wire which hosts counter propagating modes. One hamiltonian which we can use is kitaev chain model. It is written in the momentum basis as,

$$H(k) = -(2t\cos(k) + \mu)\tau_z + \Delta\sin(k)\tau_y \tag{2.1}$$

At $\mu = -2t$ we can write the above hamiltonian as,

$$H(k) = -2t(\cos(k) - 1)\tau_z + \Delta\sin(k)\tau_y \tag{2.2}$$

Near k=0 this hamiltonian possess counter propagating states which are eigenvectors of τ_y and have eigenvalue +1 or -1. So when $k \approx 0$, $H(k) \approx \Delta\sin(k)\tau_y$. And, the corresponding eigenvectors are the counter propagating modes which we are looking for.
We have successfully been able to obtain our sought after 1D hamiltonian and part of our job is complete. The next step is to combine n of these hamiltonians in two-dimensions which would finally provide our hamiltonian for the edge states.
We can write the hamiltonian for n 1D chains stacked in the y-direction as follows,

$$H(k_x) = (-(2t\cos(k_x) + \mu) + \Delta\sin(k_x)\tau_y) \oplus |n_y\rangle\langle n_y| \tag{2.3}$$

Notice that these 1D wires are not coupled to each other that means we still don't have chiral edge states. In order to achieve our objective completely we will have to introduce coupling between the adjacent wires. The term $|n_y\rangle_y + 1| \oplus (\tau_z + \iota\tau_x)$ does this job for us.
So now, writing the final hamitonian,

$$H = \sum_{n_y}[-(2t\cos(k_x) + \mu)\tau_z + \Delta\sin(k_x)\tau_y] \otimes |n_y\rangle\langle n_y| - \gamma\sum_{n_y}[|n_y\rangle\langle n_{y+1}| \otimes (\tau_z + \iota\tau_x) + h.c] \quad (2.4)$$

Here, γ is the coupling term which indicates the strength of coupling between the wires. It is possible to write the above hamiltonian completely in terms of k_x and k_y. To do this we will have to consider an infinite stack of chains in the y-direction so that we could have translational invariance along both the axes. The hamiltonian which we get consequently is as follows,

$$H(k_x, k_y) = [-(2t\cos(k_x) + \mu)\tau_z + \Delta\sin(k_x)\tau_y] - 2\gamma[\cos(k_y)\tau_z + sin(k_y)\tau_x]. \quad (2.5)$$

We can rearrange the above hamiltonian and write down all the terms with τ_x together and same with τ_y and τ_z.
When we have a hamiltonian of the form, $H = A\tau_x + B\tau_y + C\tau_z$, its energy spectrum is given by, $E = \pm\sqrt{A^2 + B^2 + C^2}$.
So after rearranging the hamiltonian we get the following spectrum.

$$E(k_x, k_y) = \pm\sqrt{\Delta^2\sin(k_x)^2 + (2\gamma\cos(k_y) + \mu + 2t\cos(k_x)^2 + 4\gamma^2\sin(k_y)^2)} \quad (2.6)$$

The dispersion relation when plotted looks like as shown in the figure.

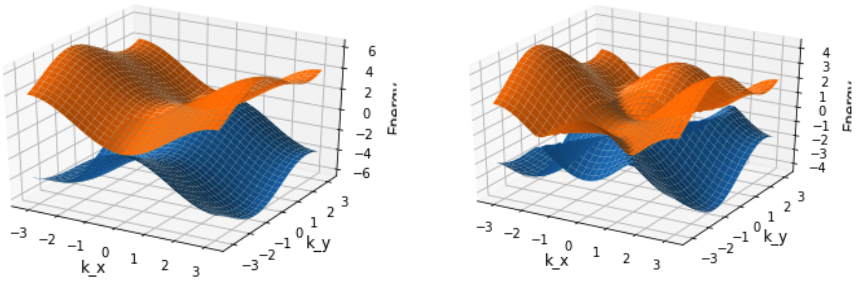

(a) Δ=0.3,γ=-0.5$\mu = -2.0$ (b) Δ=0.3,γ=-0.5, $\mu = 0.0$

Figure 2.1: Dispersion for infinite number of kitaev chains stacked in y-direction(A Chern insuator model)

Now, we can also check how the dispersion relation looks like for a finite width in the y-direction. However, unlike the earlier case when we had considered translational symmetry in the y-direction by stacking infinite number of wires we can't simply write a formula for the dispersion. We use kwant package for this purpose. The plot is only two-dimensional and not three dimensional because we have translational symmetry only along one direction. The plot looks like as shown in the figure.

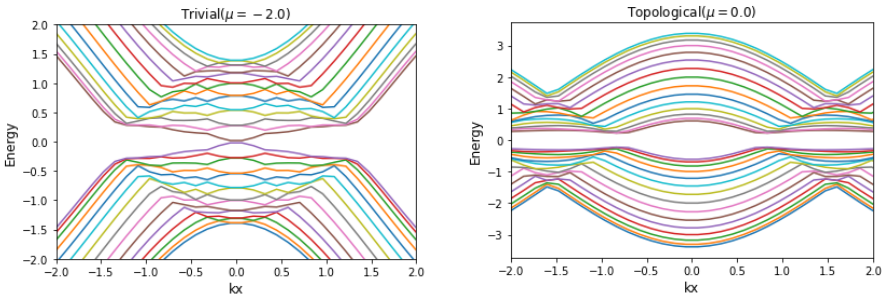

(a) Δ=0.3,γ=-0.5 (b) Δ=0.3,γ=-0.5

Figure 2.2: Dispersion for finite number of kitaev chains stacked in the y-direction(A Chern insulator model)

We note that for lower values of μ band crossing is there while for the higher values crossing disappears, however, the bulk remains gapped for all range of values. Now , when the bulk is gapped and there is no crossing at the fermi level we have nothing but a normal insulator. These are the types which we are aware of since a very long time. When the bulk is gapped but there is crossing at the fermi level that means states at the edge are ungapped and so conducting, this forms what is called a topological insulator. It is due to this property of topological insulators that at very low temperatures they have lower resistance than normal insulators, however, at higher temperatures both behave as normal insulator and have a high resistance. As we have seen, this property of insulated bulk and conducting edges was not possible without the presence of the bulk. Bulk is always required in this case to support the edge states. So, this also forms the example of bulk edge correspondence.
If we look at the figure(2.2), if we keep the chemical potential, $\mu < |2t+2\gamma|$(t=1 here) we have a band crossing at the fermi level.So, in that range of chemical potential we have a topological insulator and the system is said to be in the topological regime. While, if $\mu > |2t + 2\gamma|$ there is no crossing at the fermi level and the conduction and valence bands become completely gapped. Now, we are in trivial regime and what we have is a trivial insulator.
Note that in Quantum Hall Effect also we had edge states which were obtained as a result of bulk edge correspondence. But, in that case we needed to apply an external field to obtain the edge states, however, as we can note, in the current case, we obtained edge states without without the application of any external field. This can be thought of as another version of Quantum Hall Effect obtained without application of any external magnetic field. It has a specific name called **Chern insulator**. It is also known by the name Quantum anomalous hall effect.
Duncane Haldane was the one who first came up with a model for Chern insulator[11]. A Chern insulator was first observed experimentally in 2013 by the group of Qikun at Tsinghua University [12].
In the next sections we will see how we can realise a Chern insulator model in a real system. A favorite model system for this objective may be graphene due to its fantastic properties which makes it a wonderful material for a large number of applications.[13]

2.2 Graphene

Andre Geim and Konstantin Novoselov were the first people to isolate and characterize graphene in 2004 at the University of Manchester[14]. They used so called scotch tape technique to isolate single layers of graphene. The two went on to receive Nobel Prize for their discovery in 2010[15]. We will now try to see how we can take a graphene sheet and convert it into a topological system with edge states. Graphene has dirac cones which can be gapped or ungapped by applying some external factors, which allows us to create or break various symmetries it possess like time reversal, or inversion, and produce a bulk gap and an ungapped edge. Before proceeding to the advanced level let us look at the basic structure of graphene and write a hamiltonian for it.

The structure looks like as shown in the figure(2.3(a)). At the first glance it looks like all the

lattice sites of graphene are equivalent. But, on a closer examination it appears there are two types of sites in that there are two types of localities in which each atom is placed. In one type there is no atom on the left at a distance equal to the side length of the hexagon, while in the other type one does find an at atom at such a distance.
If we look at the nearest neighbor hoppings they are not possible between atoms of the same types. That means, if we call two types of lattice sites as A and B, hopping happens only from A to B, and A to A and B to B hoppings which are next nearest neighbor hoppings are forbidden.
Because in graphene we have two types of lattice sites, therefore two types of hoppings and two types of lattice site potentials are possible. So, the first information we have before writing the hamiltonian for graphene is that it is a 2×2 hamiltonian.
We also know that only $A \rightarrow B$ type hoppings are possible so we will have only off-diagonal terms in the hamiltonian. $B \rightarrow A$ hopping is nothing but the conjugate of $A \rightarrow B$ hopping. So, if h(k) occupies one off-diagonal position in the hamiltonian matrix, then $h(k)^\dagger$ occupies the other off-diagonal position. Diagonal positions are zero because as we have already said $A \rightarrow A$ and $B \rightarrow B$ hoppings are not possible.

$$H_0(\vec{k}) = \begin{bmatrix} 0 & h(\vec{k}) \\ h(\vec{k})^\dagger & 0 \end{bmatrix}$$

If $\vec{a}_1$,$\vec{a}_2$,$\vec{a}_3$, the vectors along which hopping takes place, are represented by $\vec{a}_i$, $h(\vec{k})$ is written as, $h(\vec{k}) = t_1 \sum_i exp(\iota \vec{k}.\vec{a}_i)$.
Expression for $h(\vec{k})$ has been written simply by using the tight binding approximation.

$$H_0(\vec{k}) = \begin{bmatrix} 0 & t_1 \sum_i exp(\iota \vec{k}.\vec{a}_i) \\ t_1 \sum_i exp(-\iota \vec{k}.\vec{a}_i) & 0 \end{bmatrix}$$

$$\Rightarrow H_0(\vec{k}) = \begin{bmatrix} 0 & t_1 \sum_i (\cos(\vec{k}.\vec{a}_i) + \iota(\sin(\vec{k}.\vec{a}_i)) \\ t_1 \sum_i (\cos(\vec{k}.\vec{a}_i) - \iota(\sin(\vec{k}.\vec{a}_i)) & 0 \end{bmatrix}$$

$$= \begin{bmatrix} 0 & t_1 \sum_i (\cos(\vec{k}.\vec{a}_i) \\ t_1 \sum_i (\cos(\vec{k}.\vec{a}_i)) & 0 \end{bmatrix} - \begin{bmatrix} 0 & -\iota(\sin(\vec{k}.\vec{a}_i)) \\ \iota(\sin(\vec{k}.\vec{a}_i)) & 0 \end{bmatrix}$$

$$= t_1 \sum_i (\begin{bmatrix} 0 & 1 \\ 1 & 0 \end{bmatrix} \cos(\vec{k}.\vec{a}_i) - \begin{bmatrix} 0 & \iota \\ -\iota & 0 \end{bmatrix} \sin(\vec{k}.\vec{a}_i))$$

$$= t_1 \sum_i (\sigma_x \cos(\vec{k}.\vec{a}_i) - \sigma_y \sin(\vec{k}.\vec{a}_i))$$

Dispersion relation for graphene is written as follows[17]:

$$E(k_x, k_y) = \pm \sqrt{1 + 4\cos(\frac{ak_x}{2}) + 4\cos(\frac{ak_x}{2})\cos(\frac{\sqrt{3}ak_y}{2})}$$

The above spectrum has been plotted in the following figure:

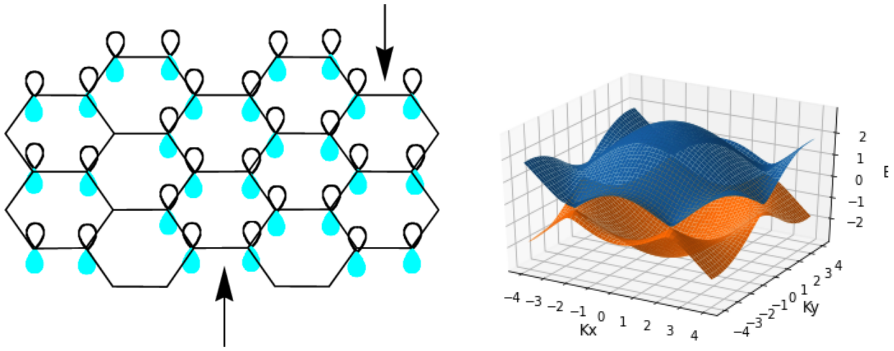

(a) (Source:(16))Graphene lattice (b) Graphene dispersion plot,a=1

Figure 2.3: Graphene lattice and dispersion

The valence and conduction bands touch each other at six points, and these are called dirac points. All the six dirac points can be generated from two dirac points $\vec{K}$ and $\vec{K}'$ by adding a reciprocal lattice vector. These $\vec{k}$ and $\vec{k}'$ points are, $\vec{K} = (2\pi/3, 2\pi/3\sqrt{3})$, and $\vec{K}' = (2\pi/3, -2\pi/3\sqrt{3})$.

2.3 Preparing a Topological Insulator using Graphene

Now, we come to our main objective which was to create a topological insulator using graphene. We have seen how we have dirac points at K and K' points, now we will see how we can use these special points to create topological insulators.
If we ask how should the bandstructure of the topological insulator look like the bulk states must be completely gapped and the edge states must ungapped. In the bandstructure of graphene bulk states are neither gapped nor completely ungapped. The conduction and valence bands touch each other at a single point, so it must be easy to lift the degeneracy at the dirac points and introduce a gap. We will see that these dirac points are protected by certain types of symmetries. Once we introduce some terms in the hamiltonian which break these symmetries, the degeneracy at the dirac points can be lifted and gap can be created.
We first look at what these symmetries are which protect these dirac points.

2.3.1 Sublattice Symmetry

As we know there are two types of lattice sites in graphene, say A and B. Now, we swap the positions of these two lattice sites, so that each lattice site which was occupied earlier by type A is now occupied with B and vice versa. If after performing this transformation the hamiltonian remains unchanged the system is said to possess **sublattice symmetry**. It is very easy to see how sublattice symmetry is possessed in graphene. We observe that in graphene hamiltonian, which is a 2×2 matrix if we simply exchange the two off-diagonal terms which are the representatives of two sublattices the hamiltonian remains unchanged. We can use unitary matrix σ_z to perform this transformation.

$$\sigma_z H(k) \sigma_z = -H_0(\vec{k})$$

2.3.2 Time reversal Symmetry

This symmetry implies if we reverse the motion of time and the hamiltonian still remains intact time reversal symmetry is preserved. Most of the times, time dependence of a hamiltonian is contained inside the derivative operator due to momentum. When we write the derivative operator for a momentum it is accompanied by a complex number. So instead of changing sign of time variable we can equivalently perform the complex conjugation of the complex number. If we are dealing with a hamiltonian with spinless particles the time reversal operator is simply a complex conjugation

operator. If

$$H_0(\vec{k}) = H_0(-\vec{k})$$

time reversal symmetry is preserved.
How is time reversal symmetry broken? The simplest way to break time reversal symmetry is to introduce terms in the hamiltonian which do not preserve this symmetry. For example, applying the magnetic field. It is very simple to understand how magnetic field breaks time reversal symmetry. Imagine an electron moving around in a closed loop inside a wire. It generates a magnetic field along the axis of the loop. The direction of the magnetic field is given by Fleming's right hand thumb rule. Now, suppose we reverse the time. The electron goes around the loop in opposite direction. This change also reverses the direction of the magnetic field. Hence, magnetic field is not preserved under time reversal.

A graphene lattice preserves both time reversal and sublattice symmetry. It is these symmetries which protect dirac cones. Our objective, therefore, is to break these symmetries and create a bulk gap and ungapped edge states.
To break sublattice symmetry we need to modify sublattices A and B in such a way that interchanging them does produces the same hamiltonian. We achieve this objective by introducing an opposite mass term at each lattice site. That means mass M for lattice sites A and -M for lattice sites B. We do this by introducing a mass term $M\sigma_z$ into the hamiltonian.

$$H(\vec{k}) = H_0(\vec{k} + M\sigma_z)$$

The energy spectrum now becomes,

$$E(\vec{k}) = \pm\sqrt{|h(\vec{k})|^2 + M^2)}$$

.

A band gap of 2M is introduced into the spectrum.
By doing this we have successfully created an insulator out of graphene. To create a topological insulator with edge states we need to put in some more efforts. We also need to break time reversal symmetry. One way to do that is to introduce an imaginary next nearest neighbor hopping term ιt_2. Note the new terms are introduced at the diagonal places because these hoppings are between the lattice sites of same type.
The new hamiltonian is written as,

$$H(\vec{k}) = H_0(\vec{k}) + M\sigma_z + 2t_2 \sum_i \sigma_z sin(\vec{k}.\vec{b}_i) \tag{2.7}$$

The hamiltonian we have arrived at has a specific name, and it is called Haldane Model[18]. One may wonder how do we introduce opposite mass term at the lattice sites. This may be achieved by applying an opposite mass term at each lattice site, which can be done by attaching the graphene lattice with another magnetic lattice with two opposite polarities.
We can see the band structure for the hamiltonian plotted using kwant in the figure. The band crossing appear at the fermi level while the bulk remains gapped. This indicates we have been successful in attaining our objective of obtaining a chern insulator using graphene.

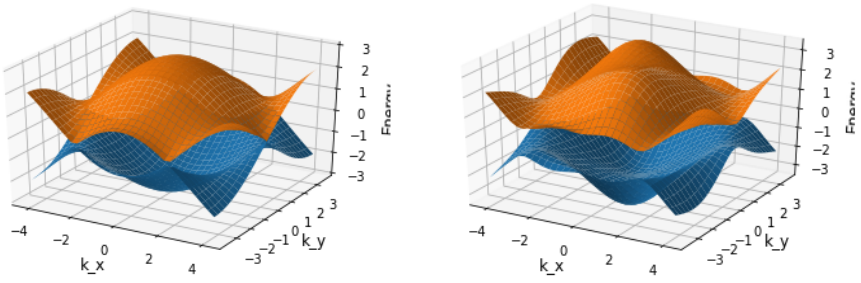

(a) Trivial($t_2 = 0.0$) (b) Topological($t_2 = 0.5$)

Figure 2.4: Dispersions for infinite lattice of graphene in two dimensions converted into a Chern insulator by introducing a mass term(M) and imaginary next nearest neighbor hopping(t_2). The system moves from trivial to topological regime on changing the value of t_2 from 0 to 0.5

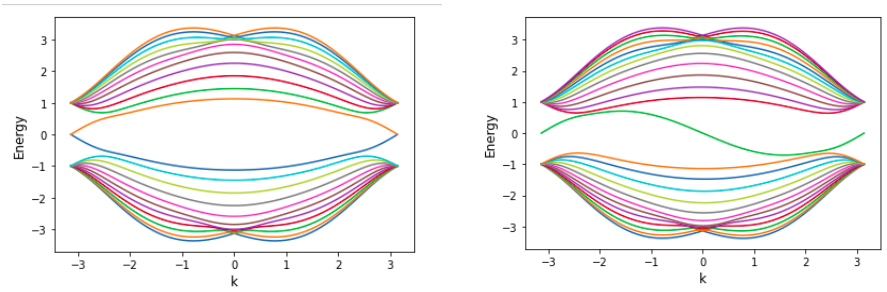

(a) Trivial($t_2 = 0.0$) (b) Topological($t_2 = 0.5$)

Figure 2.5: Dispersion for a graphene ribbon(i.e infinite only in one direction and not two) converted into a Chern insulator. There is a transition from trivial to topological state on changing the value of t_2

Duncane Haldane, the discoverer of **haldane model** was awarded Nobel Prize for his work topological phases of 2D matter[19]. He shared his Nobel Prize with David Thouless and Michael Kosterlitz.

When edge states are there, the system is in a topological state while when the edge states are not there the system is in trivial state. So, it becomes important to characterize when the system is topological and when trivial. It turns out we can perform a surface integral over the entire brillouin zone and obtain a quantity called Chern number. If the Chern number is zero the system is in trivial regime, while if Chern number is non-zero the system is in topological regime. The number of chiral states that system has on each edge is equal to the Chern number. So suppose Chern number is one then there is one chiral edge state, if Chern number is two there are two chiral edge states and so on.
In order to calculate the Chern number the quantities like berry phase, berry connection, berry curvature come into play which are calculated with the help of ground state wavefunction of the hamiltonian. .

2.4 Berry Phase

We are aware of the gauge invariant property of the magnetic potential, $\vec{A}$, which implies if we add the gradient of a scalar to this quantity the magnetic field remains invariant. We also understand, for a periodic lattice there is a crystal momentum associated with each mode. If we add another momentum to it equal to the integer multiple of the reciprocal lattice vector the crystal momentum remains same. And now we ask, how do we introduce magnetic field to a hamiltonian? We use minimal coupling formalism such that if $\vec{A}$ is the vector potential corresponding the magnetic field

momentum $\vec{p}$ transforms to $\vec{p} + e\vec{A}$. If we have a hamiltonian $H(\vec{k})$ in which we wish to include the effect of magnetic field we can do so by transforming $H(\vec{k})$ to $H(\vec{k} + e\vec{A})$. So suppose we have a one-dimensional hamiltonian and we wish to swipe from one end of the brillouin zone to the other, we can do so by changing $\vec{A}$ term in the hamiltonian which adds to the crystal momentum. This much preparation is enough for understanding berry phase.
Before berry phase was discovered[20] there was only one type of phase gain known which was time dependent phase which was gained by the wavefunction due to time dependent schroedinger equation.

Now suppose we change $\vec{A}$ and move the wavefunction around in a closed loop. As we change $\vec{A}$ we change the momentum in such a way so as to sweep a closed loop in the momentum space. It turns out by doing so there is an additional phase gained by the wavefunction other than the time dependent phase called **berry phase**. It has a unique property that this phase doesn't depend upon the time taken to close the loop, instead it depends only upon the path taken by the loop. It is given by,

$$\Gamma(C) = \oint_c \vec{A}(\vec{k}).d\vec{k}. \tag{2.8}$$

Here, $A(\vec{k}) = \iota\langle\Psi(\vec{k})|\nabla_k|\Psi(\vec{k})\rangle$. $|\Psi(\vec{k})\rangle$ is the ground state wavefunction of the hamiltonian in the momentum space, and we perform its gradient in all the three directions with $\vec{\nabla}_k$. The vector $A(\vec{k})$ is called Berry connection. This phenomenon was named after Michael Berry, however, he was not the one who discovered the phenomenon, though he was the one who generalized it. Before Berry it had been discovered independently by T.Kato in 1950 and Pancharatnam in 1956. Due to this reason it is also called Pancharatnam-Berry phase or Pancharatnam phase[21].
How we arrive at the formula of berry phase can be directly seen in the article[22].
We can define another quantity called **berry curvature** with which it is easier to write down the formula for Chern number.

$$\Omega(\vec{k}) = \vec{\nabla}_k \times A(\vec{k}) = \iota[\langle\frac{\partial\Psi(\vec{k})}{\partial k_x}|\frac{\partial\Psi(\vec{k})}{\partial k_y}\rangle - \langle\frac{\partial\Psi(\vec{k})}{\partial k_y}|\frac{\partial\Psi(\vec{k})}{\partial k_x}\rangle] \tag{2.9}$$

As can be seen, berry curvature can simply be obtained by taking curl of berry connection.
Chern number in the new form can be written as,

$$W = \frac{1}{2\pi}\iint_{BZ}\Omega(\vec{k}).d\vec{S} \tag{2.10}$$

Chapter 3

Quantum Spin Hall Insulator

Recently, a new class of topological states has emerged, called quantum spin Hall (QSH) states or topological insulators. Topologically distinct from all other known states of matter, including QH states, QSH states have been theoretically predicted and experimentally observed in mercury telluride quantum wells, in bismuth antimony alloys, and in Bi2Se3 and Bi2Te3 bulk crystals. QSH systems are insulating in the bulk—they have an energy gap separating the valence and conduction bands—but on the boundary they have gapless edge or surface states that are topologically protected and immune to impurities or geometric perturbations.—(Qi and Zhang)

3.1 Quantum Spin Hall insulator out of a Chern insulator

We now ask what happens if we add time reversal symmetry to a Chern insulator? We know Chern insulator edges have chiral edge states moving in either forward of backward direction. Suppose chiral state at an edge is moving in forward direction. What is its time reversed mode? The time reversed form is a chiral state moving in the backward direction.
If we combine both forward moving chiral state and its time reversed backward moving chiral state we get both forward and backward moving states at each edge. This gives net current to be zero. If forward and backward moving states have opposite spins the device gives rise to a net spin current which may have very interesting applications[22].
How do we mathematically create a system with a Chern insulator along with its time reversed part? One easy way is to expand the dimensions of the original hamiltonian and introduce the time reversed form.
If H_0 is the hamiltonian of Chern insulator, the required hamiltonian is written as,

$$H = \begin{bmatrix} H_0 & 0 \\ 0 & \tau H_0 \tau^{-1} \end{bmatrix} \tag{3.1}$$

where, τ is time reversal symmetry operator.
It is notable, if H_0 has N chiral modes, another N time reversed forms of these modes will be added to the system with hamiltonian H. So, our new system will have N modes moving in forward direction and N modes moving in the backward direction at each edge. These forward and backward moving modes can be exchanged into each other by applying time reversal symmetry. On applying τ to H the two diagonal terms simply exchange their positions and the hamiltonian remains same which means it satisfies time reversal symmetry.
Time reversal symmetry is an important component of the system. We will see that it protects forward and backward moving states from scattering due to impurities. As long as time reversal symmetry is preserved a forward moving state cannot be scattered into a backward moving state

and vice versa.
That implies, unless we have magnetic impurities which break time reversal symmetry our system is protected from any scattering and transport along the edge happens ballistically.
Now we see how it happens.

3.1.1 Perfect Transmission

Figure 3.1: (source:(23)) Figure showing transmission across the scattering region

Suppose we have a scattering region along the edge of our device. The region has N incoming modes and N outgoing modes on each side. We note that the outgoing modes on one side are are just the time reversed partners of the incoming modes on that side. We can label modes which are moving towards left along the edge as $|n, L\rangle$ and the modes moving towards right as $|n, R\rangle$.
The state on the left side of the scattering region is the superposition of forward moving states and backward moving states on that side. We also note that the backward moving states are just the time reversed part of the forward moving states. So, representing the scattering state on left side with $|\Psi, L\rangle$ it can be written as,

$$|\Psi, L\rangle = \sum_{n=1}^{N} \alpha_{n,L}|n.L\rangle + \beta_{n,L}\tau|n, L\rangle \tag{3.2}$$

Similarly, for the scattering state on the right,

$$|\Psi, R\rangle = \sum_{n=1}^{N} \alpha_{n,R}|n, R\rangle + \beta_{n,R}\tau|n, R\rangle \tag{3.3}$$

Now, the states which move away from the scattering region on the left are those which are transmitted from the right and those parts of the incoming states which are reflected back.
So,

$$\beta_{n,L} = \sum_{i=1}^{N} r^{n}_{i,L}\alpha_{i,L} + \sum_{n=1}^{N} t_{i,R}\alpha_{i,R} \tag{3.4}$$

$$\beta_{n,R} = \sum_{i=1}^{N} t'^{n}_{i,R}\alpha_{i,L} + \sum_{n=1}^{N} r'^{n}_{i,R}\alpha_{i,R} \tag{3.5}$$

These two equations above are written for N values of n, ranging from n=1...upto N. So, these form 2N equations.

We can write a $2N \times 2N$ matrix for the above set of equations as,

$$\begin{pmatrix} \beta_{1,L} \\ \beta_{2,L} \\ \vdots \\ \beta_{N,L} \\ \beta_{1,R} \\ \beta_{2,R} \\ \vdots \\ \beta_{N,R} \end{pmatrix} = \begin{pmatrix} r^1_{1,L} & r^1_{2,L} & \dots & r^1_{N,L} & t^1_{1,L} & t^1_{2,L} & \dots & t^1_{N,L} \\ r^2_{1,L} & r^2_{2,L} & \dots & r^2_{N,L} & t^2_{1,L} & t^2_{2,L} & \dots & t^2_{N,L} \\ . & . & \dots & . & . & \dots & . & \\ . & . & \dots & . & . & \dots & . & \\ . & . & \dots & . & . & \dots & . & \\ t'^1_{1,R} & t'^1_{2,R} & \dots & t'^1_{N,R} & r'^1_{1,R} & r'^1_{2,R} & \dots & r'^1_{N,R} \\ . & . & \dots & . & . & \dots & . & \\ . & . & \dots & . & . & \dots & . & \\ . & . & \dots & . & . & \dots & . & \\ t'^N_{1,R} & t'^N_{2,R} & \dots & t'^N_{N,R} & r'^N_{1,R} & r'^N_{2,R} & \dots & r'^N_{N,R} \end{pmatrix} \begin{pmatrix} \alpha_{1,L} \\ \alpha_{2,L} \\ \vdots \\ \alpha_{N,L} \\ \alpha_{1,R} \\ \alpha_{2,R} \\ \vdots \\ \alpha_{N,R} \end{pmatrix} \tag{3.6}$$

Writing the above matrix in a shorter form and using the following notations,

$$\beta_L = (\beta_{1,L}, \beta_{2,L}, \beta_{3,L}, \dots, \beta_{N,L}, \beta_{1,R}, \dots, \beta_{N,R})$$

$$\alpha_L = (\alpha_{1,L}, \alpha_{2,L}, \dots, \alpha_{N,L}, \alpha_{1,R}, \dots, \alpha_{N,R})$$

$$r = \begin{pmatrix} r^1_{1,L} & \dots & r^1_{N,L} \\ . & & . \\ . & & . \\ . & & . \\ r^N_{1,L} & \dots & r^N_{N,L} \end{pmatrix}$$

$$t = \begin{pmatrix} t^1_{1,L} & \dots & t^1_{N,L} \\ . & & . \\ . & & . \\ . & & . \\ t^N_{1,L} & \dots & t^N_{N,L} \end{pmatrix}$$

Similarly, we can write matrices for r' and t'.
Hence, the scattering matrix S is written as,

$$S = \begin{pmatrix} r & t \\ t' & r' \end{pmatrix} \tag{3.7}$$

and,

$$\begin{pmatrix} \beta_{n,L} \\ \beta_{n,R} \end{pmatrix} = S \begin{pmatrix} \alpha_{n,L} \\ \alpha_{n,R} \end{pmatrix} \tag{3.8}$$

We had said earlier, if no magnetic impurities are present in the scattering region, that means if time reversal symmetry is preserved everywhere, then there can be no back scattering in such a system. So, our problem now boils down to proving that t, $t' = 0$.
We know that S is unitary which means $S^\dagger S = 1$. So, if perfect transmission happens we get $r^\dagger r = r'^\dagger r' = 0$.
Let's apply time reversal operator to the earlier two equations which yield,

$$\tau|\Psi, L\rangle = \sum_{n=1}^{N} \alpha^*_{n,L} \tau|n, L\rangle + \beta^*_{n,L} \tau^2 |n, L\rangle$$

$$\tau|\Psi, R\rangle = \sum_{n=1}^{N} \alpha^*_{n,R} \tau|n, R\rangle + \beta^*_{n,R} \tau^2 |n, R\rangle$$

When τ acts on a complex number it performs its complex conjugation.
Incoming and outgoing states are now reversed. Incoming states are $\tau^2|n,L\rangle$ and $\tau^2|n,R\rangle$ and outgoing states are $\tau|n,L\rangle$ and $\tau|n,R\rangle$.
Some scattering matrix again acts on the incoming states and gives back the outgoing states therefore,

$$\begin{pmatrix}\alpha^*_{n,L}\\ \alpha^*_{n,R}\end{pmatrix} = S\tau^2 \begin{pmatrix}\beta^*_{L}\\ \beta^*_{R}\end{pmatrix}$$

Multiplying both sides by $\tau^2 S^\dagger$.

$$\tau^2 S^\dagger \begin{pmatrix}\alpha^*_{n,L}\\ \alpha^*_{n,R}\end{pmatrix} = \begin{pmatrix}\beta^*_{n,L}\\ \beta^*_{n,R}\end{pmatrix}$$

Because,

$$\tau^2 = +1 or -1$$

$$\tau^4 = 1$$

Taking the complex conjugation of the above equation we get,

$$\begin{pmatrix}\beta_{n,L}\\ \beta_{n,R}\end{pmatrix} = \tau^2 S^T \begin{pmatrix}\alpha_{n,L}\\ \alpha_{n,R}\end{pmatrix} \tag{3.9}$$

Comparing (3.9) with (3.8) we have,

$$S = \tau^2 S^T \tag{3.10}$$

τ^2 above may take two values either +1 or -1 depending upon the type of the system. For, example if the system consists of +1/2 particles τ^2 takes -1 value and for spinless fermions it takes +1 value.
Let us consider the case when $\tau^2 = -1$. We see it gives very interesting consequences.
In this case, it turns out $S^T = -S$. If $t = t' = 0$, that means if there is no transmission, then $r^T = -r$. Also by unitary property of S, i.e. $S^\dagger S = \mathbf{1}$, it turns out $r^\dagger r = 1$. So, r matrix is both anti-symmetric and unitary.
There is a property of anti-symmetric matrices that if e is an eigenvalue, then -e is also an eigenvalue. So, if the order of the matrix N is an odd number, there is an eigenvalue situated at $e = 0$.
Unitary matrices always have the property that their eigenvalues have a unit norm.
Combining these two arguments, above it turns out, it is not possible to have a situation where there is an odd number of modes, and $t = t' = 0$.
Also, since for $\tau^2 = -1$ case r matrix is antisymmetric that is $r^T = -r$ we have atleast one eigenvalue equal to zero and it is for this mode that the transmission happens with unit probability.
So, we conclude from the above discussion, if we have an odd number of modes moving in forward or backward direction in a time reversal symmetric Chern insulator there is atleast one mode for which transmission happens with unit probability through the disordered scattering region.
The above statement is true only when there is an odd number of modes while when there is an even number of modes we can not talk about the protection of the states due to time reversal symmetry.
Hence, there are two possible scenarios, the first is when the number of modes is odd and the states are protected by time reversal symmetry, these are represented by an invariant -1, while when the system contains an even number of modes the system is represented by +1 and the system is said to be in a trivial phase.
These counter propagating modes are called helical edge states. In 2007, Molenkamp's group became the first group to observe 1D helical edge states[23].
After we provide time reversal symmetry to our Chern insulator the hall current disappears. This happens because there is an equal number of modes travelling in forward and backward direction. But, this scenario gives rise to another important effect called Quantum spin Hall effect. If we look at the figure(3.2) the situation becomes clear.

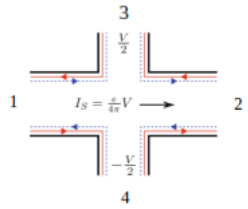

Figure 3.2: (source:(24)) Schematic showing quantum spin hall effect in a quantum hall bar

There is a net spin current between terminals 3 and 4 because the electrons which move from 3 to 1 and 1 to 4 have exactly opposite spin to those travelling from 4 to 1 and 1 to 3.

3.2 Quantum spin hall insulator: Mathematical Model

We treat quantum spin hall insulators now somewhat more formally. As we derived a mathematical model for Chern insulators by stacking together a large number of kitaev chains, and then we obtained a more realistic model using graphene which we called Haldane model, in this section we will derive a mathematical model which describes a quantum spin hall insulator.
If we remember our starting discussion of quantum spin hall insulator, we just appended the time reversed partner of Chern insulator to the original system. We will do a similar thing again. The time reversed partner of Chern insulator will be included into the original system which will expand the dimensionality of the hamiltonian.
The hamiltonian is written as,

$$H_{BHZ} = \begin{pmatrix} h(\vec{k}) & 0 \\ 0 & h^*(-\vec{k}) \end{pmatrix} \tag{3.11}$$

where,

$$h(\vec{k}) = \epsilon(\vec{k}) + \vec{d}(\vec{k}).\vec{\sigma} \tag{3.12}$$

.

$\vec{\sigma} = (\sigma_x, \sigma_y, \sigma_z)$

$\epsilon(\vec{k}) = C - D(k_x^2 + k_y^2)$

$\vec{d} = [Ak_x, -Ak_y, M(\vec{k})]$

$M(\vec{k}) = M - B(k_x^2 + k_y^2)$

H_{BHZ} is called **Bernevig Hughes Zhang model**. The model is named after Bernevig and Zhang who discovered it in 2006[25]. The model was discovered after an another model which was given by Kane and Mele in 2005[26].Bernevig, Hughes and Zhang later used this model to predict the possibility of realisation of 2D topological insulators with 1D helical edge states in the heterostructure created by combining mercury telluride and cadmium telluride layers[27].
We can check for ourselves whether the above model does give ungapped modes, that is helical states at the edges. We can obtain E vs (k_x, k_y) plot using kwant.

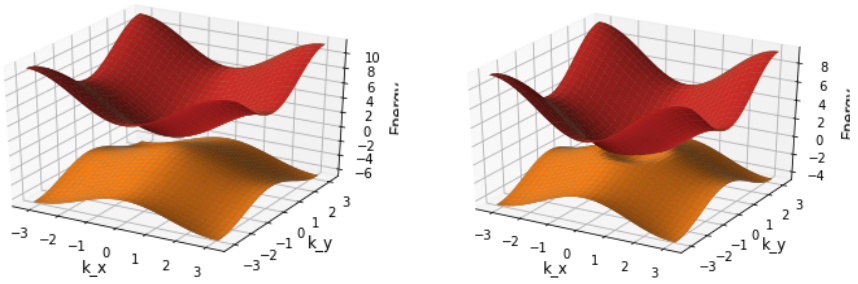

(a) Trivial(M=+1) (b) Topological(M=-1)

Figure 3.3: Bernevig Hughes Zhang model(Bandstructure for the above hamiltonian for a quantum spin hall insulator) plotted for the following parameter values:A=0.5,B=1,C=0,D=0.3.

We see that the model does provide gap closing at $k = 0$ as M changes sign from negative to positive.

3.3 Corbino disk for quantum hall effect(Spin Pumping)

While studying quantum spin hall effect we observed that we could transfer the charge from one edge to other by pumping flux at the centre of the annular disk. We used this as an argument for the quantization of hall conductance.
In the current case what we have is a conduction in both the directions from the inner to the outer edge and from the outer to the inner edge. Because we have hall current along with its time reversed, so we have the net current flowing equal to zero. On the contrary there is a spin current and on completing one cycle of pumping there is an unequal number of both the spins at the two edges.
We now see what happens with the two possible states of the system that is when the system is topological and there are ungapped states present at the edges and when the system is in trivial state that is when the system behaves as a normal insulator.
We prepare two plots using kwant in topological and trivial case to observe how the states behave as we turn the magnetic flux (Φ) from (Φ=0) to (Φ=h/2e).

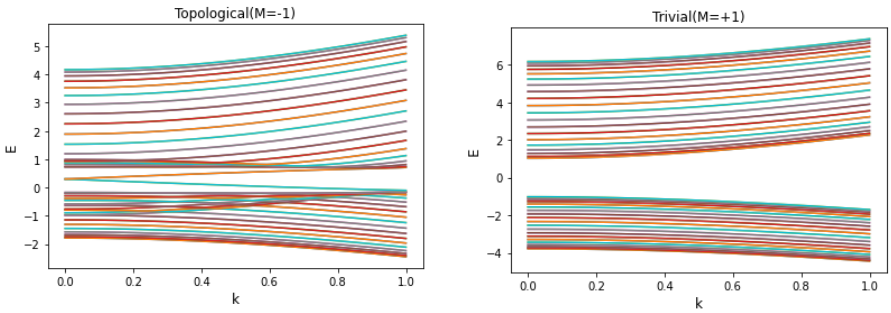

(a) (b)

Figure 3.4: BHZ model plotted for a corbino disk with a finite length along one dimension and periodicity along the other. Following parameter values are used:A=.5,B=1.0,C=0.0,D=0.3.

These plots provide a clear picture about how fermion pumping happens in topological case but does not happen in the trivial case.

3.4 Quantum spin hall effect and experiments

Reference([28]) discusses the experimental realisation of spin quantum hall effect in $HgTe/CdTe$ quantum well. The hamiltonian which explains the experimental model is written as[29]:

$$H(\vec{k}) = \begin{pmatrix} \epsilon_e(\vec{k} & \Delta(\vec{k})) \\ \Delta^\dagger & \epsilon_0(\vec{k}) \end{pmatrix} \tag{3.13}$$

where, $\Delta(\vec{k}) = \alpha\sigma_z(k_x + \iota k_y)$, $\epsilon_e = \delta_e + m_e k^2$, $\epsilon_o = \delta_o + m_o k^2$, and, $\delta_e < \delta_0$.

This model describing quantum spin hall effect in $HgTe/CdTe$ quantum well is known as Bernevig Hughes Zhang model.

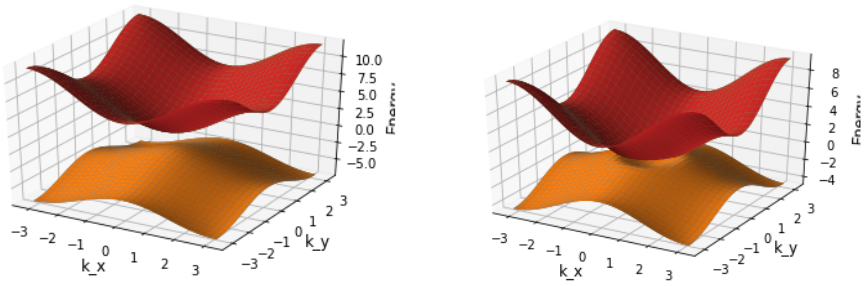

(a) Trivial(M=1.5)

(b) Topological(M=-1)

Figure 3.5: Quantum spin hall effect model for HgTe/CdTe quantum well plotted for the above hamiltonian with the following parameter values:A=.5,B=1.0,C=0.0,D=0.3

Above we see the plot for both trivial and topological case. When we are in the trivial case there is no band crossing and the system behaves as a normal insulator with no edge states. After the band crossing happens the system becomes topological and edge states appear. If we keep the chemical potential at $E = 0$, in the trivial case the system will be totally insulating because there are no states to carry the current. While in the topological case, there will be a no conduction due to bulk but it will be there due to the edges. For the chemical potential at any place other than $E = 0$ both topological and trivial insulators behave in a similar way and show bulk conductance. Though, the conductance for topological insulator is still higher, obviously due to conduction from the edge states. The situation is easily represented by the following plot obtained by calculating the conductance at different chemical potentials using kwant package.

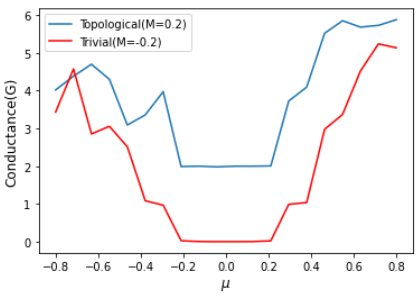

(a) Conductance vs μ plot created for for both trivial and topological case

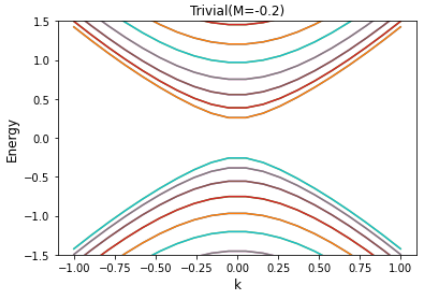

(b) Band diagram for the trivial case

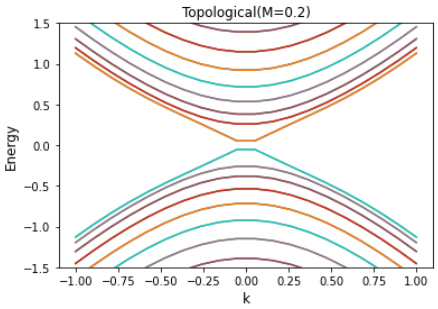

(c) Band diagram for the topological case

Figure 3.6: Conductance plot and the band diagrams plotted for trivial and topological cases for a HgTe/CdTe quantum well. There are states present at zero energy in the topological case so the conductance is always higher. Parameter values are the following:A=0.5,B=1,C=0,D=0.

The conductance is minimum near $\mu = 0$ because the density of states drops down to minimum, anywhere else the conductance increases with increasing chemical potential as the density of states increases.
We know that edge states are protected from scattering due to time reversal symmetry and so the conduction happens ballistically, which gives the conduction equal to $2e^2/h$.

3.5 Quantum spin hall edge states and magnetic field:

The edge modes in quantum spin hall effect are protected due to time reversal symmetry and the transport happens without scattering which provides the maximum possible conductance value that is for ballistic conductance which is $2e^2/h$.
If we apply a magnetic field we break the time reversal symmetry and in the process we also make the edge states less protected. So, we expect the conductance at zero chemical potential to drop with increasing magnetic field.
We can write the hamiltonian corresponding to edge states as,

$$H = v_F k_x \sigma_z$$

If we introduce a magnetic field it enters the hamiltonian as follows,

$$H = v_F k_x \sigma_z + \vec{B}.\vec{\sigma}$$

In this case transport happens only along x-axis, so if the magnetic field is applied only along x-direction, the hamiltonian looks as,

$$H = v_F k_x \sigma_z + B\sigma_x,$$

and the energy spectrum is written as,

$$E = \pm\sqrt{v_F^2 k_x^2 + B^2}$$

We set the chemical potential at $\mu = 0$ and calculate the conductance at each magnetic field using kwant package.

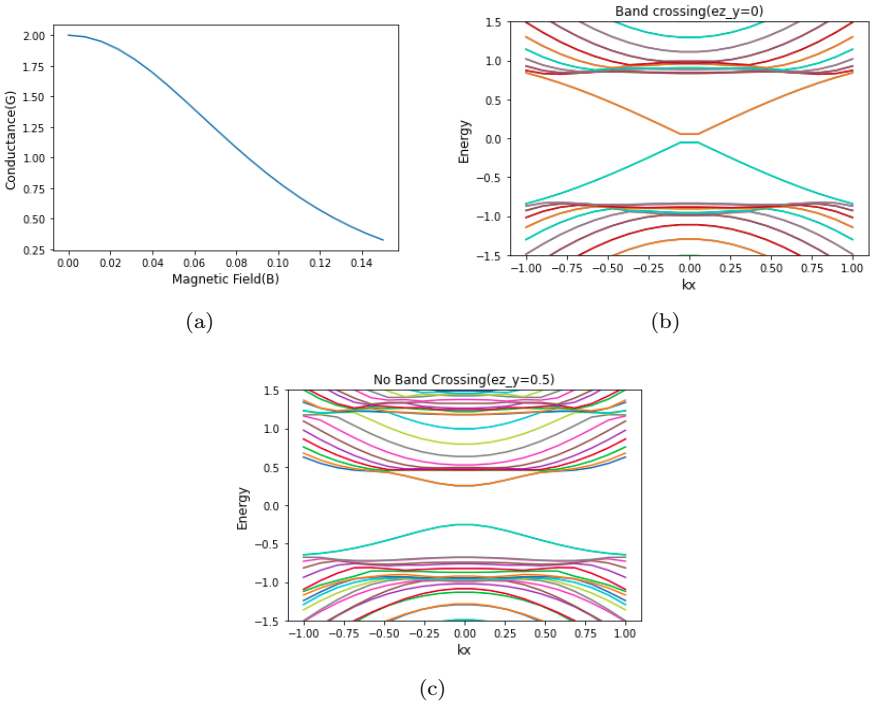

(a) (b)

(c)

Figure 3.7: Fig(a) shows drop in the conductance for the quantum spin hall insulator with an applied magnetic field which breaks the time reversal symmetry and makes the propagating modes unprotected. Fig(b) and (c) show the band diagram without and with an applied magnetic field. There is a band opening in fig(c) due to the applied magnetic field. Following parameter values were used for the plot:A=0.5,B=1.0,C=0.0,D=0.0

The result obtained is as expected. The conductance starts from $2e^2/h$ at $B = 0$ and falls upto zero as we increase the magnetic field.

Chapter 4

3D Topological Insulator

But only when topological insulators were discovered experimentally in 2007 did the attention of the condensed-matter-physics community become firmly focused on this new class of materials. A related topological property known as the quantum Hall effect had already been found in 2D ribbons in the early 1980s, but the discovery of the first example of a 3D topological phase reignited that earlier interest.—(Kane and Moore)

4.1 Quantum spin hall effect: Extended to three dimensions

In the earlier sections, we studied how to create a 2D quantum spin hall insulator out of a 2D Chern insulator, then we studied about the helical edge states, the states travelling along edge of the sample without scattering and protected due to time reversal symmetry.
Now, after studying all that a natural question arises in mind what happens if we build a three dimensional topological insultor? Will we then have 2D edge states propagating along faces of the cube? Will they be protected due to time reversal symmetry? How will time reversal symmetry act in three dimensions? We are going to study about all such questions in this section. There is one important concept to be discussed which may be useful in our later discussion.
Strong topological insulator: We have seen before that each quantum hall insulator can take any of the two values depending upon whether the insulator is in trivial or topological state. Idea behind a 3D topological insulator is that we can combine 2D topological insulators in three dimensions to build a three dimensional topological insulator, and we see that each face of the 3D insulator has a topological invariant of its own. Based on these topological invariants we define a property for the combined system called **Strong topological invariant.**
In the figure below is shown a cubic brillouin zone for a cube in real space.

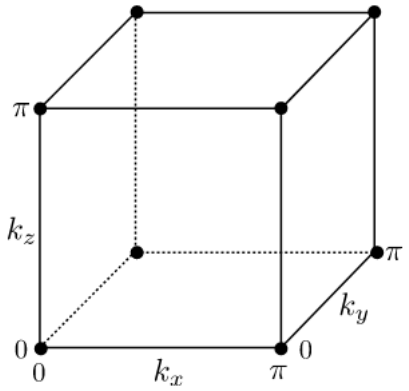

Figure 4.1: 3D brillouin zone.

There is a topological invariant associated with each face represented as, $Q(k_x = 0)$ for face corresponding to $k_x = 0$, $Q(k_y = 0)$ for face corresponding to $k_y = \pi$, and so on.
If the following property is satisfied, $Q(k_x = 0)Q(k_x = \pi) = Q(k_y = 0)Q(k_y = \pi) = Q(k_z = 0)Q(k_z = \pi)$, we have a strong topological insulator and the product is called strong topological invariant.

4.2 A mathematical model for 3D topological insultor

Our approach next would be to write a hamiltonian which describes a 3D topological insulator. This hamiltonian we will arrive at by combining together 2D topological insulators. We will next plot the three dimensional bandstructure and see what parameters can we change to close the gap and go from trivial state, when we have no edge states, to the topological state, when edge states are there.
Without providing the argument for why the following model holds we will simply write the hamiltonian for 3D topological insulator and look at its bandstructure.

$$H(\vec{k}) = \epsilon.\mathbf{1} + \begin{pmatrix} M(\vec{k}) & Ak_+ & 0 & \tilde{A}k_z \\ Ak_- & -M(\vec{k}) & \tilde{A}k_z & 0 \\ 0 & \tilde{A}k_z & M(\tilde{k}) & -Ak_- \\ \tilde{A}k_z & 0 & -Ak_+ & -M(\vec{k}) \end{pmatrix} \tag{4.1}$$

In this,
$k_\pm = k_x \pm \iota k_y$,
$M_0(\vec{k}) = M - B(k_x^2 + k_y^2)$
$\epsilon(\vec{k})$ here varies from material to material.
3D toplogical insulator was first predicted to exist in bismuth compounds in 2007[30], and was verified experimentally in $Bi_{1-x}Sb_x$[31].

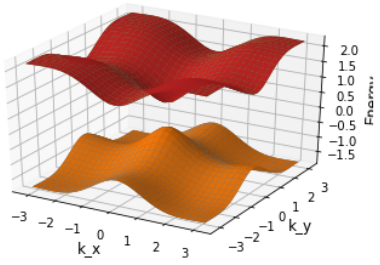

(a) Trivial(M=-0.6)

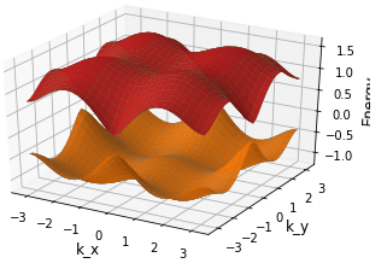

(b) Topological(M=-2.0)

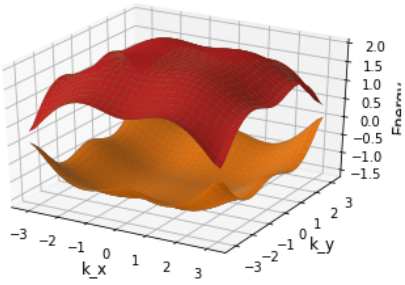

(c) Topological(M=-2.75)

Figure 4.2: Bandstructure for a 3D topological insulator plotted for the above hamiltonian with the following parameter values:A1=1,A2=1.0,B1=1,B2=0.2,C=0,D1=0.1,D2=0.0. System moves from trivial to topological state on changing the value of M

The system transforms from trivial to topological state as we change M from -ve(-1) to +ve(+1).
Surface states of a 3D topological insulator: Remember we formed our 3D topological insulator by combining two-dimensional topological insulators so each face of the cube is just a 2D quantum spin hall insulator. So we can conclude that surface contains edge states which counter propagate, when the system is in the topological regime. These states are best described by the following hamiltonian:

$$H = v\sigma_y k_y,$$

which is the hamiltonian of the states propagating in the opposite directios. The dimensionality of two provided by σ_y is due to two possible directions of propagation, hence the system has two degrees of freedom. The above hamiltonian is symmetric under time reversal symmetric operator, $\tau = \iota\sigma_y k$.

4.3 Quantum hall conductance

What happens if we apply a magnetic field perpendicular to one of the surfaces and an electric field along that surface? If we apply probes perpendicular to the electric field we will measure a hall current and the system will possess a quantum hall conductance.
We plot the landau levels for such system. The effect of perpendicular magnetic field is included into the system by multiplying a phase factor to the hopping parameter given by peierls hopping. If B_z is the magnetic field the phase multiplied to the hopping parameter is $e^{-\frac{\iota}{2}B_z(x_1-x_2)(y_1+y_2)}$, where (x_1, y_1) and (x_2, y_2) are the initial and final hopping sites. The landau levels are obtained with the help of kwant package, as shown in the figure.

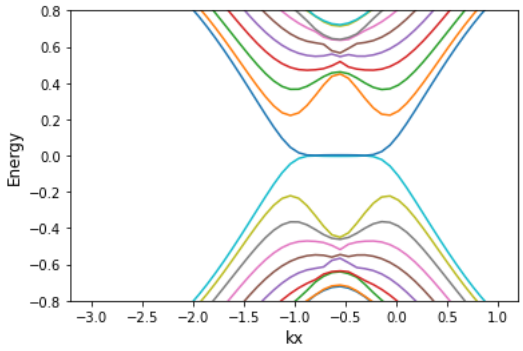

Figure 4.3: Landau levels for a 3D topological insulator with an applied perpendicular magnetic field and an electric field parallel to the surface. Following parameter values were used:A1=1,A2=1.0,B1=1,B2=1.0,C=0,D1=0.0,D2=0.0

We see that if there is an energy level below $E = 0$, corresponding to that there is another level above $E = 0$. All these opposite levels are paired and these two levels of each pair come from opposite surfaces of the cube, i.e. if one comes from top the other comes from the bottom.
Quantum hall conductance corresponding to each surface is given by $(n+\frac{1}{2})\frac{e^2}{h}$, hence, the combined conductance measured for both the surfaces is $\sigma_{xy} = (2n+1)\frac{e^2}{h}$.
While studying 2D quantum hall effect we plotted conductance at various values of chemical potential μ and observed that the conductance was maximum when the chemical potential was such that there were maximum number of states at that level. We observed the conductance to be dropping as we moved towards $E = 0$ level as the density of states there is minimum.
We obtain a similar plot for 3D topological insulator and obtain conductance versus chemical potential curve and compare it with the energy spectrum to see how conductance drops and increases with the corresponding density of states.

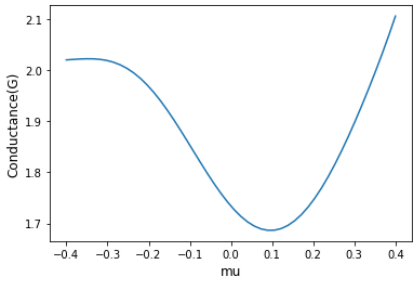

(a) Conductance vs μ at Bz=0

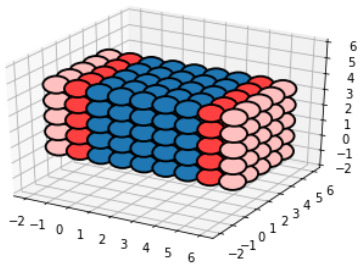

(b) 3D Lattice with the leads attached

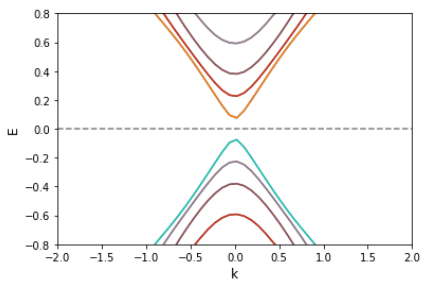

(c) Band sructure for a 3D topological insulator.

Figure 4.4: Fig(a) shows drop in the conductance of a 3D topological insultor as μ is moved closer to zero. Fig(b) shows the 3D toplogical insultor and the leads attached to its opposite surfaces. Fig(c) shows the band structure for the 3D topological insultor block.

If we come back to the landau levels which give as a result the hall conductance, $\sigma_{xy} = (2n + 1)e^2/h$, this implies the separation between two plateaus is expected to be $[2(n+1)+1-(2n+1)] = 2e^2/h$. This is our conclusion, but the real experimental plot doesn't confirm our analysis.

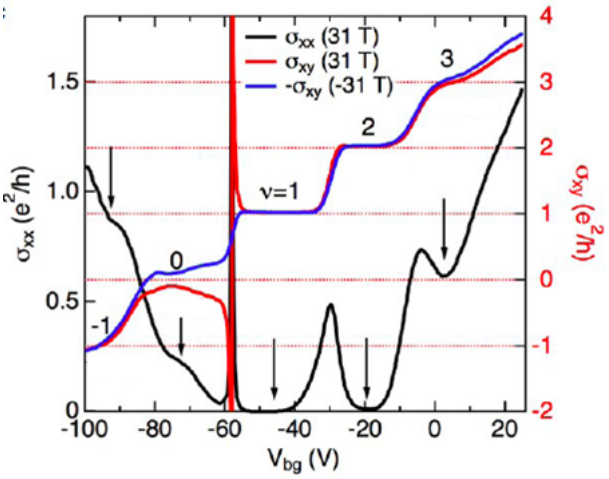

Figure 4.5: (source:(32)) Hall plateaus for a 3D topological insulator.

The real plot still shows a separation of e^2/h between the consecutive plateaus. The reason for this anomaly is that the top and bottom surfaces both contribute to the conductance, however, both the surfaces may not be exactly the same, that means if the top surface has the conductance given by $(n_{top} + \frac{1}{2})e^2/h$, the bottom surface may have a conductance given by $(n_{bottom} + \frac{1}{2})e^2/h$, so σ_{xy} is written as,

$$\sigma_{xy} = (n_{top} + n_{bottom} + 1)e^2/h$$

The separation between two nearest pleateus is given by,

$$((n_{top} + 1) + n_{bottom})e^2/h - (n_{top} + n_{bottom} + 1)e^2/h = e^2/h$$

or as,

$$(n_{top} + (n_{bottom} + 1))e^2/h - (n_{top} + n_{bottom} + 1)e^2/h = e^2/h$$

4.4 Methods used to probe surface states of a 3D topological insulator

We will discuss now two methods used by experimentalists to probe the surface states of a 3D topological insulator. One method is striking the surface of a 3D topological insulator with high energy photons and then plotting the brillouin zone for the surface based on the momenta of excited electrons. This method is called ARPES(Angle Resolved Photo Emission Spectroscopy)[32].
Another method is to obtain real space picture of the surface by tunneling electrons into the surface from a metallic tip. We then obtain perform a fourier transform to obtain brillouin zone picture of the surface. THis method is known as Quasiparticle Interference(QPI).

4.5 ARPES(Angle Resolved Photo Emission Spectroscopy)[Ref:32]

As discussed before ARPES can be used to map out the entire bandstructure of the surface of a 3D topological insulator. A beam of x-rays is sent to the surface of the insulator and the ejected

electrons are collected. Since the momentum is conserved, the momentum of the ejected electrons have the same value as they have inside inside the crystal. Due to this property entire fermi surface can be mapped out. Since only the electrons at the fermi level are ejected from the surface, to obtain the entire bandstructure we have to adjust the chemical potential and take measurements for different heights of the fermi level.

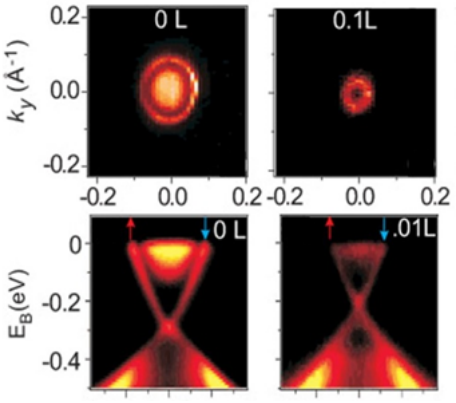

Figure 4.6: (source:(33)) Band structure for the surface of a 3D topological insulator

4.6 Scanning Tunneling Microscopy(STM)

(Ref:[34])

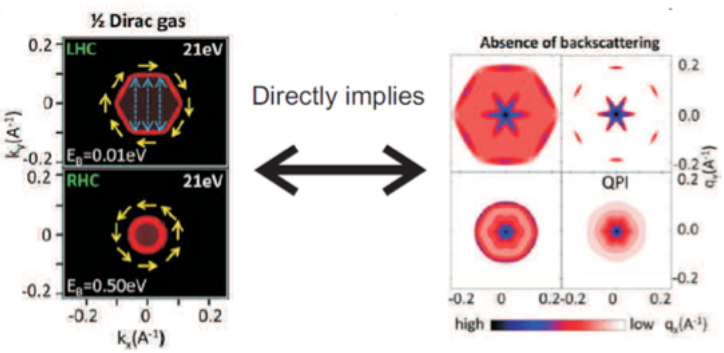

Figure 4.7: [source(33):Hasasn Lab, princeton]

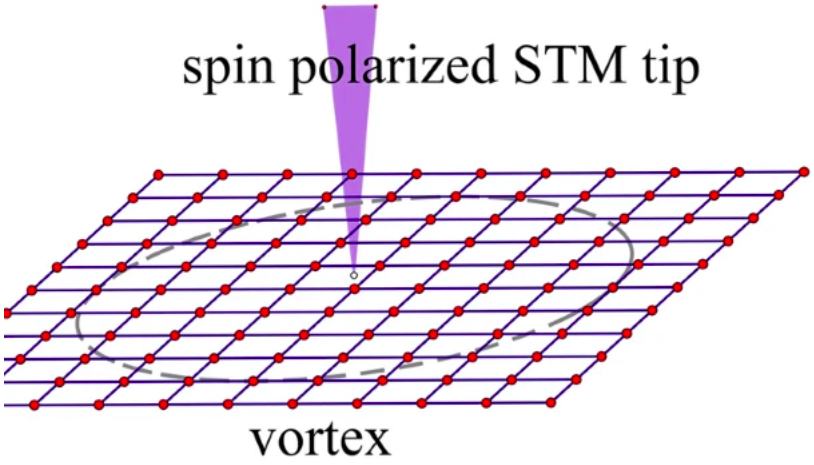

Figure 4.8: source(35):STM imaging performed on a 2D lattice with a spin polarised tip.

Scanning Tunneling Microscopy is a method by which electrons are tunnelled into the surface from a metallic tip. This method is useful for obtaining atomic level resolution. However, we don't gain any information about the momenta. We can sweep the metallic tip across the surface and obtain information about various atomic orbitals occupied by the electrons. The pattern which is obtained is called Quasiparticle Interference(QPI).

4.7 Correction in the dirac hamiltonian of the surface states

In the last section, we wrote down the dirac hamiltonian for the surface of a 3D topological insulator as,

$$H = v\vec{\sigma}.\vec{k}$$

This hamiltonian shows that the fermi surface must be circular. However, moving away from this circular region another region was found in scanning tunneling microscopy, which was hexagonal[36]. So, it is important to write a corrected hamiltonian which also explains the hexagonal part of the fermi surface. We see that if cubic terms k_+^3 and k_-^3 and a dirac velocity proportional to $\alpha\vec{k}^3$ are introduced, the hexagonal part of the fermi surface can be explained.
The new terms are added in such a way that time reversal symmetry is still preserved. The modified hamiltonian is written as:

$$H(\vec{k}) = E_0(k) + v(1 + \alpha\vec{k}^2)(k_x\sigma_y - k_y\sigma_x) + \frac{\lambda}{2}(k_+^3 + k_-^3)\sigma_z \tag{4.2}$$

We plot the corrected hamiltonian using kwant package as shown in the figure.

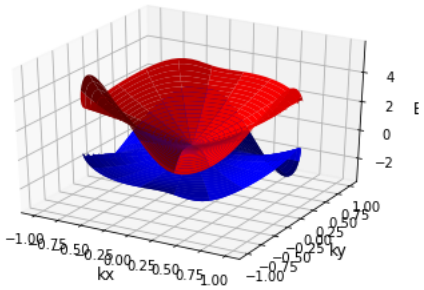

Figure 4.9: Hexagonal warping. Bandstructure plotted for the corrected hamiltonian for the surface states of a 3D toplogical insulator.(Parameters used:$v(1+\alpha\vec{k}^2) = 1.8$,$\lambda = 1.5$)

Chapter 5

Majorana Fermions

"There are various categories of scientists, people of a secondary or tertiary standing, who do their best but do not go very far. There are also those of high standing, who come to discoveries of great importance, fundamental for the development of science. But then there are geniuses like Galileo and Newton. Well, Ettore Majorana was one of them."—Enrico Fermi

5.1 Majorana fermions in the topological systems

We utilize the expertise we have gained so far in the understanding of topological systems to obtain Majorana fermions. Majorana fermions were proposed originally as zero energy particles which exist in nature as a consequence of dirac equations. In nuclear physics we have a spectrum of particles with negative and positive energies called particles and antiparticles. In condensed matter systems also we have a similar scenario with particles occupying the states below the fermi level and holes occupying the states above the fermi level. As a consequence, we expect the particles to be also present at the zero energy level. These are not actual particles but zero energy states which are produced as a consequence of the superposition of negative and positive energy states. We call these states Majorana modes. They are interesting because of their non-abelian statistics which projects them as an important candidate for topological quantum computation. In this section we, study the methods by which Majorana fermions can be obtained in these systems:
(a) 2D quantum spin hall insulators (b) p-wave superconductors (c) 3D-Topological insulators

Superconductors will be an important material for our use, this is because of the particle-hole spectrum and gap at zero energy which is important to provide protection to the edge modes present at zero energy.

5.2 Majorana fermions in Quantum spin hall insulator

1D topological superconducting wire has a property that it has isolated Majorana modes present at the edges. It is a fact which we will discuss in detail in a later section, but we keep it in our mind for now.
We prepare a quantum spin hall insulator in the form of a Corbino disk. The disk has helical states propagating along both inner and outer edge. Now we fix a superconducting wire at the outer edge of the corbino disk in the form of a ring while leaving a small gap which is a Josephson Junction. As a result, Majorana fermions are produced at the two ends of the Josephson junction. However, there is a caveat. By bringing the superconductor in proximity of the Quantum spin hall insulator, the edge becomes gapped everywhere except the area which is exposed due the Josephson junction. This causes the Majorana fermions which are present at the two ends of the superconducting ring to be coupled.
Obtaining two coupled Majorana modes, as we will see later, is as good as a single fermionic mode,

which is not required for our purpose. So, we need to make the region under the Josephson junction to be gapped.
If we remember, a 2D quantum spin hall insulator obeys time reversal symmetry which is also responsible for the ungapped edge states. If we break this time reversal we may expect to produce a gap at the edge. We can apply a magnetic field to break the time reversal symmetry, for which we place a magnet inside the gap of the Josephson junction.
The situation looks like as shown in the figure and we obtain two isolated modes.

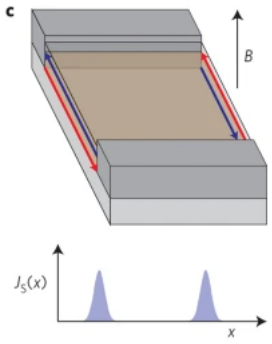

Figure 5.1: source(37):Majorana modes produced at the ends of the superconductor shown by gray blocks. Peaks in the below diagram show the Majorana modes.

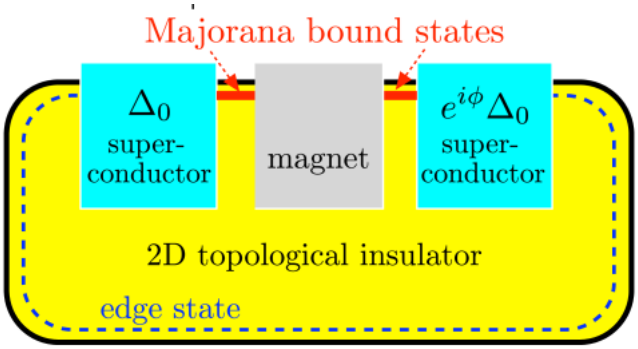

Figure 5.2: source(38):Majorana bound states at the interface of magnet and superconductor

We now attempt to write the hamiltonian for our model, which gives Majorana modes. There are three components in our model, helical edge states, superconducting pairing, and magnetic field. We need to combine these hamiltonians for these three to write the complete hamiltonian. The term corresponding to helical edge states is $(-\iota v_x \partial_x - \mu)$. This hamiltonian should be on the diagonal of the complete hamiltonian so it is written as $(-\iota v_x \partial_x - \mu)\tau_z$. The particle-hole pairing term due to superconductor comes on the off diagonal places, so it is written with the pauli matrix τ_x as, $\Delta(x)\tau_x$. The magnetic field is applied along z-direction so the zeeman term comes as $m(x)\sigma_z$. Since the zeeman field is equivalent for both, particles and holes, so it is crossed with pauli matrix τ_0 which is an identity matrix. So the last term is written as $m(x)\sigma_z\tau_0$.
The final hamiltonian after summing up all the components is written as follows:

$$H_{BdG} = (-\iota v \sigma_x \partial_x - \mu)\tau_z + m(x)\sigma_z + \Delta(x)\tau_z$$

We can finally use our hamiltonian and plot the solutions to see if it really gives the expected zero energy modes at the superconducting wire and magnet interface.

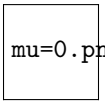

Figure 5.3:

5.3 Majorana fermions in p-wave superconductors:

We see in the section, how Majorana modes can be obtained inside the vortices in a p-wave superconductor. When magnetic field is applied to a superconductor it penetrates inside the vortices. Superconducting pairing term drops down to zero at the center of the vortex. Also the superconducting phase winds by 2π on going around the vortex.
Our claim is that Majorana zero modes are present inside the superconducting vortices. To prove our claim we first need to find the hamiltonian for a 2D-pwave topological insulator and pass a perpendicular magnetic field then plot the zero energy solution.
The process we are going to use here is already familiar to us. We start with a low dimensional material and stack it up to obtain the higher dimensional material. The 1D kitaev chain model written as,

$$H_{1D} = -2t(cosk - 1)\tau_z + \Delta sink\tau_y$$

can be stacked together and written in two dimensions as,

$$H_{2D}(k_x, k_y) = -[2t(\cos k_x + \cos k_y) + \mu]\tau_z + \Delta(sink_x\tau_y - sink_y\tau_x)$$

If we recall our derivation for the hamiltonian of a 2D Chern insulator, it took the similar route and the hamiltonian which we used for wire with 1D counter propagating modes was same as H_1D written above. After stacking 1D kitaev chains we obtained a 2D Chern insulator with counter propagating edge modes. These modes were standing waves at the edge. The hamiltonian for our p-wave superconductor has been derived in a similar way and hosts edge modes which propagate ballistically and form standing waves at the edge. The energy of the edge modes is thus, $E = \hbar vk$. Since standing waves are formed at the edge we can apply periodic boundary conditions of a wave and obtain the values which can be taken by k.

$$KL = 2\pi n$$

$$k = \frac{2\pi n}{L}$$

$$\Rightarrow E_n = \frac{\hbar v 2\pi n}{L}$$

These are the possible energy values which can be taken by the edge states. Keeping in mind the particle-hole spectrum of a superconductor all the integer values of n are allowed and n doesn't only take the positive but also the negative energy values. $n = \ldots -2, -1, 0, 1, 2, \ldots$.
This discussion implies that it is possible that the edge state takes a zero energy value.
Since, the energy states of a superconductor come in pairs of negative and positive if there is a state at zero energy level there must be another state present at the same energy level. And there is no place other than the centre of the vortex where this state can be present because the superconducting pairing term here drops down to zero. We can plot the zero energy solutions for our hamiltonian using kwant package as shown in the figure.

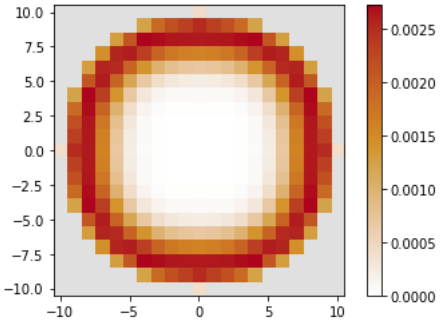

Figure 5.4: Zero energy states on the 2D-pwave superconductor lattice, t=1,$\Delta = 0.5$

5.4 Majorana modes in a 3D topological insulator

It is also possible to obtain Majorana fermions on the surface of a 3D topological insulator. We simply attach a superconductor and a magnet to the surface and write the corresponding hamiltonian. We know that each of the components will contribute their own term to the hamiltonian. The term for the edge states on the surface of the insulator is given by $-\iota(\sigma_x\partial_x+\sigma_y\partial_y)-\mu$. This term occupies the diagonal position so it comes with the pauli matrix τ_z. While the pairing term and zeeman field term enter the hamiltonian as $\Delta(x)\tau_x$ and $m(x)\sigma_z\tau_0$ respectively. The final hamiltonian is written as,

$$H_{BdG} = (-\iota\sigma_x\partial_x - \iota\sigma_y k_y - \mu)\tau_z + m(x)\sigma_x + \Delta(x)\tau_x \tag{5.1}$$

We can solve the above hamiltonian using kwant package and plot the zero energy eigenvectors. The result is as follows:

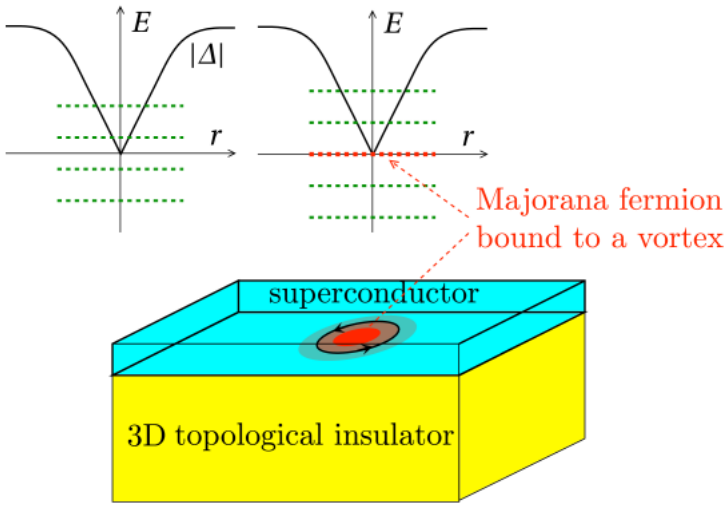

Figure 5.5: source(39): Majorana modes on the surface of a 3D topological insulator attached with a superconductor and a magnetic field applied perpendicular to the surface.

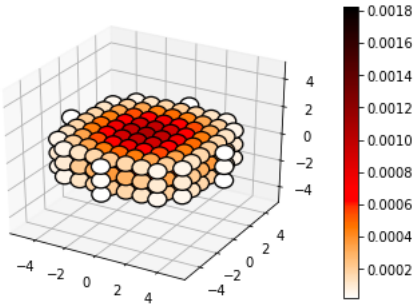

Figure 5.6: Zero energy modes produced at the opposite surfaces of a 3D topological insulator. Parameter values:A1=0.5,A2=0.5,B1=0.5,B2=0.5,C=-0.2,D1=0.1,D2=0.0,M=-0.2,Delta=0.15

5.5 Some important concepts

In this section, we review some of the important concepts that one comes across while studying the topological systems.

5.5.1 Topology

If there are properties of a system or an object which do not change upon a continuous deformation, it comes under the study of topology. Topology is a well defined mathematical discipline, and it finds applications in a number of sciences like physics, biology, computer science, engineering material science etc. Our focus will be to understand, what do we mean by topology when we talk about condensed matter systems.
In physics, a system is defined by a hamiltonian. After we write the hamiltonian the next step is to calculate its eigenvalues and eigenvectors. Suppose now we deform the hamiltonian. One way of deforming the hamiltonian is to change the parameter α on which it depends. We take the value of α from say 0 to 1, and calculate the eigenvalues at each point. The hamiltonian is said to be topologically equivalent as long as the eigenvalues do not cross. Now, this is a continuous deformation because we are changing the parameter α continuously, and H also changes continuously. One important feature is apparent here which is we cannot talk about the topology of a system if its eigenvalues are continuous. In that case, we would never know when one energy level has crossed the other. We can put it in another way as saying that topology is defined only for the systems for which energy spectrum is gapped. If upon a continuous deformation of hamiltonian the gap closes the hamiltonian doesn't remain topologically invariant anymore, and the system is said to have undergone topological phase transition. It is possible to characterize each topological phase of the system by a number. This number can be an integer and is called topological invariant. We can track the progress of our system upon changing some external parameter, changing the hamiltonian continuously, by checking the value of topological invariant. If there is change in the topological invariant then there is a phase transition.
Topological invariant simply keeps track if there has been a bulk gap crossing and can be defined in different ways for different systems.
For example, for a quantum dot we can define topological invariant for a system by counting the number of energy levels below the fermi surface that is $E = 0$. If an energy level crosses $E = 0$ there is a band crossing and the number of energy levels below $E = 0$ reduces by one. So, instead of calculating the number of energy levels below $E = 0$ there is another method which can be used. We can simply start from zero and for each level crossing above $E = 0$ level the topological invariant reduces by one and similarly for each energy level crossing below $E = 0$ level the topological invariant increases by one. In this way, the topological invariant takes integer values and the system is said to belong to a $\mathbb{Z}$ topological class.
Similarly, we can define the topological invariant based on the parity of the system. This we do in the case of superconductors. We know that superconductors have cooper pairs as charge carriers. And if we bring a superconductor in proximity to another system, say a 2DEG, or a topological

insulator, it introduces cooper pairs into the system so that the number of electrons changes but that doesn't change the parity of the system. Each cooper pair is formed of two electrons, so it can only add an even number of electrons which doesn't change the parity. Now, if the band closes, that changes the parity. So, odd or even parity acts as the topological invariant.
We characterised our quantum spin hall insulator in a previous section by topological invariants +1 and -1. 1 was for the case when there were an even number of forward or backward propagating modes and the system was unprotected due to time reversal symmetry. We called it to be trivial state of the system. The system was topological when there were an odd number of modes, and forward moving modes were protected from backscattering due to time reversal symmetry.

5.5.2 Symmetries of a system

We observe from the last example that symmetry can play an important role in defining the topology of a system. A certain symmetry may be preserved in one topological phase and it may not be preserved in the other. It is a general practice, when a certain symmetry preserves some property of the system and the symmetry is preserved as long as the system is in that particular topological phase, we call the system to be topological. For example, in the last example of the earlier section we said the system to be topological when there were an odd number of edge modes which were protected from backscattering due to time reversal symmetry. While when the system is in a trivial phase, no symmetry protects a certain property of the system and we call it to be in a trivial or topologically trivial phase.
A system may have several types of symmetries including translational, or rotational symmetries, but there are three types of symmetries which are most important to us in topology. We use only these types of symmetries to characterise the topological class of a system. For example, if a system satisfies two of these three symmetries the system belongs to one type of topological class while if there is a system which satisfies all the three symmetries, it belongs to another topological class.
These three symmetries are:
(1) Time reversal symmetry
(2) Particle hole symmetry
(3) Chiral Symmetry or sublattice symmetry.
We will discuss each of these symmetries one by one in the following:

5.5.2.1 Time reversal symmetry

We have already seen time reversal symmetry working in quantum spin hall insulator and a 3D topological insulator. Time reversal symmetry is a symmetry, as the name suggests, which dictates that the system stays symmetrical even after the time is reversed. As a physical example of time reversal symmetry we can consider a spin half electron. On reversing the time, a positive spin half particle becomes a negative spin half particle. Another example is that of a magnetic field. We can understand it as follows. Suppose an electron is revolving around a positive charge in a circle. It generates a magnetic field along the axis of the circle, whose direction is given by right hand thumb rule. Now, we reverse the time. The effect is the electron starts moving in the counterclockwise direction if it was moving clockwise earlier, which reverses the direction of magnetic field along the axis. This example shows that time reversal symmetry does not preserve time reversal symmetry.
Several times when we need to break time reversal symmetry we apply a magnetic field, as we had to do when we wanted to open a gap in the ungapped edge states of the quantum spin hall insulator. Then we were trying to obtain Majorana fermions by covering the edge of quantum spin hall insulator with superconductor, and we introduced a magnet inside the gap of Josephson junction in order to gap out the helical edge states which are protected by time reversal symmetry to uncouple the Majoranas produced at the ends of the superconductor.
We also applied a magnetic field to break the time reversal symmetry and open a gap at the dirac points when we tried to prepare a Chern insulator from graphene.
The operator corresponding to time reversal symmetry is an anti-unitary operator and it is represented by greek letter τ. Whenever, a hamiltonian obeys time reversal symmetry it satisfies, $\tau^{-1}H(k)\tau = H(-k)^*$. Since, τ is an anti-unitary operator it can be written as a product of a

unitary operator and a complex conjugation operator;

$$\tau = U\kappa$$

A time reversal operator which reverses the spin is of the form, $\tau = \iota\sigma_y\kappa$.
Time reversal operator comes in two varieties, one of them squares to 1 and the other to -1.
$\tau^2 = -1$ forms a more interesting case because it gives rise to another property called kramer's degeneracy. The property states, when a hamiltonian is time reversal symmetric and the time reversal symmetry operator squares to -1 each energy level is doubly degenerate. This gives rise to interesting properties. For example, as we have discussed earlier if a system has particle-hole symmetry the parity changes from odd to even or vice versa, each time there is a zero energy crossing, if there is time reversal symmetry also in the system each crossing is a double crossing and the parity of the system can not change. Hence, time reversal symmetry provides an extra protection to the topological state of the system.

5.5.2.2 Sublattice symmetry

We have come across this type of symmetry also in our previous discussion. We talked about sublattice symmetry in our discussion of graphene. Graphene lattice has this symmetry and it plays an important role in the protection of dirac points. While trying to obtain a Chern insulator using graphene we had to break this symmetry by applying an opposite mass term at each lattice site belonging to type A or B.
Sublattice symmetry is possessed by systems with a bipartite lattice. If we exchange all the lattice sites belonging to type A with the lattice sites belonging to type B, and the hamiltonian is symmetric under such a transformation, the system is said to possess sublattice symmetry. The operator corresponding to sublattice symmetry is a unitary operator. σ_z exchanges the two lattice sites in graphene and the hamiltonian satisfies,

$$\sigma_z H \sigma_z = -H$$

5.5.2.3 Particle hole symmetry

Now, we move on to the third type of symmetry called particle-hole symmetry. It is most prominent in superconductors and provides them some very important defining properties. It simply means if we replace all the electrons with holes and all the holes with the electrons the system remains symmetric. Holes are actually the empty quantum mechanical states which can be occupied by electrons so they act as vacant seats for the particles and are thought of as particles themselves with an opposite charge.
Holes occupy the region above zero energy. These are the antiparticles of the electrons which occupy the region below the the fermi surface at T=0. An electron and hole annihilate each other when they come very close.
Particle-hole symmetry operator is an anti-unitary operator. It acts on a hamiltonian H as follows:

$$PH(k)P^{-1} = -H(-k)$$

As an example, a particle hole symmetry unitary operator is,

$$P = \tau_x\kappa$$

For a hamiltonian which satisfies particle hole symmetry if there is a state at energy E given by eigenvector, $\Psi = \begin{pmatrix} u \\ v \end{pmatrix}$, there is another state at -E with eigenvector $\Psi' = \begin{pmatrix} v^* \\ u^* \end{pmatrix}$

$$P\Psi = \Psi^{'}.$$

Due to this property, superconductor forms an important ingredient for the realisation of Majorana fermions because it generates particles corresponding to the equal superposition of negative and

positive energy states in the topological phase which are the zero energy Majorana modes. These modes can be spatially separated by various means which we will discuss later. Once these modes are spatially separated they cannot be perturbed from zero energy because both of them have to be perturbed simultaneously, otherwise particle hole symmetry will be violated. Again, due to this symmetry, these zero energy modes always come in pairs.

We are now a couple of steps away from starting our Majorana story. We will discuss now Bogoliubov degennes hamiltonian for superconductors and then about pfaffian.

5.5.3 Bogoliubov de gennes hamiltonian

We know that charge carriers inside a superconductor are a pair of electrons with opposite spins called cooper pairs. We can write down the hamiltonian for such a system in second quantized notation as follows. We can write down the term corresponding to kinetic energy of the individual electrons as a hopping operator in the tight binding form. The next term corresponds to the pairing between electrons in a cooper pair with pairing coefficient Δ. The hamiltonian can be written as follows without including the spin.

$$H = \sum_{nm} H_{nm} c_n^\dagger c_m + \frac{1}{2}(\Delta_{nm} c_n^\dagger c_m^\dagger + \Delta_{nm}^* c_m c_n) \tag{5.2}$$

The term $c_m^\dagger c_n$ corresponding to pairing between electrons at site n and m is not hermitian so its hermitian conjugate needs to be added and the whole needs to be divided by $1/2$ to make the hamiltonian hermitian.
Because of the terms like $c_m^\dagger c_n^\dagger$ and $c_m c_n$ the total number of electrons is not constant inside the superconductor. It shows electrons can always be added or removed in pairs. It, however, shows that parity of a superconductor always remains same. That means, if there are even number of electrons they remain even, if there are odd number of electrons they remain odd.
The hamiltonian just written has some important properties:
Usually, there is nearest neighbour hopping, therefore,

$$H_{nm} = \begin{cases} -t & , |n-m| = 1 \\ 0 & , |n-m| \neq 1 \end{cases} \tag{5.3}$$

Similarly, there are conditions for superconducting pairing term Δ_{nm}. There are two options for pairing to happen. Electrons on adjacent sites can pair up or pairing can happen between electrons on the same site. Superconductors for which pairing happens between the electrons on the adjacent sites are called p-wave superconductors. This is so because if we take fourier transform of a p-wave superconductor and write the hamiltonian in momentum basis the pairing term is k dependent.

If the pairing happens on the same site, the superconductor is called s-wave. On taking a Fourier transform pairing term comes out to be independent of momentum. We can write Δ_{nm} for a p-wave superconductor as follows,

$$\Delta_{nm} = \begin{cases} \Delta_0 & |n-m| = 1 \\ 0 & |n-m| \neq 1 \end{cases} \tag{5.4}$$

c and $c^\dagger$ are the usual fermionic operators so they satisfy anti-commutation relations,

$$c_n^\dagger c_m + c_m c_n^\dagger = \delta_{mn}$$

also,

$$c_n c_m + c_m c_n = 0$$

The hamiltonian we wrote is not a BdG hamiltonian but we can derive H_{BdG} out of it. We prepare a column vector C which consists of all the creation and annihilation operators combined together. It is written as,

$$C = \begin{pmatrix} c_1 \\ c_2 \\ \vdots \\ c_n \\ c_1^\dagger \\ c_2^\dagger \\ \vdots \\ c_n^\dagger \end{pmatrix}$$

The first n-components are annihilation operators and the next n-components are creation operators. It is possible now to write hamiltonian H in the following form,

$$H = \frac{1}{2} C^\dagger H_{BdG} C$$

Here,

$$H_{BdG} = \begin{pmatrix} H & \Delta \\ -\Delta^* & -H^* \end{pmatrix} \tag{5.5}$$

We discussed in the previous section that a superconductor has particle hole symmetry. We can understand now how it is so. The vector C consists of first n-components as annihilation operators. These operators can also be thought as creation operators for holes. The next n-components are creation operators for electrons. Hence, there is an extra degree of freedom in the system. We can replace all the creation operators with annihilation operators in the hamiltonian and that doesn't change the system at all.

5.5.4 Pfaffian

We have seen that the number of particles isn't constant in a superconductor, but the parity stays constant. Parity of the superconductor changes when there is a band gap crossing from even to odd or vice versa. So noting the fermion parity helps us in keeping a track of the topological phase transition of the superconductor. To use fermion parity as a topological invariant we need to find a method which gives us any of the two numbers corresponding to each parity. Method we use for this purpose is the calculation of pfaffian, which can be obtained using the BdG hamiltonian.
We first to need to perform a unitary transformation of the hamiltonian to convert it into an anti-symmetric matrix, $U = \begin{pmatrix} 1 & -\iota \\ 1 & \iota \end{pmatrix}$.

$$H_{BdG} = \frac{1}{2} \begin{pmatrix} 1 & 1 \\ \iota & -\iota \end{pmatrix} H_{BdG} \begin{pmatrix} 1 & -\iota \\ 1 & \iota \end{pmatrix}$$

Antisymmetric matrices have a property that their eigenvalues come in pairs, that is, if one eigenvalue is E the other one is -E. Hence, if we take the determinant of an anti-symmetric matrix which is the product of all the eigenvalues it takes the following form:

$$det(\tilde{H}_{BdG}) = E_1(-E_1)E_2(-E_2)\dots E_n(-E_n)$$

$$= \pm E_1^2 E_2^2 \dots E_n^2$$

We can define the pfaffian as,

$$pf = sign[(\iota det(\sqrt{H_{BdG}}))]$$

As we can see, pfaffian takes either +1 or -1 value.
But how does the value of pfaffiann change? $\sqrt{det(\tilde{H}_{BdG})}$ can be written as,

$$\sqrt{det(\tilde{H}_{BdG})} = \pm \prod_n \iota E_n \tag{5.6}$$

Each time an energy level crosses $E = 0$ E_n changes the sign. This is how pfaffian acts as a topological invariant and changes only when there is a topological phase transition.

When Majorana fermions were predicted by Ettore Majorana they came out as a natural consequence from Dirac's equation of spin half particles. At that time they were predicted as a model for chargless neutrons. After years of time they were predicted to be occuring in the condensed matter systems under special circumstances. What we have in condensed matter systems is electrons and holes, both having either positive or negative energy, while Majorana fermions are the particles with zero energy. It is possible to superimpose the positive and negative energy states corresponding to electrons and holes and obtain the zero energy states. We show now how Majorana fermions can be obtained at the ends of a chain of fermions. And later we show how the situation can be modelled using a kitaev chain model by tuning the parameters and how the zero energy modes thus obtained are protected by the topology of the system.

5.6 Majorana modes at the ends of a fermionic chain

We work in the second quantisation formalism, in which creation and annihilation operators for the fermionic modes are given by c and $c^\dagger$. The vacuum state which is devoid of any fermions is given by $|0\rangle$, and the first excited state is given by $|1\rangle$. The following relationships exist between the states and the operators:

$$c|0\rangle = 0, c^\dagger|0\rangle = |1\rangle$$

$$c|1\rangle = 0$$

The creation and annihilation operators satisfy the following relations:

$$c|0\rangle = 0$$
$$c^\dagger|1\rangle = 0$$

The second one are due to pauli's exclusion principle.
Now, operators c and $c^\dagger$ can be written as a superposition of another pair of operators as folows:

$$c^\dagger = 1/2(\gamma_1 + \iota\gamma_2)$$
$$c = (1/2)(\gamma_1 - \iota\gamma_2)$$

It turns out that on rearranging, γ_1 and γ_2 satisfy the following properties:
$\gamma_1 = \gamma_1^\dagger$, $\gamma_2 = \gamma_2^\dagger$

These properties clearly imply that γ_1 and γ_2 are zero energy modes which are a superposition of positive and negative energy modes.

Making use of the commutation properties of the fermionic operators we can show that Majorana fermionic operators show the following properties:

$$\gamma_1\gamma_2 + \gamma_2\gamma_1 = 0, \gamma_1^2 = 1, \gamma_2^2 = 1$$

Imagine a vacuum state $|0\rangle$, which is devoid of any fermions. Now, we add a single fermionic mode to this state using $c^\dagger$. The state becomes $|1\rangle$. The system is raised by an energy ϵ. Hence, the corresponding hamiltonian is given by, $H = \epsilon c^\dagger c$. Using the relations between fermionic and Majorana operators the same operator can be written as, $H = (1/2)\epsilon(1 - \iota\gamma_1\gamma_2)$.
Now, we come to our initial question, is it possible to isoltate individual majorana modes? Fermions are indivisible particles, so it seems far fetched to isolate individual majorana fermions.

Imagine a chain of sites and put one fermion at each lattice site. Each fermion can be seen as to be composed of a pair majoranas, as in the figure. The corresponding hamiltonian looks like,

$$H = (\iota/2)\mu \sum_{n=1}^{N} \gamma_{2n-1}\gamma_{2n}$$

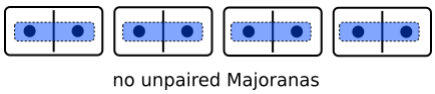

Now we perform the pairing between majoranas on the adjacent lattice sites. The hopping parameter is -t, the corresponding hamiltonian is given as,

$$H = \iota t \sum_{n=1}^{N-1} \gamma_{2n}\gamma_{2n+1}$$

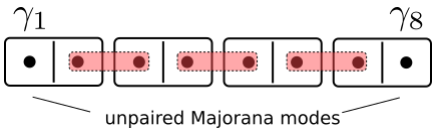

This setting leaves the first and last sites unpaired and they do not enter into the hamiltonian making them zero energy. All the states that are present in the bulk of the system have energy t.

5.7 Majorana modes in a kitaev chain

If we write γ_1 and γ_2 above in terms of c and $c^\dagger$, substituting $\gamma_{2n-1} = (c_n^\dagger + c_n)/2$ and $\gamma_{2n} = -\iota(c_n^\dagger - c_n)/2$ we obtain a hamiltonian which can be written by tuning the parameters of another hamiltonian,

$$H = -\mu \sum_n c_n^\dagger c_n - t \sum_n (c_{n+1}^\dagger c_n + h.c) + \Delta \sum_n (c_n c_{n+1} + h.c)$$

Here, μ = onsite energy, t = hopping parameter, Δ = Superconducting pairing.
If we now set $\mu = 0$ and, $\Delta = t$, we get a hamiltonian which has zero energy states at the edges. It may seem that the zero energy modes appear only for highly tuned parameters and zero modes will disppear as soon as we deviate from the $\mu = 0$. We make energy vs μ plot for the above hamiltonian starting from $\mu = 0$ and try to see how long the zero modes persist.

The following parameters have been used in all the plottings : t=1, $\Delta = 1$, L=25.

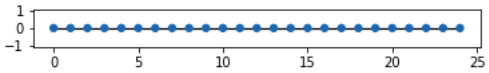

Figure 5.7: 1D kitaev chain lattice

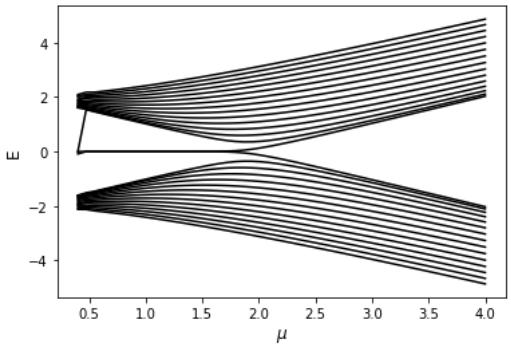

Figure 5.8: Energy vs μ plot for the above kitaev chain. Zero modes persist as long as $\mu < t$ after which the bulk gap collapses and the zero edge modes disappear. Parameters:t=1, $\Delta = 1$, L=25

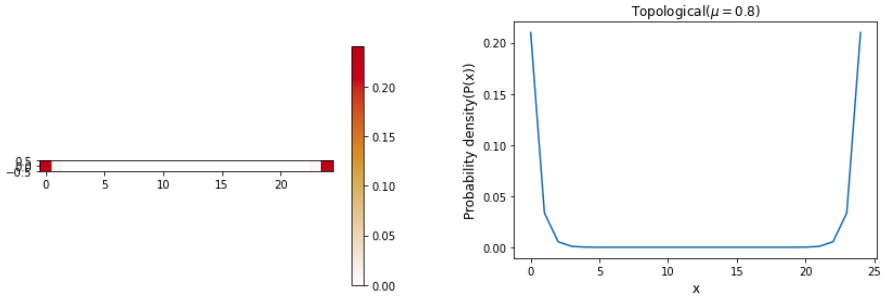

(a) Topological(Majoranas at the ends(μ = 0.8))

(b)

Figure 5.9: Zero modes are situated at the ends of the kitaev chain as seen in the diagram on the left. Probability of finding zero energy modes at the edges is plotted on the right at $\mu = 0$. We can see the zero energy wavefunctions are highly localised at the edges.

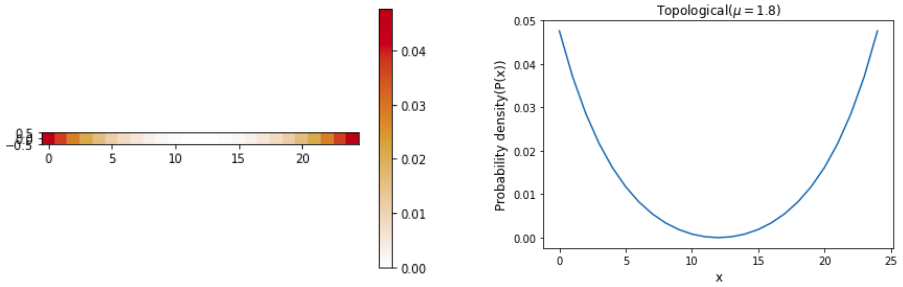

(a) Topological(Majoranas at the ends(μ=1.0))

(b)

Figure 5.10:

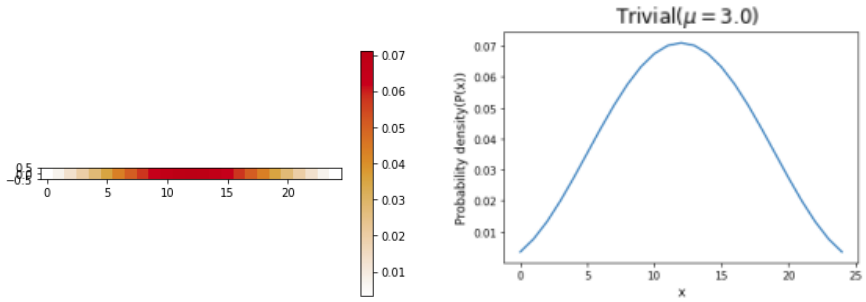

(a) Trivial(No Majoranas at the ends($\mu = 3$)) (b)

Figure 5.11: Density of zero modes has been plotted for a kitaev chain on left and right in different forms, for different values of μ. As μ becomes greater than 2t the zero modes no longer remain at the edges and the system goes into the trivial state. Parameters: t=1, $\Delta = 1$, L=25.

We make a few observations here from the above figure. The zero energy modes do not disappear until $\mu = 2t$, after that the zero modes split equally on both sides of the x-axis. When zero energy modes split it is also the point when the bulk gap closes. For small μ values the wavefunction corresponding to the zero energy modes is localised at the edges while on increasing μ the zero modes become less localised.
The reason why the zero modes stay protected even for larger μ values is due to the topology of the system. The zero energy modes localised at the edges have no states available in the middle due to the bulk gap. As we increase μ the bulk gap starts reducing and the zero modes localised at the edges start coupling to each other. When the bulk gap closes completely the zero energy modes are completely delocalised. The coupling between the unpaired Majorana modes at the edges is now allowed, which causes the deviation in their energy from zero.

5.8 Majorana modes at the domain wall

Kitaev chain hamiltonian after fourier transformation can be written into the momentum space:

$$H(k) = (-2t \cos k - \mu)\tau_z + 2\Delta \sin k \tau_y$$

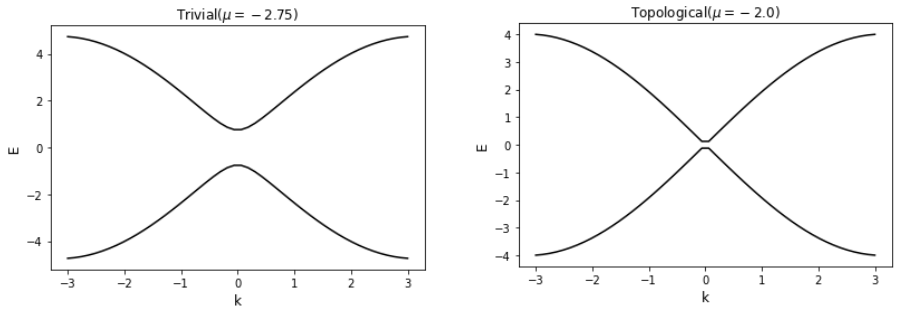

(a) (b)

Figure 5.12: Bandstructure for the above written hamiltonian in the trivial and topological state.

On expanding this hamiltonian close to $k = 0$ we get the following:

$$H(k) = m\tau_z + 2\Delta k \tau_y$$

where $m = -\mu - 2t$. This is Dirac hamiltonian. m here is the mass parameter whose value at any point in the spectrum is equal to the band gap at that point.

Writing down this hamiltonian in the real spaces:

$$H = -v\tau_y \iota \partial_x + m(x)\tau_z$$

Now, we take the mass m(x) in such a way that it changes sign from negative to positive as x crosses zero and m(x) is $-\infty$ at the negative end and $+\infty$ at the positive end. We say that zero modes are obtained at the domain wall at $x = 0$. To find the eigenfunction corresponding to the zero energy we set, $H\psi(x) = 0$.

$$-v\tau_y \iota \partial_x \psi(x) + m(x)\tau_z \psi(x) = 0$$

Multiplying with $\iota\tau_y$ on both sides of the equation, and then using, $\iota\tau_z\tau_y = \tau_x$, we get

$$\partial_x \psi(x) = (1/v)m(x)\tau_x \psi(x)$$

$$\psi(x) = exp(\tau_x \int_0^x \frac{m(x')}{v} dx')\psi(0)$$

τ_x has eigenvalues ± 1 and corresponding eigenvectors equal to $(1, \pm 1)^T$. We write the same solution as,

$$\psi(x) = exp(\pm \int_0^x \frac{m(x')}{v} dx') \begin{pmatrix} 1 \\ -1 \end{pmatrix}$$

Because m(x) changes sign from -ve to +ve on crossing $x = 0$ $\psi(x)$ is normalizable on either of the sides, without which the wavefunction integration would be infinite and no solution would exist.

5.9 Majorana modes in a periodic kitaev chain

Take the chain of the fermions as taken in the previous case and express each fermion as a pair of Majorana modes. Now, we perform the pairing of the Majorana modes on the adjacent sites such that two Majorana fermions on each end of the chain come out unpaired. Now, we perform the pairing of the two unpaired majoranas with hopping parameter equal to $t(1 - 2\lambda)$. λ belongs to the range $[0, 1]$. So that, when $\lambda = 1/2$ the hopping parameter t is zero and we have an open chain with the unpaired ends, otherwise hopping parameter varies from t to -t. When hopping parameter is t the chain is anti-periodic and when it is -t the chain is periodic.

We look at the band structures for the different values of μ. The following parameters have been used: t=1, $\Delta = 1$, L=25.

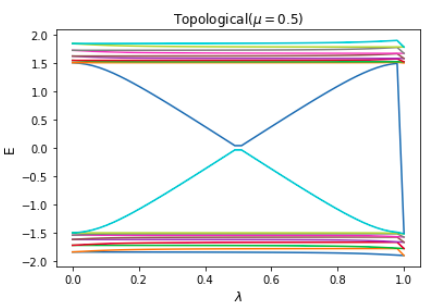

(a) $\mu < 2t$ in this case. Zero energy crossing is present at $\lambda = 1/2$

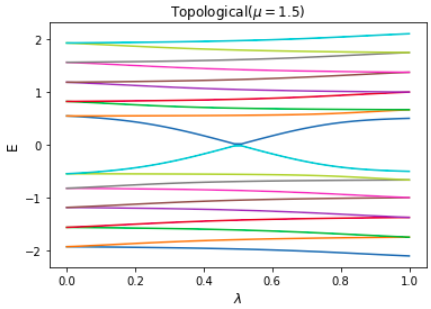

(b) $\mu < 2t$ in this case. Zero energy crossing present at $\lambda = 1/2$

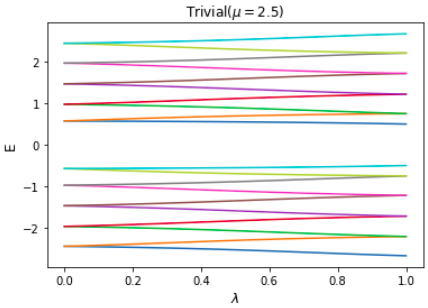

(c) $\mu > 2t$ in this case. We can see that no zero energy crossing is present.

Figure 5.13: Energy vs λ plot where λ value going from 0 to 1 changes the system from periodic to anti-periodic with the pairing between the ends being cut off completely at $\lambda = 1/2$

5.10 Theory for the experimental realisation of Majorana fermions

There are a few components which are essential in an experimental system to realise Majorana fermions. These are superconductor, semiconductor and magnetic field. Topological superconductor is the most important part and we already know that a superconducting wire contains unpaired Majorana modes at the ends. Semiconductor is used because it is easier to manipulate experimentally and we have been using semiconductors for decades, so we are quite familiar with its properties and how to manipulate it to be useful in experiments. An earlier proposal [40] suggested topological insulator to be used to obtain Majorana fermions. Later, it was proposed[41] to use semiconductor instead of a topological insulator. For the magnetic field part we can apply an external magnetic field or fix a magnet with the semiconductor-superconductor heterostructure. Fixing the magnet doesn't allow us to manipulate the magnetic field so it was suggested[42] to use a semiconductor with Dresselhaus coupling to which an in-plane magnetic field can be applied to create a band gap. We will discuss in this section a step by step procedure by which we can arrive at the final hamiltonian which can be realised in the experiments and produce Majorana zero modes.

We start with Kitaev model. It is notable that kitaev model is also the model for a p-wave superconductor. Let us see how we can modify this hamiltonian to be realisable in lab.

$$H_{kitaev} = (-2tcosk - \mu)\tau_z + 2\Delta\tau_y sink$$

Semiconductor has a very low chemical potential so we can expand $\cos k$ and $\sin k$ terms upto the first order. We have seen in the previous section that the edge states appear or say the system is topological when $-2t < \mu < 2t$. We can make the following change in μ, $\mu \to \mu - 2t$ so that when $\mu < 0$ we are in topological phase. We can write the same hamiltonian in the modified form as,

$$H = (\frac{k^2}{2m} - \mu)\tau_z + 2\Delta\tau_y k$$

Plotting the bandstructure for the above hamiltonian for both in trivial regime i.e. when $\mu > 0$ and topological regime that is when $\mu < 0$ gives the following result as shown in the figure.

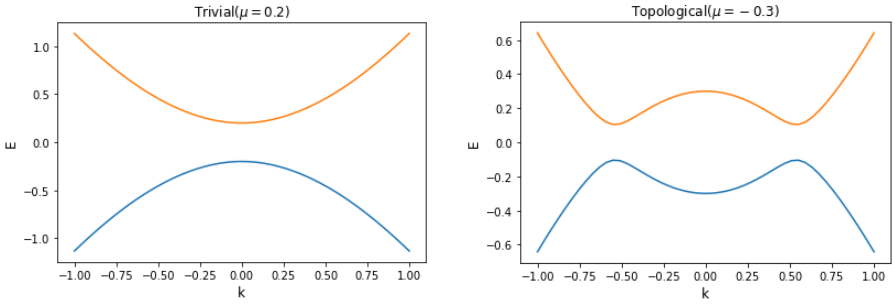

(a) (b)

Figure 5.14: Band structure for the above hamiltonian in trivial and topological case. After the transformation of μ we obtain topological modes for $\mu < 0$ and trivial modes for $\mu > 0$.

So far we have been dealing with a hypothetical system of electrons which doesn't have spins. There exists no such system in nature so we will have to give our hamiltonian an extra degree of freedom which accounts for the spin. But, it creates a problem, because adding the spin creates a degeneracy in the system. This implies, now instead of having a single Majorana at the edge we will have two Majoranas. And, as we have already seen two Majoranas is nothing but a single fermion. So instead of having an isolated Majorana fermion we would have an electron fine tuned to zero energy at the edge.
To tackle this problem we will have to make such an arrangement that out of two spin species only one of them is in topological state and the other is in trivial state. For this purpose, we can apply an external magnetic field. Magnetic field has such an effect that it makes the chemical potential for one species greater than zero and for the other species less than zero, so that one is in the trivial regime while the other in the topological regime.

$$H = (\frac{k^2}{2m} - \mu - B\sigma_z)\tau_z + 2\Delta\tau_y k \tag{5.7}$$

We can prepare the bandstructure for the above hamiltonian using kwant and visualize the effect of increasing the magnetic field applied to the system.

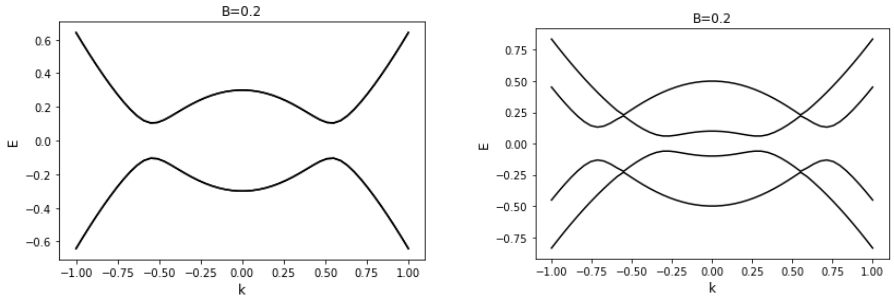

(a)

(b)

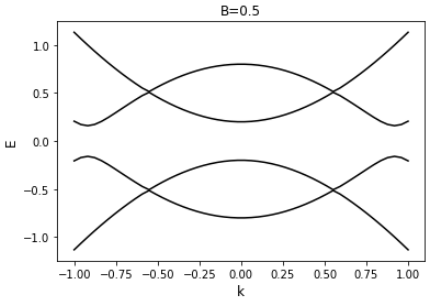

(c)

Figure 5.15: Bandstructure plotted at different magnetic fields for the above hamiltonian. There is spin degeneracy in the system and the magnetic field causes one spin species to be in the trivial state and the other in the topological state, so that there are single Majorana modes present at the edges.

Our analysis so far has been limited to a special class of superconductors called p-wave. Such superconductors are difficult to find in nature which makes our analysis non-practicable. There is another class of superconductors called s-wave and most of the popular superconductors are of this type. We can modify our hamiltonian to work with an s-wave pairing. S-wave pairing is different than p-wave paring in that there is no momentum dependence in the pairing. When the pairing between the electrons is on the adjacent site after we take the Fourier transform and write the hamiltonian in momentum basis there appears a momentum dependence in the pairing term, which forms a p-wave superconductor. However, in s-wave pairing the coupling happens for electrons on the same site, the hamiltonian written for which after Fourier transform does not have k dependence in the pairing term.
Writing the hamiltonian for the modified system looks like,

$$H = (\frac{k^2}{2m} - \mu)\tau_z + B\sigma_z + \Delta\tau_x \tag{5.8}$$

We can diagonalize the above hamiltonian and to do that we rewrite it in the following form,

$$H = (\frac{k^2}{2m}\sigma_0)\tau_z + (B\sigma_z)\tau_0 + (\Delta\sigma_0)\tau_x$$

If there is a hamiltonian of the following form,

$$H = A\tau_0 + B\tau_x + C\tau_y + D\tau_z$$

Its spectrum can be written as,

$$E = A \pm \sqrt{B^2 + C^2 + D^2}$$

This implies, the energy levels for our experimental system can be given by,

$$E = B \pm \sqrt{\mu^2 + \Delta^2} \tag{5.9}$$

Topological phase transition happens after there is band gap closing and the system enters into the topological phase.
So we put $E = 0$ to see at what value of B does the band gap close,

$$B = \sqrt{\mu^2 + \Delta^2}$$

We know that for $B = 0$ the system lies in the trivial regime. As we discussed earlier, this is because there is spin degeneracy which gives two Majoranas instead of one at the edge.
As we increase B spin degenracy breaks and band crossing happens when $B = \sqrt{\mu^2 + \Delta^2}$. So the condition for the system to be in the topological regime is,

$$B > \sqrt{\mu^2 + \Delta^2} \tag{5.10}$$

We can again try to plot the spectrum using kwant and it looks as in the figure.

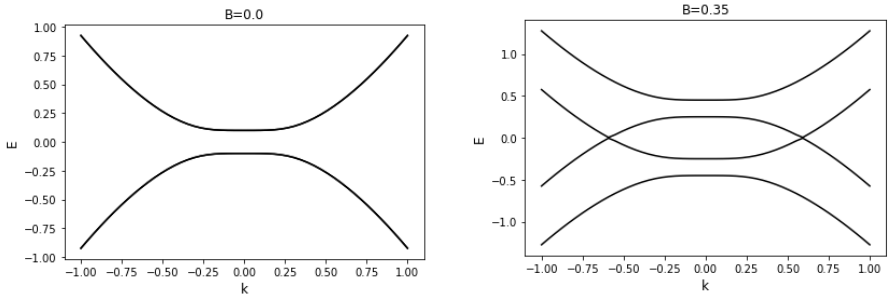

(a) (b)

Figure 5.16: Bandstructure plotted for hamiltonian(5.8) at different values of B. At B=0 there is spin degeneracy in the system. At non-zero B the spin degeneracy breaks and there is only one spin species which enters the topological regime while the other one remains in the trivial regime. Parameter values:$\Delta = 0.1$,$\mu = 0.0$

We see that that bulk is not gapped and we still don't obtain the Majorana edge modes. It happened because the way we have defined our system implies that Majoranas must have a spin. But Majoaranas can't have a spin because if they have a spin this would imply spin degeneracy which would again prevent us from having isolated Majorana modes.
We can add an additional term, $\alpha\sigma_y k$ called Rashba spin-orbit coupling term to come out of this problem.
So the final hamiltonian is written as,

$$H = (\frac{k^2}{2m} + \alpha\sigma_y k - \mu)\tau_z + B\sigma_z + \Delta\tau_x \tag{5.11}$$

Adding the new term allows us to open a gap in the bulk and obtain zero energy modes at the edges. It should be noted that spin orbit coupling is non-zero only for finite k values. Which implies it doesn't open a gap at $k = 0$.

Let's look at the energy spectrum of the final hamiltonian, obtained using kwant.

This is the energy spectrum obtained for different values.

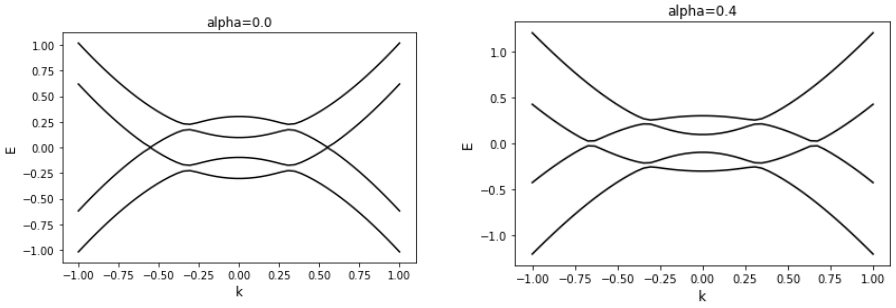

(a) (b)

Figure 5.17: Bandstructure is plotted for the above hamiltonian with spin orbit coupling included to prevent spin degenerate Majorana modes to enter the system which prevents us from having isolated Majorana modes at the edges. On the left $\alpha = 0$ and no bulk gap is opened while on the right $\alpha = 0.4$ and a bulk gap is opened. Paramters:$\Delta = 0.025$,$\mu = -0.1$,B=0.2

Hence, we can see the bulk gap does open up for the non zero values of α.

Finally, we look at how the band gap behaves for different values of α as we change the magnetic field.

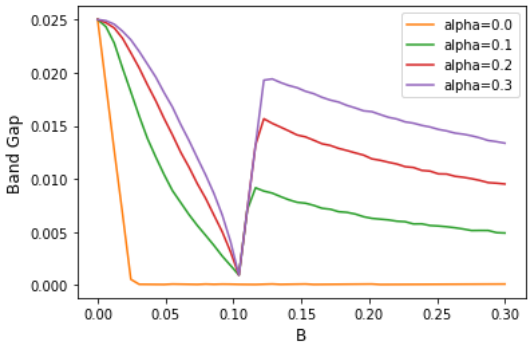

Figure 5.18: Band gap plotted with respect to magnetic field for different values of α. Bulk gap closes and drops to zero as the system enters into the topological regime then rises again.Parameters:$\Delta = 0.025$, $\mu = -0.1$

Band gap closes at a certain value of B and then it reopens. It increases on further increasing the magnetic field.
We also observe the larger the spin orbit coupling α faster the drop in the band gap.

5.11 Conduction with Majorana modes

In this section, we will discuss a method which can be used for the detection of the Majorana modes at the ends of a superconductor. This method was suggested in a paper by Jay D Sau[43] using the Josephson effect. It is the Zero Bias peak(ZBCP) that we will talk about which has been the main hunting target of experimentalists in the field of Majorana fermions 2010 onwards. In 2012, Mourik et al's group was successful in obtaining a Zero Bias Peak[44] but it received a heavy criticism and only recently the group has announced that the conclusions of the 2012 experiment were incorrect and the paper would be retracted from Nature. Since 2010, there have been several claims about obtaining a Zero Bias peak but there are theoretical papers also which indicate that no Zero Bias Peak(ZBP) has ever been observed which is due to Majorana[45], and not due to an

impurity or disorder.
To understand how a Zero Bias Peak appears due to Majorana we will first have to understand about Andreev Reflection.
When a normal metal and a superconducting wire are connected together and a bias is applied at the ends such that the applied bias eV is smaller than the superconducting energy gap Δ then the conduction happens in a special way.
When a single electron arrives at the normal metal- superconductor junction it can either get reflected or transmitted. For the transmission it should have some states available at energy eV, but due to superconducting gap there are no states available from $-\Delta$ to $+\Delta$.
So, instead of one, two electrons are transmitted through the superconductor as a cooper pair, and a hole is reflected. When an incoming electron is reflected back as an electron, it is called normal reflection, while, if an incoming electron is reflected as a hole it is called Andreev reflection.

The probability of normal reflection is given as $|r_{ee}|$ and that of Andreev refflection as $|r_{eh}|$. Conductance due to Andreev reflection has the following form:

$$G = 2G_0|e_{eh}| \tag{5.12}$$

where, $G_0 = \frac{e^2}{h}$. The factor of 2 comes because the conductance happens due to a pair of electrons.
Now conductance has a property, if the bias applied is such that it is of the level of an energy level inside the system the conductance is maximum.
Now, we can prepare a normal metal, superconductor junction. If superconductor is in the topological regime there should be Majorana modes present at zero energy at the edge of the superconductor, which is also the normal metal superconductor junction. Now we prepare a plot of conduction vs voltage bias. If Majorana modes are present at the edge we should observe a resonance at the zero bias.

At the resonance, $|r_{eh}| = 1$, so $G = G_0 = 2e^2/h$. We can prepare the plot using kwant package.

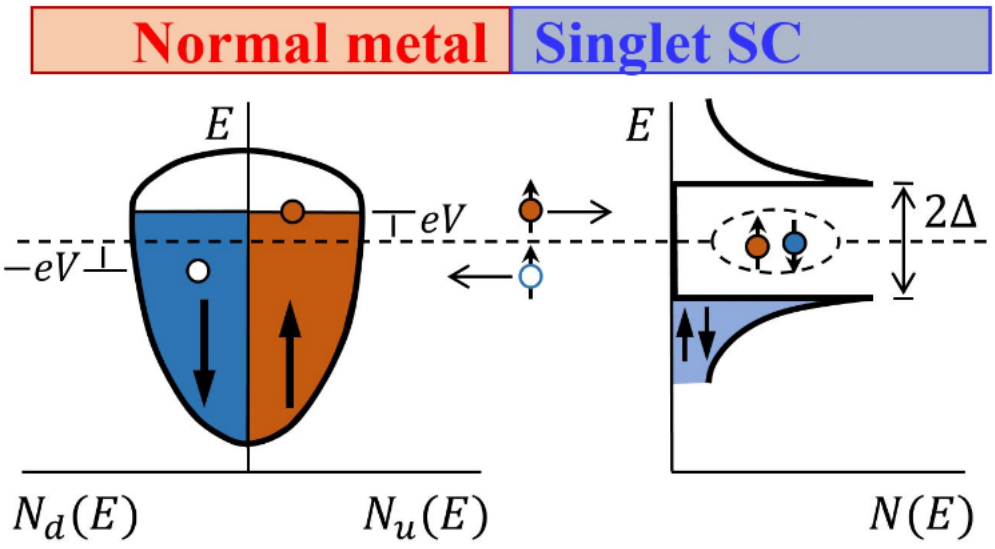

Figure 5.19: source(46): A depiction of Andreev reflection happening at the junction of a normal metal and superconductor.

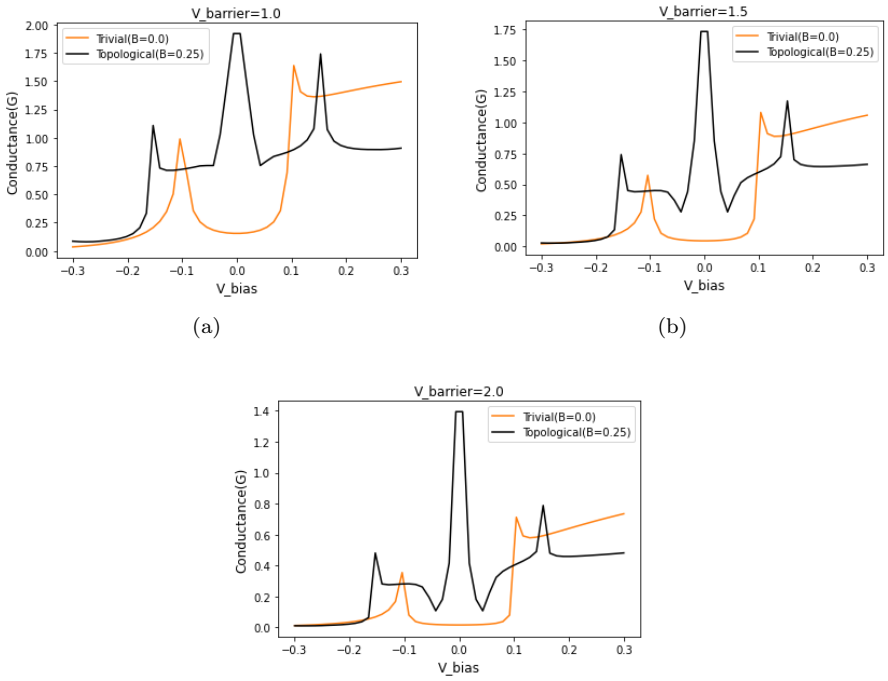

Figure 5.20: Black curve represents Andreev reflection in the topological case while orange curve represents Andreev reflection in the trivial case . Plots are prepared for different potential barriers between normal metal and superconductor. Majorana modes remain persistent even at higher barrier heights which shows their robustness.

When we are in the topological regime, edge modes are protected due to gap in the bulk and the conductance peak is robust. We can see that zero bias peak is not suppressed even for higher barrier strengths.

We can perform another test to know if the system is in trivial regime or topological regime by preparing a Josephson junction and measuring the progression of the Josephson current as we change the flux through the centre.
We first look at how the how the energy levels change as we turn the magnetic flux through the centre of a superconducting ring with a Josephson junction. This type of setup is called squid(Superconducting Quantum Interference Device). It is as shown in the figure.

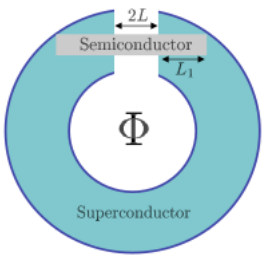

Figure 5.21: (source:(43)) Majorana fermions are produced at the ends of an incomplete superconducting ring

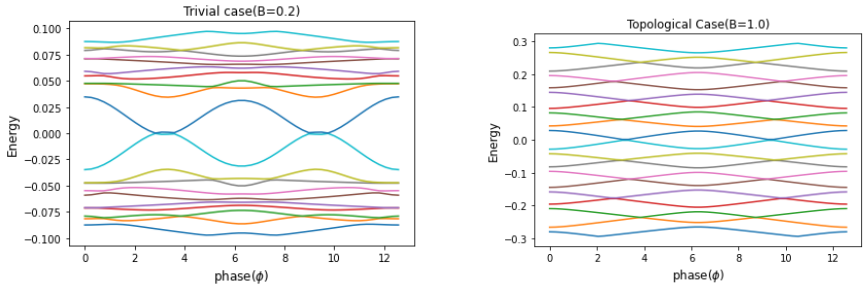

(a) (b)

Figure 5.22: We prepare a plot for the energy spectrum vs phase(Φ) for the setup in the above figure as the phase is turned from 0 to 4π. We can see in the trivial case there is a periodicity of 2π while in the topological case there is a periodicity of 4π.Parameter values:α=0.2,Δ=0.1,μ=0.4

We know that each time there is a band crossing at zero energy there is a change in the parity. We have two plots above, prepared using kwant package, for the energy levels of the superconductor as we vary the flux through the center. Flux enters the superconductor by changing the hopping term as $t \to te^{\iota\phi}$, where $\phi = \Phi/\Phi_0$.
We can see for the energy spectrum in the trivial regime there is no band gap crossing and there is a periodicity of Φ_0 in the spectrum. While in the topological regime there is a parity change at $\frac{\Phi_0}{2}$ and $\frac{3\Phi_0}{2}$. This implies at $\frac{\Phi_0}{2}$ superconductor reaches an excited state so that when we turn the flux by Φ_0 the system is not the same as it was at $\Phi = 0$. Now, if we further turn the flux there is again a band crossing at $\frac{3\Phi_0}{2}$and there is a parity change. The system returns to its original state as it was when there was no parity change so that when the flux reaches $2\Phi_0$ the system is in the same state as it was at $\Phi = 0$.

Consequence of the above discussion is that the total energy of the system and the Josephson junction calculated as a function of flux Φ shows a $2\Phi_0$ periodicity when the system is topological. While these quantities show a Φ_0 periodicity when the system is in trivial regime.
Changing the flux through the superconducting ring also changes the superconducting phase. So if a flux Φ_0 is turned through the center of the superconducting phase changes by 2π and if a flux $2\Phi_0$ is turned through the centerthe flux changes by 4π.
When the system is in topological regime there is a periodicity of $2\Phi_0$ in the Josephson current on changing the flux through the centre and this is called 4π Josephson effect. It can be used as an important measurement to test the presence of Majorana modes at the ends of a superconductor.

Total energy $E(\Phi)$ is calculated by summing over all the energy levels below $E = 0$. Josephson current $I(\Phi)$ is calculated by taking the first order derivative of $E(\Phi)$ as follows:

$$I(\Phi) = \frac{dE(\Phi)}{d\Phi}$$

The plots for $E(\Phi)$ and $I(\Phi)$ for both when the system is in trivial and topological regime are shown in the below figure.

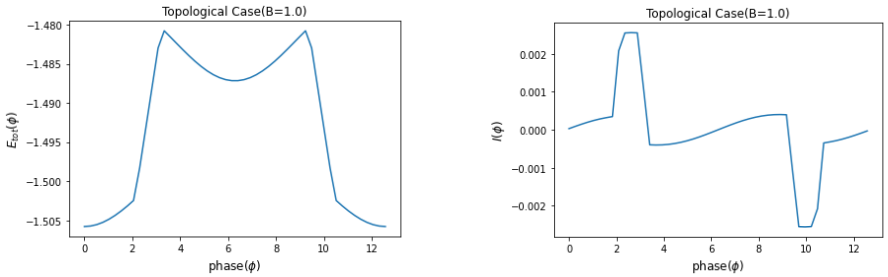

(a) (b)

Figure 5.23: E_{tot} vs Φ plot on the left and $I(\Phi)$ vs Φ plot on the right for the setup of type Fig(5.21). There is a periodicity of 2π in both energy and current in the trivial case. Parameter values:α=0.2,Δ=0.1,μ=0.4.

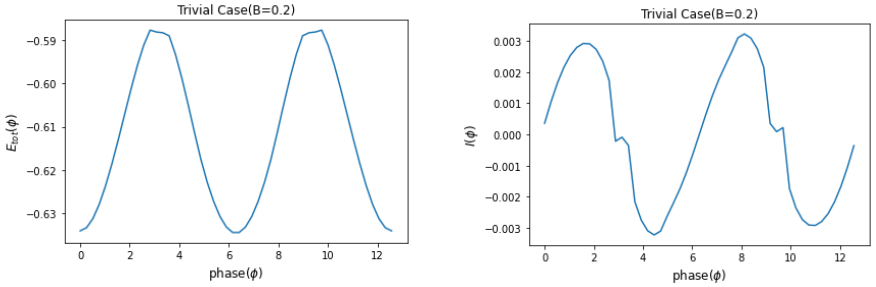

(a) (b)

Figure 5.24: E_{tot} vs Φ plot on the left and $I(\Phi)$ vs Φ plot on the right for the setup of type Fig(5.21). There is a periodicity of 4π in both energy and current in the topological case. Parameter values:α=0.2,Δ=0.1,μ=0.4

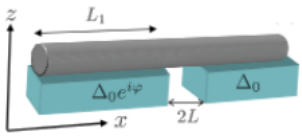

Figure 5.25: source:(43) An experimental setup proposed for the detection of Majorana fermions

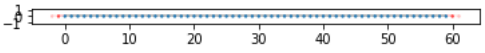

Figure 5.26: Lattice representation of the above model

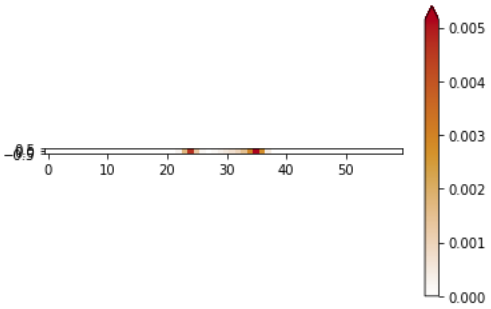

Figure 5.27: Majoranas appearing at the ends of the superconductors. Parameters:$\alpha = 0.1$,$\Delta = 0.5$

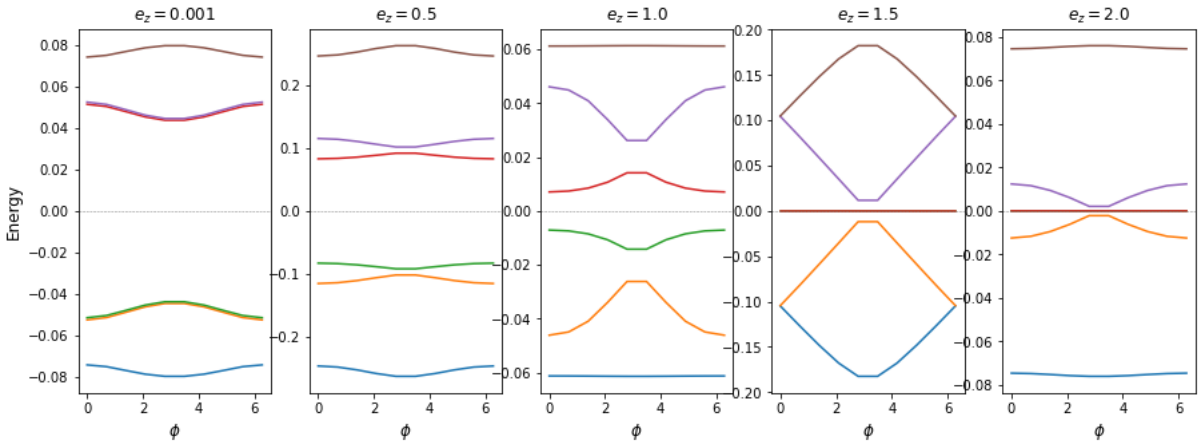

Figure 5.28: Energy vs phase diagram shows closing of the the bulk gap with increasing magnetic field for the above setup.

Chapter 6

Majorana Fermions in experiments

"I don't know for sure what was in their heads, but they skipped some data that contradicts directly what was in the paper. From the fuller data, there's no doubt that there's no Majorana."— Sergey Frolov on Kouwenhoven group's experimental discovery of Majorana

6.1 Majorana fermions in experiments

We have discussed the theoretical proposal which would lead to the realisation of Majorana fermions in semiconductor-superconductor heterostructures. Let us now look at the developments that have taken place in the field after the discovery of the theoretical model.
Mourik et al' group at Delft University was the first one to claim to have obtained the zero energy modes in semiconductor-superconductor heterostructures[44]. They prepared a setup as shown in the figure:

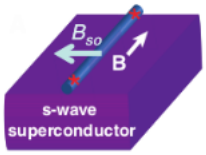

Figure 6.1: source:(44) The schematic for the realisation of Majorana modes.

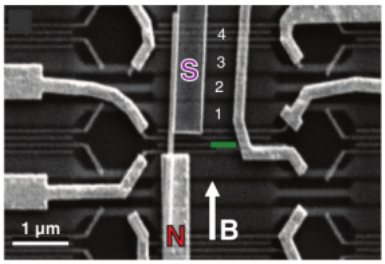

Figure 6.2: source:(44) The actual experimental setup for the realisation of Majorana modes.

They put an InSb nanowire on top of an s-wave superconductor, with the direction of spin orbit coupling perpendicular to that of the nanowire. An external field was applied along the nanowire which was perpendicular to spin orbit coupling. Real experimental setup is also shown in the figure. The system should enter the topological regime if, $V_z > \sqrt{\Delta_0^2 + \mu^2}$.
Hence, when $B = 0$ we expect no zero bias modes. We gradually increase the magnetic field, and as

it crosses the value set by $\sqrt{\Delta_0^2 + \mu^2}$ the system is in topological regime.
Shown in the figure(6.3) is the plot of differential conductance vs bias. We know that for a superconductor there are electronic states present above the energy $+\Delta$ and below the energy $-\Delta$. However, there are no states available inside the electronic gap 2Δ. So that when a bias is applied above and below 2Δ energy gap a peak is seen in the conductance while the conductance is minimal if the bias is applied in between the energy gap. However, this is not the case when there are states available at zero energy, which happens when the system is in the topological state that is when there are zero energy modes situated at the ends of the nanowire. If the magnetic field is small we should obtain the conductance plot similar to fig 6.3 and 6.4.

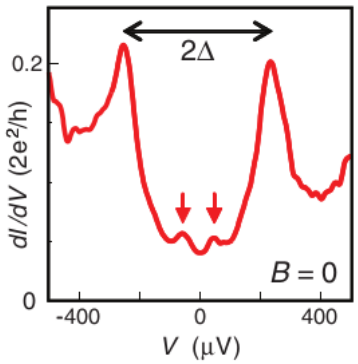

Figure 6.3: source:(44) Experimentally obtained conductance vs bias plot for a superconductor

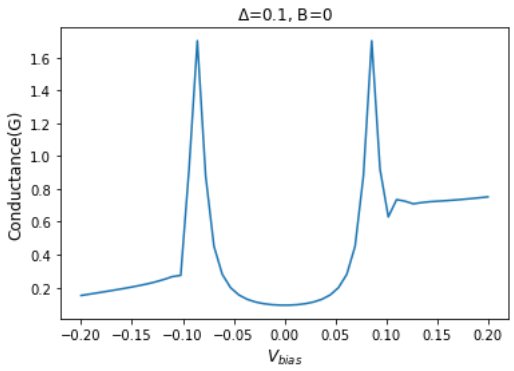

Figure 6.4: Theoretical conductance plot representing bulk gap in a superconductor

But, for large enough magnetic field there should be a peak situated at zero bias corresponding to Majorana bound states.

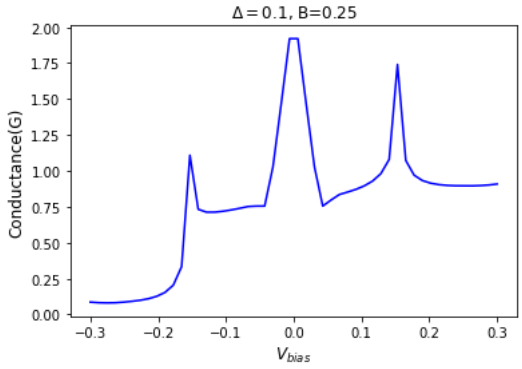

Figure 6.5: Zero modes produced at zero energy show a peak at zero bias in the conductance plot

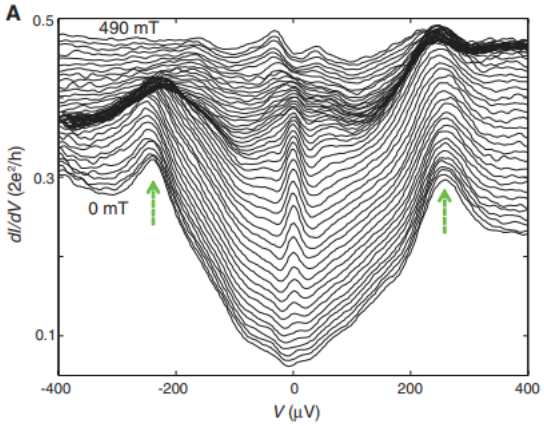

Figure 6.6: source:(44) The actual conductance vs bias plot obtained by Mourik et al for different magnetic fields which confirmed the presence of Majorana modes.

Figure 6.6 is the one which provided an evidence for Majorana modes. As we can see, the line near zero bias is almost flat for smaller magnetic fields. As we go higher in the plot, we see that for larger magnetic field there is a small peak at zero bias.
Now, to verify that these results are indeed due to Majorana the group tried to disturb the peak by adding external perturbations by changing gate voltages, and magnetic field. They found the zero bias peak to be robust under such perturbations. Other than that, they tried removing one of the prescribed components for obtaining the Majorana modes like magnetic field parallel to the spin orbit field, or superconductivity. The zero bias peak disappeared on removing any of these components. Such tests confirmed that the zero bias peak was robust and was indeed according to as prescribed by the theoretical proposal.
Zero bias plot at different temperatures was also obtained. It appeared, the peak was tallest and sharpest when the temperature was highest, while the peak diminished for larger temperatures(fig6.7).

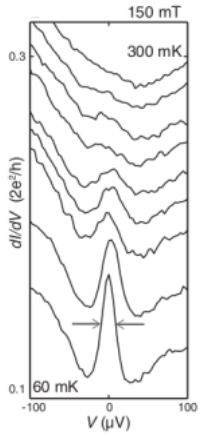

Figure 6.7: source:(44) Conducatance vs bias plot in the topological regime obtained at different temperatures.

The group concluded after these experiments that these zero bias modes were due to Majorana, but we will see, in the later experiments the peaks couldn't pass some of the very important tests and were accused of being there due to disorder in the nanowire or due to Andreev Bound States.

6.2 Theoretical corrections in the model

In the original proposal there are some of the factors which were not included but are present in the experiments which lead to the results varying from theoretical predictions. Experimental results of Mourik et al also suffered some miss-alignments with the theoretical predictions.
Theoretically, it was predicted that zero bias peak should have a height of $2e^2/h$. But, the experimentally obtained peak was much shorter. There was another observation, that ZBP splits at high magnetic field.
Such effects were explained in Lin et al's paper[47] in which they included some of the additional factors into the simulations to explain the experimental results.
There are some of the ways in which experimental systems are different:
1. Disorder: There may be disorder present in the nanowire which makes it difficult for the system to enter into the topological regime.
2. Temperature: As we already saw in the previous section, the peak grew weaker for larger temperatures. In the theory, it was assumed that the experiments are performed at $T = 0$.
3. Finite wire length: In the experimental system, the length of the wire is not more than a few nanometers. Hence, the Majorana modes produced at the ends are not infinitely away from each other.
All these effects above give rise to ZBPs which are suppressed and split at higher magnetic field.
The starting hamiltonian is written as,

$$H = (-\frac{\hbar}{2m}\partial_x^2 - \mu)\tau_z + V_x\sigma_x + V_y\sigma_y + \iota\alpha_R\partial_x\sigma_y\tau_z + \Delta\tau_x \tag{6.1}$$

The term $V_y\sigma_y$ has been included to allow us to apply magnetic field in a direction along the spin orbit coupling(B_{SO}). General expectation is, the magnetic field(B) applied along B_{SO} has no effect whatsover.
Writing the above hamiltonian in a discreatized form,

$$H = \sum_{i,j,\sigma} t_{ij} c^{\dagger}_{i\sigma} c_{j\sigma} - \sum_{i\sigma} \mu_i c^{\dagger}_{i\sigma} c_{i\sigma} + \sum_{i\sigma\sigma'} \frac{\alpha_i}{2} [c^{\dagger}_{i+1,\sigma} (\iota\sigma_y)_{\sigma\sigma'} c_{i\sigma'} + h.c.] +$$
$$\sum_{i\sigma} c^{\dagger}_{i\sigma} [V_x(i)\sigma_x + V_y(i)\sigma_y]_{\sigma\sigma'} c_{i\sigma'} +$$
$$\sum_{i} \Delta_i (c^{\dagger}_{i\uparrow} c^{\dagger}_{i\downarrow} + h.c.) \tau_x$$

After this step the hamiltonian can be easily implemented using kwant and all the relevant quantities can be obtained.
To include the effect of temperature following formalism was used. We use the fermi function[48],

$$G(V,T) = \int d\epsilon G_0(\epsilon) \frac{1}{4\pi \cosh^2[(V-\epsilon)/2T]} \tag{6.2}$$

Following are the temperature dependent results:

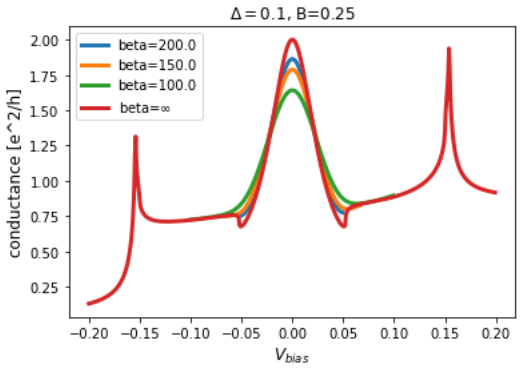

Figure 6.8: Theoretical plot for the temperature dependence. The peak height goes down with increasing temperature or decreasing β value.

As we can see the peak height drops rapidly with the increasing temperature.

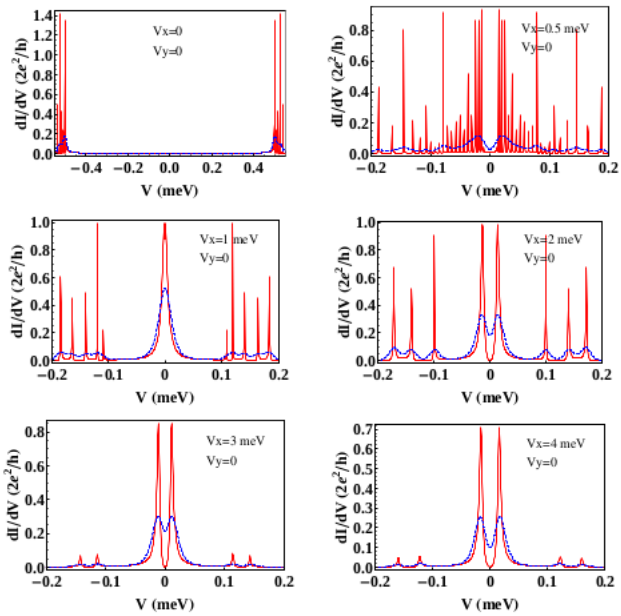

Figure 6.9: source:(47) Formation of zero bias peak as the magnetic field is increased and splitting of the Majorana peak on applying even higher magnetic fields.

Above figure(fig6.9) shows the effect of larger magnetic field. As we can see, at $B = 0$ the peaks are far apart. As the magnetic field is increased superconducting gap closes which happens at around $V_x = 1meV$ after which the system enters into the topological regime. On further increasing the magnetic field the central peak splits. The width of the split increases further with increasing magnetic field. The splitting happens due to finite size effect. In the original proposal the wire is of infinite size and the two Majorana modes never see each other. When the wire length is smaller, as in the experiments, the Majorana modes first separate to the two ends of the wire but on further increasing the magnetic field the two Majorana wavefunctions start overlapping with each other which gives rise to split ZBP.

6.3 Experimenting with dissipation less nanowire with ballistic transport

The main problem at this stage was that ZBP obtained in the experiments was suppressed. So, it was doubted if the Majorana is actually present there or not. Theorists gave dissipation in the nanowire as a possible reason due to which the peak was suppressed. Zhang et al[49] prepared an experiment in which the nanowires were practically dissipation less. The transport happened through them ballistically. They prepared high quality InSb-NbTiN interface to obtain their results. Surprisingly, it was observed the Majorana peak was still much suppressed. The group provided the formation of vortices as the reason which was suppressing the peak. Their main result is as shown in the figure.

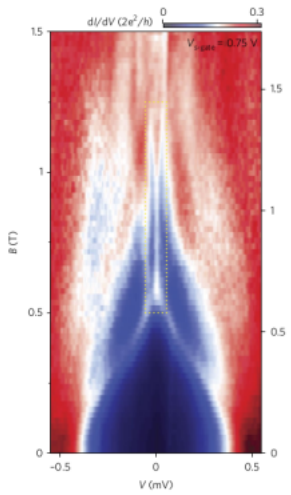

Figure 6.10: source:(49) Zero bias peak obtained for a dissipation less nanowire

A peak is observed at around 0.55T of height $0.15 * 2e^2/h$ which is still much suppressed than $2e^2/h$.

6.4 Andreev Bound States and zero bias peak

After non-observance of all the theoretical features of Majorana Bound States it was suggested that possibly the system doesn't even enter the topological regime and the zero bias peaks are coming up in the experiments entirely due to alternate mechanism. It was proposed[50] that the ZBP in the experiments was instead due to Andreev Bound States(ABSs). ABSs are generated at the junction of semiconductor and superconductor due to reflection of electrons at the surface of the superconductor, coming from normal conductor. It was said that the ABS produced at the interface of nanowire and superconductor on adjusting the parameters like magnetic field and gate potential may coalesce together at $E = 0$, which gives a peak at zero bias in the conductance measurement.
We start with the hamiltonian of original theoretical proposal,

$$H = (-\frac{\hbar^2}{2m^*}\partial_x^2 - \iota\alpha_R\partial_x\sigma_y - \mu)\tau_z + V_z\sigma_x + \Delta_0\tau_x$$

The model is also shown in the figure,

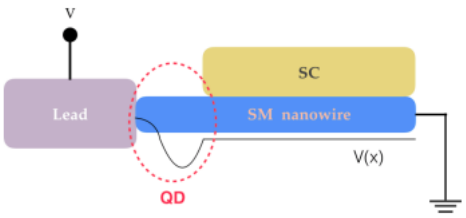

Figure 6.11: source:(50) Quantum dot at the end of the nanowire appearing due to the applied bias

A quantum dot(QD) is included at the beginning of the nanowire. This QD is responsible for the generation of Andreev Bound States. The QD is modelled as $V(x) = V_0 cos(\frac{3\pi x}{2l})$. The QD is assumed to be present in the beginning of the wire in the current analysis, but it can be present anywhere, even inside the nanowire. This QD is included in the original hamiltonian which is written as,

$$H = (-\frac{\hbar^2}{2m}\partial_x^2 - \iota\alpha_R\partial_x\sigma_y + V(x) - \mu)\tau_z + V_z\sigma_x$$

The results have been analysed for the case when QD is there and when no QD is there.

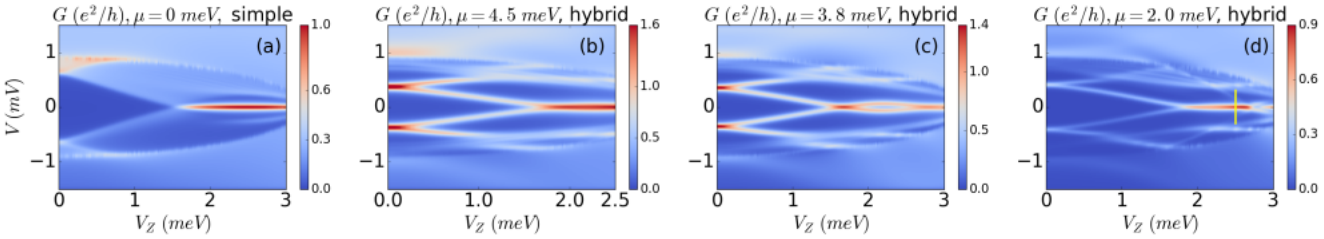

Figure 6.12: source:(50) Shown ZBPs for the systems with and without a quantum dot. ZBP appears even in the trivial regime due to Andreev modes, in the systems with a quantum dot.

The above plots(fig6.12) show the color plots for the conductance obtained at each voltage bias(V) vs Zeeman field(V_z). All four plots above are at different chemical potentials. The case with no QD is shown in fig(a). While figure (b), (c), and (d) represent the cases with a QD in the beginning of the nanowire.

Now, we already know about one common result, that is, when the peak is obtained at a Zeeman field below $\sqrt{\Delta_0^2 + \mu^2}$ it is in the trivial regime while above this field peak is in the topological regime.

In fig(a), chemical potential is set at $\mu = 0$, $\Delta = 1.5meV$ for all the cases. ZBCP is obtained at around $V_z = 1.5$ which indicates a zero bias peak due to Majorana in the toplogical regime.

Fig (b) is obtained at chemical potential, $\mu = 4.5meV$. In this case, we obtain one peak at around $V_z = 1.8$ which is in the trivial regime going by our formula.

Fig (c) is obtained at chemical potential, $\mu = 3.8meV$, which gives two peaks, one at $V_z = 1.2meV$ and the other at $V_z = 3meV$. Both the peaks are in the trivial regime because both V_z values are less than μ.

Fig(d) is obtained at chemical potential, $\mu = 2.0meV$. In this case, we see first ZBCP appears at around $V_z = 1.8meV$, which is in the trivial regime and the peak continues upto the topological regime.

The above results show that we do not need to be in the topological regime to see ZBCP. We can obtain these peaks even in the trivial regime due to ABSs.

6.5 Need for Step like spin orbit coupling

Experiments suffered from one more difficulty which was the non-observance of Majorana oscillations. As we have seen before, the Majorana fermionic wavefunctions situated at the ends of the nanowire start overlapping with each other at higher magnetic field. There is a hybridisation energy δE associated with the overlap. On further increasing the magnetic field overlap of the two Majorana modes should further increase which should lead to an increased δE. So, we expect δE to oscillate with an increasing amplitude and decreasing time period. We call it enhanced oscillations. This scenario is something which is not observed in the experiments. What is observed in the experiments is rather reversed. That is, the oscillations are deceasing in amplitude with increasing time period. We call them decaying Majorana oscillations. Decaying oscillations is also a generic property of Andreev Bound States. So it was alleged that these ZBPs observed in the experiments

are indeed due to ABSs and not due to MBSs.
Theorists, however, tried to prove that decaying Majorana oscillations are indeed due to Majorana bound states(MBSs) under the experimental circumstances[51]. It was claimed that spin orbit coupling is not constant throughout the wire which was assumed to be constant in the original theory. There is a region of the nanowire in the experiments which is not under the superconductor and the coupling there is much different than the region which is deep under the superconductor.

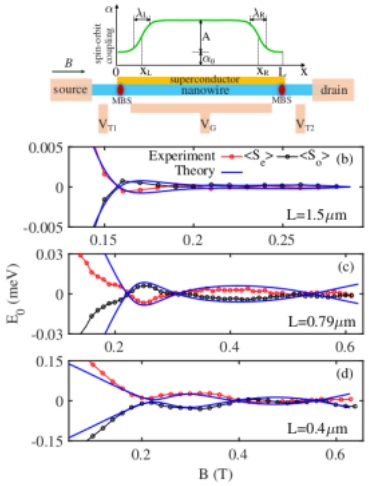

Figure 6.13: source:(51) Step like spin orbit coupling model depicted on the top. Other plots depicting decaying Majorana oscillations for the nanowires of different lengths.

Above diagram shows comparison of theoretically obtained Majorana oscillations with step like spin orbit coupling with the experimental plot. And, we can see both are in a good agreement.

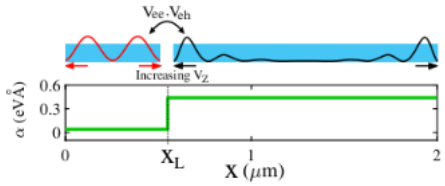

Figure 6.14: source(51): Nanowire behaves as broken into two independent parts combined together due to step like spin orbit coupling.

When there is a step like spin orbit coupling we can take the nanowire to be composed of two parts; one with lower spin orbit coupling (α) while other with a higher spin orbit coupling. Now, both the parts would have a different spectrum of energies so that when both are combined the Majorana wavefunctions do not overlap in the usual way which gives rise to the decaying oscillations.
The type of corrected SO coupling taken in the theory is,

$$\alpha(x) = \frac{A}{2}[tanh(\frac{x - x_L}{\lambda_L}) + tanh(\frac{x_R - x}{R})] + \alpha_0 \tag{6.3}$$

6.6 Decaying Majorana Oscillations: A generic property of Andreev Bound States

The decaying Majorana oscillations instead of enhanced ones raised doubts over the presence of Majorana fermions in semiconductor-superconductor heterostructures. Cao et al[51] pointed the step like spin orbit which is generated due to experimental conditions as a possible reason for decaying

Majorana oscillations even with the presence of Majorana modes at the two ends of the nanowire. However, it was pointed out later in a theoretical paper by sharma et al[45] that the region in the parameter space in which such a phenomenology occurs is vanishingly small. The statement means there is a very small set of external parameters like magnetic field, chemical potential etc for which we obtain decaying oscillations even with the presence of Majoranas. And if experiments were able to access such a region where the oscillations decay they should have also been able to access the region where the oscillations grow, because the two regions are nearby. Other than that, they were also able to show that this region of Majorana oscillations is practically removed if we consider some more factors present in the experiment. During the experiment, the external bias which is applied to the nanowire is also position dependent. This potential is modelled as,

$$V(x) = V_{dot}(\frac{1 + tanh[(x - x_0)\beta_v]}{2}) \tag{6.4}$$

After including the potential the hamiltonian looks like,

$$H = [-\frac{\partial_x^2}{2m} - \mu + \iota\alpha(x)\partial_x\sigma_y + V(x)]\tau_z + h\sigma_z + \Delta(x)\tau_x \tag{6.5}$$

Where all the factors $\alpha(x)$, $V(x)$, and $\Delta(x)$ are position dependent as,

$$V(x) = V_{dot}(\frac{1 + tanh[(x - x_0)\beta_v]}{2}) \tag{6.6}$$

$$\alpha(x) = (\alpha - \alpha')\frac{1 - tanh[(x - x_0)\beta_\alpha]}{2} + \alpha' \tag{6.7}$$

$$\Delta = (\Delta - \Delta')\frac{1 - tanh[(x - x_0)\beta_\Delta]}{2} + \Delta' \tag{6.8}$$

After including all these factors the parameter region associated with decaying Majorana oscillations is practically removed. And, it was also shown that decaying oscillations is a generic property of Andreev Bound States.

In the earlier experiments, ZBCP had been successfully used to detect Majorana fermions in the nanowires. But, on later, more detailed analysis it was found that a ZBCP could be observed for n number of reasons with many of them having no concern with the Majorana. A ZBCP can be produced due to Andreev Bound States, quasi- Majoranas and impurities, etc. It appears that none of the experiments which have attempted to observe signals of the Majorana in the nanowire experiments have been successful despite having observed a ZBCP. There are other traits attached with a ZBCP representing Majorana which includes Majorana oscillations and quantized peak. While it has been shown that quantized peaks can be generated even without the Majorana and just by carefully adjusting the parameters, Majorana oscillations are a sure proof of existence of the Majorana, which has not been observed. Looking at the fallability of the ZBCP test it is suggestive that we should come up with a more conclusive way of finding the Majorana. We want a method which clearly distinguishes when the system is in trivial regime and when in the topological regime without ambiguity. One such method which has been proposed is non-local conductance measurement[52]. Three terminal non-local measurement is also capable of providing the information about the bulk of the system which is not true for two terminal local conductance measurements. In the current section the results of a three terminal non-local conductance for various impurity and disorder conditions including quantum dots and inhomogenous potential has been provided. Various impurity and disorder conditions which arise in the experiments has been provided which acts as a guide for the future experiments to compare their results.

6.7 Non-local conductance and thermal conductance

Non-local conductance can directly be used to detect opening or closing of the bulk gap as the magnetic field applied to the system is varied. This is because non-local conductance vanishes above and below the gap. Along with non-local conductance thermal conductance and Topological Visibility(TV) were also calculated in the ref(51). TV is a purely theoretical phenomenon so it cannot be measured in the experiments, however, it provides a guide while observing the theoretical plots of non-local conductance, that, which features of the plot are topological and which are trivial.

A SM-SC hybrid structure can be modeled by the following hamiltonian, which includes the terms for impurity and disorder:

$$H = H_{SM} + H_Z + H_V + H_{SC} + H_{SC-SM}$$

H_{SM} is for semiconductor, H_Z for the externallty applied magnetic field, H_{SC} for superconductor and H_{SC-SM} for the coupling between semiconductor and superconductor.

The following Bogoliubov de Gennes hamiltonian then describes the model:

$$H_{BdG} = \frac{1}{2}\int dx \hat{\psi}^\dagger H \hat{\psi}$$

Where,

$$H = (\frac{-\hbar^2}{2m^*}\partial_x^2 - \iota\alpha\partial_x\sigma_y - \mu)\tau_z + V_z\sigma_x + \Sigma(\omega)$$

$V_Z = \frac{1}{2}g\mu_B B$, where B is the field applied in the x- direction.
In the figure the setup is shown for which the non-local conductance is measured:

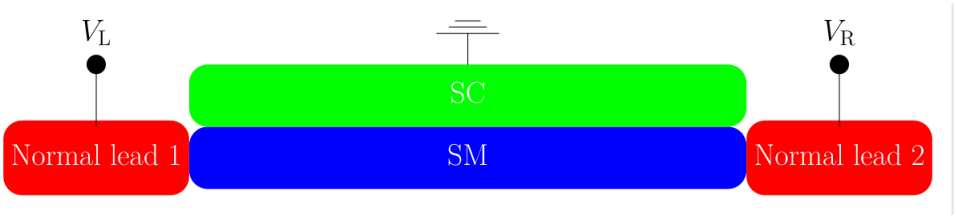

Figure 6.15: source:(52) Schematic to measure the non-local conductance for the experimental confirmation of Majorana modes.

The following matrix can be calculated for the above setup:
S = $\begin{pmatrix} S_{LL} & S_{LR} \\ S_{RL} & S_{RR} \end{pmatrix}$
Thermal conductance is also calculated for the above S-matrix.
For nonlocal conductance,
G= $\begin{pmatrix} G_{LL} & G_{LR} \\ G_{RL} & G_{RR} \end{pmatrix}$

$= \begin{pmatrix} dI_L/dV_L & dI_L/dV_R \\ dI_R/dV_L & dI_R/dV_R \end{pmatrix}$

where, I_L or I_R stands for the current coming from the left or right direction respectively. V_L or V_R stands for the bias applied at the left or right normal lead respectively. Ground is always applied at SC.
G_{LL} and G_{RR} are the local conductances.

There is a formalism called Blonder-Tinkham Klapwijk formalism, which gives an expression for the local and non-local conductance,

$$G_{ii} = \frac{e^2}{h}(N_i - T_{ii}^{ee} + T_{ii}^{)}eh$$

$$G_{ij} = \frac{e^2}{h}(T_{ij}^{ee} - T_{ij}^{eh}$$

Definition of thermal conductance:

$$\kappa = \kappa_0(T_{ij}^{ee} + T_{ij}^{eh})$$

$\kappa_0 = \pi^2\kappa_B^2\tau/6h$.
Definition of Topological visibility:
Positive value of $det(S_{LL})$ and $det(S_{RR})$ indicates trivial regime while negative value indicates topological regime.

Good, trivial and ugly ZBCP:

We classify ZBCP in different types so that it is easy to ascertain when a ZBCP represents a topological mode and when not.

Good: This is when there is no impurity in the sample. ZBCP in this case represents a topological transition. No pure sample has been obtained for the experimentation so this ZBCP may not have been observed yet.
Bad: This is when there is some impurity in the sample, or there is a weak disorder. This also may represent a TQPT.
Ugly: This is the case of strong disorder. And all topology is destroyed in the sample.

6.8 Quantum dot, disorder and inhomogenous potential

At the SM-SC junction a potential barrier is generated in the experiments. This potential barrier can be model as a quantum dot:

$$H_V = V_D exp(\frac{-x^2}{l^2})\theta(l-x)$$

$\Delta_0(x) = \Delta_0\theta(l-x)$,
V_D=potential barrier.
Inhomogenous potential is again modeled in Gaussian form.

$$H_V = V(x) = V_{max} exp(\frac{-x^2}{2\sigma^2})$$

V_{max}=peak of the potential, σ=line width.

We look at the pristine nanowire first with no quantum dot and no disorder:

The plots for different measurements for pristine nanowire are provided:

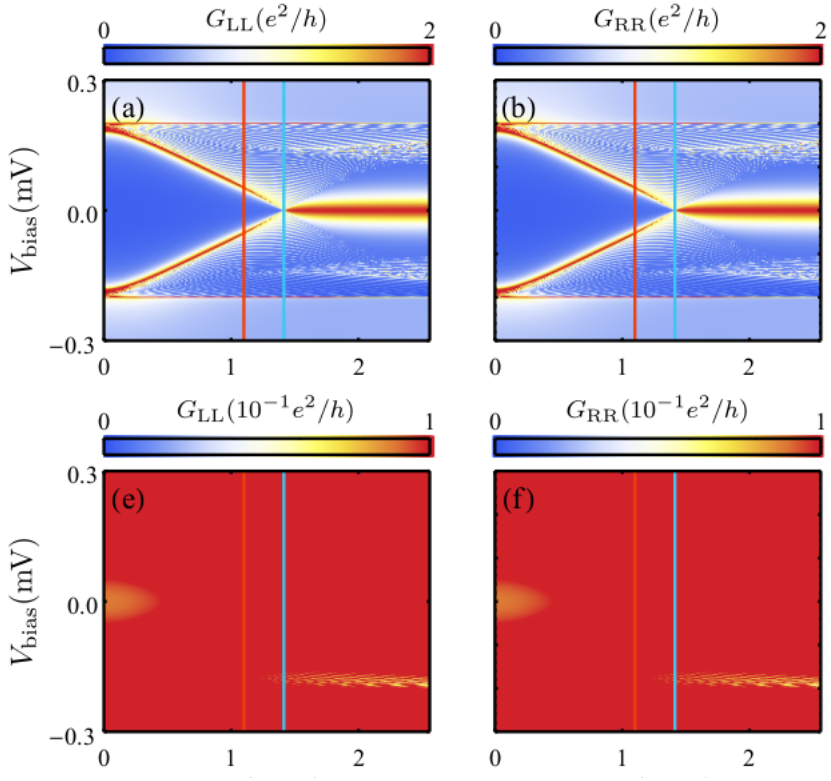

Figure 6.16: [source:Haining Pan(2020)]

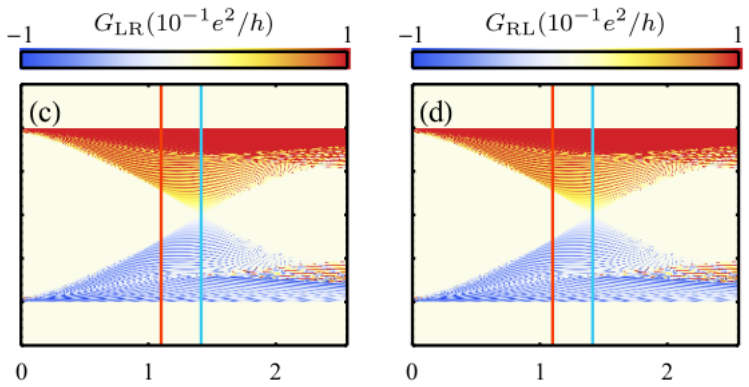

Figure 6.17: [source:Haining Pan(2020)]

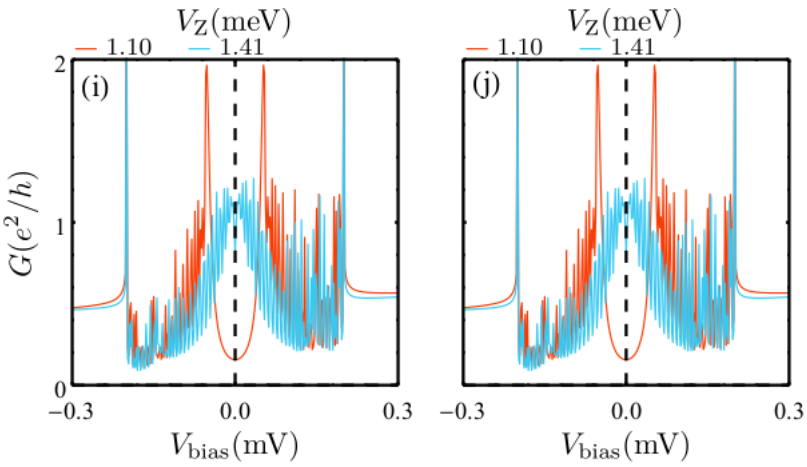

Figure 6.18: [source:Haining Pan(2020)]

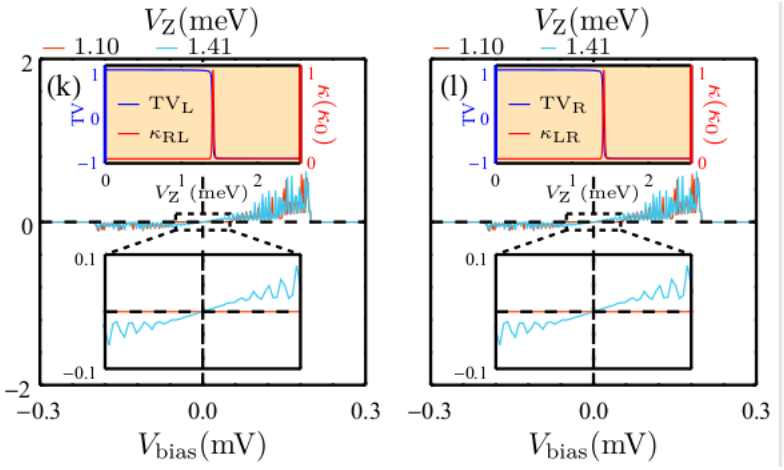

Figure 6.19: [source:Haining Pan(2020)]

Figures (a) to (d) show the plots for different types of conductances. Figures (e) to (h) are also for the same type of conductances but measured at different scales.

In figures (a) to (h) V_{bias} and V_z are the parameters for y and x-axis respectively. For each pair of x, and y values there is a conductance. There is a colour associated with each conductance value, which is indicated by the colour bar shown on top of each plot. Plots (c) and (d) are for the nonlocal conductance. They are very useful in determining the V_z at which the gap closes and the system passes into the topological regime.

In figures (a) to (d) each plot has its own scale. The scale of conductance measurement is e^2/h for local conductance. These are shown in figures (a) and (b) While, scale is $0.1e^2/h$ for non-local conductance, which is shown in figures (c) and (d). This implies higher precision would be required to observe nonlocal conductance experimentally.
We only exchange the scales in the next set of figures i.e in (e) to (h), we see that nothing is decipherable in them. Figures (e) and (f) which are plotted for local conductance are uniformly coloured throughout at the highest scale colour, while (g) and (h) which are for the non local conductance are uniformly coloured at the colour scale of zero value.

In figure (i) and (j) non-local conductance plots have been calculated at different values of Vz, Vz=1.1 and Vz=1.41 meV. Vz is representative of the external magnetic field. At the lower value the plot is in trivial regime while at the higher value it is in topological regime. In figures (k) and

(l) plots for thermal conductance and and topological visibility(TV) have been shown. Thermal conductance shows a peak at the point of topological quantum phase transition(TQPT) so in the experiments it can be used as an indication for the transition to a topological state. The TV is also shown in the plots (k) and (l) with respect to V_z. TV takes a positive value of +1 in the trivial regime while it takes -1 value when the system transitions into the topological regime. TV cannot be measured experimentally but it can be used as a theoretical tool to determine when a TQPT has happened.

In the last section, we showed how nonlocal measurement can be used to detect the bulk properties of the nanowire proximity coupled with a superconductor. We saw there was no difference in the analysis of local and nonlocal conductance. In short, both provided the same information, and peak in the local conductance represented topological quantum phase transition(TQPT). The Vz value of bulk gap closing observed in nonlocal conductance was same as the peak of local conductance at zero bias conductance measurement. The results in the previous section were for the pristine wire case. The nanowires available with the current technology are far from the ideal case. The nanowires which are available, are filled with impurities and disorder. The theoretical results in the previous section do not represent any of the experimental data which has been available so far. To correctly model the kind of data which can be taken with the currently available technology we need to add the effects of impurity and disorder to the theory. These effects can be modeled by adding a quantum dot, inhomogenous potential and disorder in the chemical potential. In this section we see the effect of what happens when we add any one of them, or some of them together to the nanowire, in the theoretical model. We see first the results for a long wire, and later we see the same results in the short wire limit. I would like to emphasize that all the experimental results which are currently available are in the short wire limit.

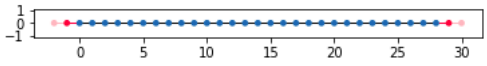

Figure 6.20: 1D superconducting lattice with Rashba spin orbit coupling

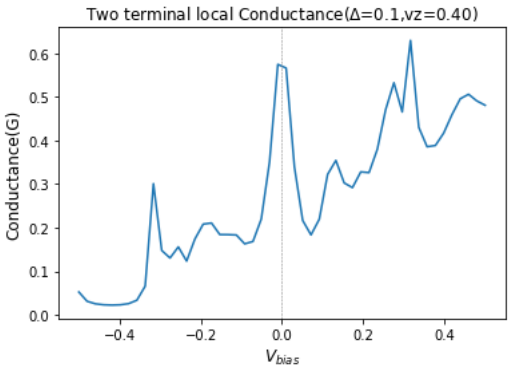

Figure 6.21: Local conductance vs bias potential plot for the local conductance. There is a peak at the zero bias due to Majorana modes.

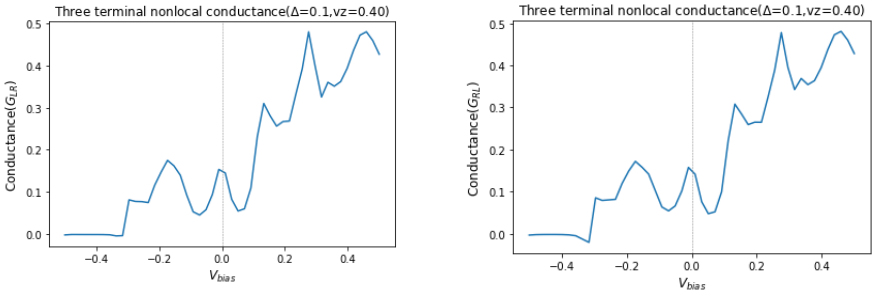

(a) (b)

Figure 6.22: Nonlocal conductance vs bias plot for the setup of fig(6.15). The left hand side plot is for conductance(G_{LR}) and the right hand side plot is for conductance(G_{RL}). Both the plots are identical which shows that it doesn't make a difference whether we measure G_{LR} or G_{RL}.

6.9 Quantum dot at one end of the nanowire

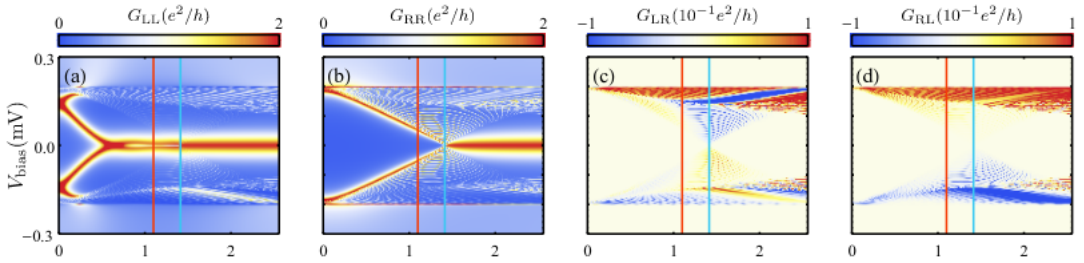

Figure 6.23: [source:Haining Pan(2020)]

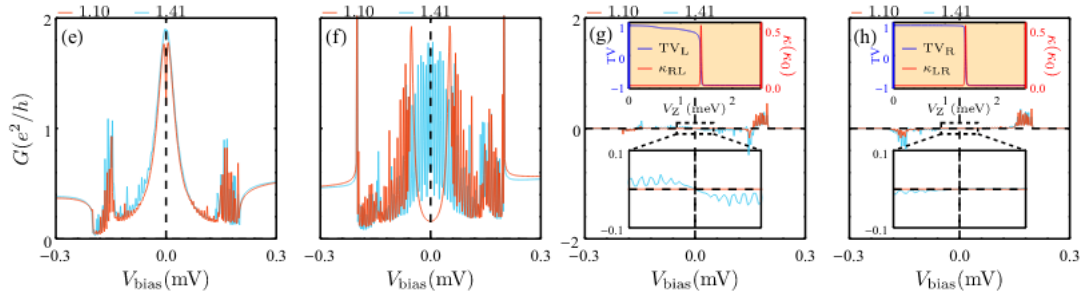

Figure 6.24: [source:Haining Pan(2020)]

The above figure shows the results for adding quantum dot at one end of the nanowire. As usual figures (a) and (b) present the results for local conductance, while figures (c) and (d) are for nonlocal conductance. Figs (e) and (f) present the plots for non-trivial(shown with light blue color) and trivial(shown with red color) values of the magnetic field. The same convention is followed for all the plots throughout this section. Red color stands for trivial case, light blue stands for the non-trivial, and dark blue stands for topological case at the same parameters for the pristine nanowire. It is called nominal case. It gives us the information about how much the real TQPT point deviated from the pristine case, due to impurities and disorder.

In fig (a) a ZBCP is obtained at Vz=0.5, below the point of real topological phase transition. If local conductance were the only data available in an experiment this would give a false perception of a TQPT. In fig (c) there is a gap closure at Vz=1.41. This is the point of real topological phase tran-

sition. Fig(a) also shows a ZBCP at this point. This ZBCP represents the true TQPT. How do we know that the gap closure in fig(c) really represents a real TQPT? In figs (g) and (h)TV(Topological Visibility) have been plotted. Although, TV is a purely theoretical measure and it cannot be measured experimentally, it provides us a method to calculate in our theory the point of topological phase transition. In figs (g) and (h) TV changes sign from 1 to -1 at Vz=1.41mev. This is the same point at which nonlocal conductance in fig (c) shows a bulk gap closure.

The results of thermal conductance are also shown in the figs (e) and (f). It is shown in red color. We observe that thermal conductance shows a peak at the point of TQPT. This shows that thermal conductance in this case correctly represents the point of topological quantum case transition.

The results for the nanowire with a single quantum dot added at the end show that local conductance is unreliable to show the point of real TQPT, but nonlocal conductance, and thermal conductance correctly represent TQPT.

6.10 Nanowire with inhomogenous chemical potential

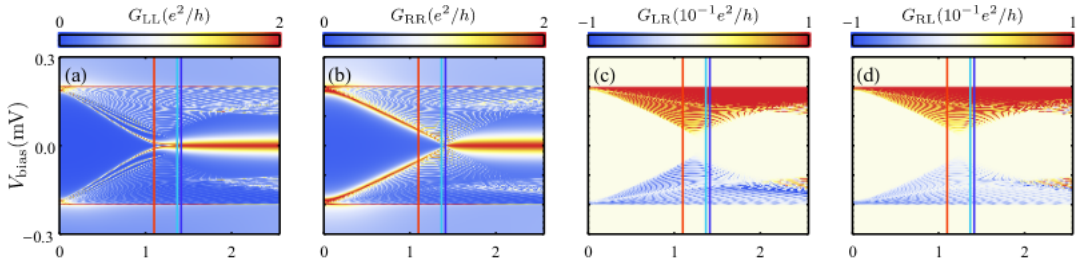

Figure 6.25: [source:Haining Pan(2020)]

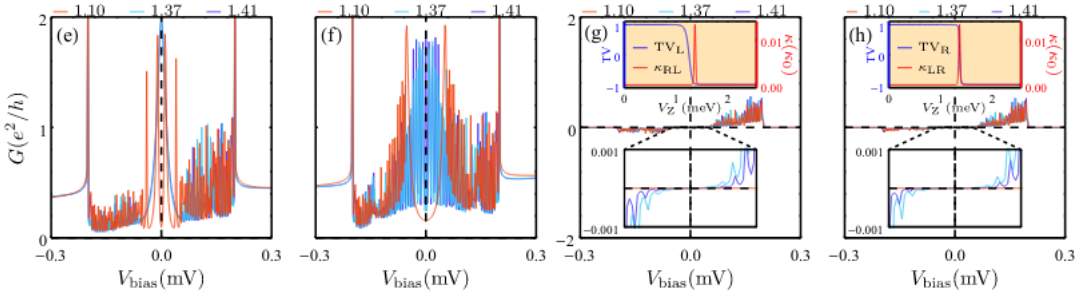

Figure 6.26: [source:Haining Pan(2020)]

In this section, we see the effect of inhomogenous potential on the results of local conductance, nonlocal conductance and thermal conductance. See that in this section quantum dot has not been included, but just the inhomogenous potential has been included. We will compare the results of the this section with the previous section.

As before Figs(a) and (b) present the result for local conductance. Figs(c) and (d) present the result for nonlocal conductance, while Figs (g) and (h) for thermal conductance. Figs (e) and (f) show results for the nonlocal conductance near the zero bias. Results for real TQPT are shown with light blue and for nominal TQPT are shown with dark blue.

We again see a trivial ZBCP below TQPT as in the above case. Nonlocal conductance gap closes at real TQPT. However, the gap is not as small as in the previous case. Thermal conductance correctly represents the point of TQPT. The height of thermal conductance is smaller than the quantized

height due to finite dissipation. Finite dissipation was added in the theoretical calculations to simulate for the realistic situations where the dissipation is present. Real TQPT is shifted from nominal TQPT in this case. The gap is also smaller at the real TQPT in the nonlocal conductance.

The result of this section is that local conductance is unreliable to detect TQPT. Peak of thermal conductance is the most accurate measure of TQPT. Nonlocal conductance can also give some accurate idea.

6.11 Nanowire with weak disorder in chemical potential

This case is similar to the pristine wire case. There is not much effect of the weak disorder so the results of this case are not shown.

6.12 Nanowire with intermediate disorder

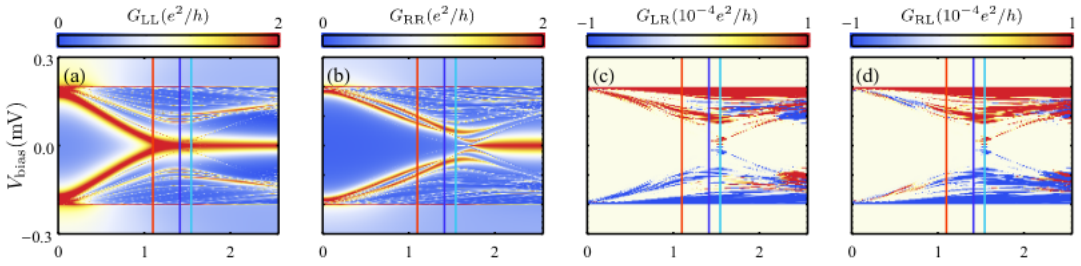

Figure 6.27: [source:Haining Pan(2020)]

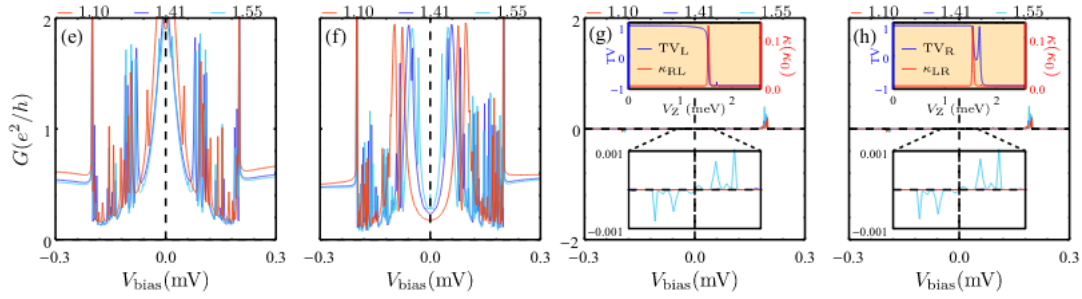

Figure 6.28: [source:Haining Pan(2020)]

In the above figure we see a trivial ZBCP below TQPT in local conductance measurement. Nonlocal conductance shows the gap closure but the signal is very weak. Although, TV shows a few spikes, it indicates a phase transition as the value properly moves from +1 to -1. Thermal conductance again shows a peak where TV value drops to -1.

Results with intermediate disorder indicate that ZBCP cannot be used as a measure to detect TQPT. Nonlocal conductance measurement can be used to some extent but the values are very weak. Very precise measurement may be required for the nonlocal conductance which may not be feasible in the experiments. Thermal conductance shows best results for the intermediate disorder case. Based on the results of this section it is suggested that thermal conductance measurements are better than all the other measurements to detect a TQPT.

6.13 Nanowire with strong disorder

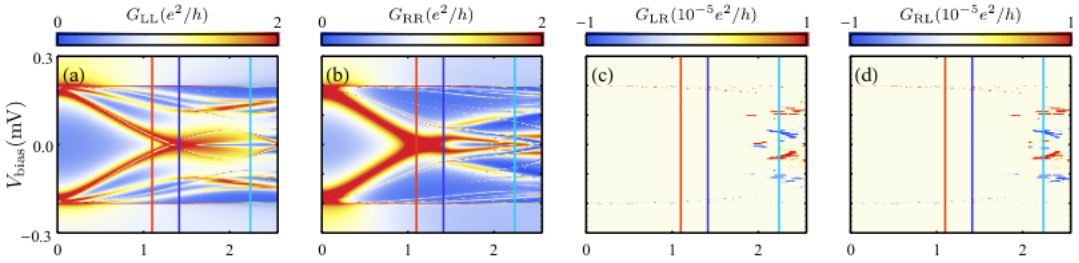

Figure 6.29: [source:Haining Pan(2020)]

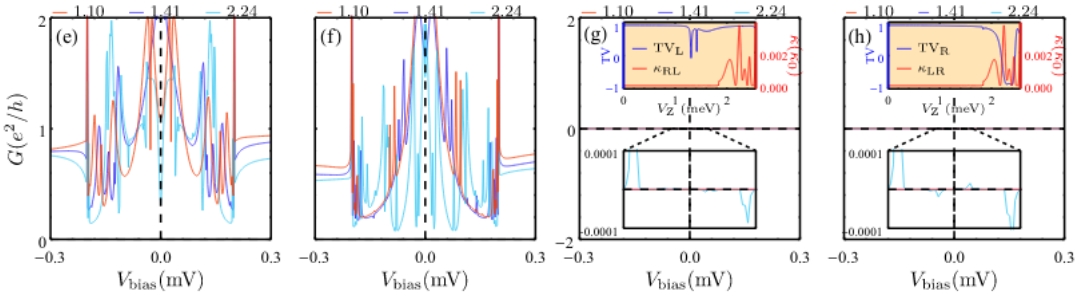

Figure 6.30: [source:Haining Pan(2020)]

In this section, the effect of strong disorder is shown. We see topological state is not defined properly at such large disorder. There is a strong signal of trivial ZBCP. This is what mostly happens in the current experiments. Strong signal of trivial ZBCP due to disorder is falsely taken as the signature for Majorana modes. We see that even nonlocal conductance does not help. Its value is very diminished and it is scattered everywhere. There is no signature of gap closing or reopening. Thermal conductance is zero at small values of Vz and oscillates abruptly at higher values. TV is also very irregular and does not drop to -1, which indicates that no topological phase is defined at such large disorders.

6.14 Nanowire with quantum dot and strong disorder

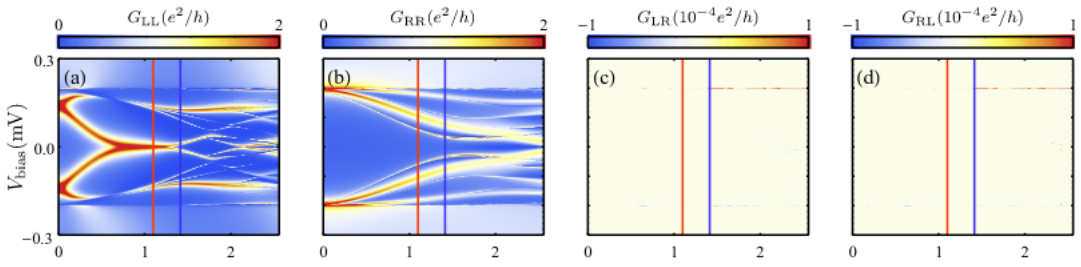

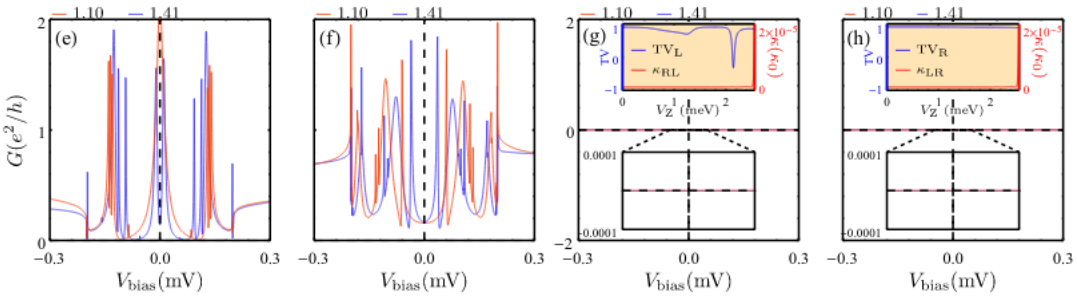

Figure 6.31: [source:Haining Pan(2020)]

So far, we have studied the effect of quantum dot and disorder separately. But, there is no reason why they should occur separately in realty. To simulate a more realistic situation the effects of quantum dot and nanowire are combined and we see how the system behaves as a result. When both are combined, we see the separate results for each of them are superimposed. In the earlier sections, we have seen that in the presence of weak and intermediate disorder the topological phases persist, despite observing a trivial ZBCP. And, there were signatures of TQPT observed with the help of nonlocal conductance and thermal conductance which correctly represented the situation, as verified from TV. In the weak and intermediate disorder case, the results are predominated by the quantum dot. That means, the results are similar to that of the quantum dot case. If we increase the disorder to very large values, the results are now predominated by disorder. As in the strong disorder case, topological phase is completely destroyed as indicated by TV, which does not drop to zero. Thermal and nonlocal conductances are unable to provide any conclusion.

6.15 Pristine short nanowire

The analysis so far has been for long wires. If we look at the size of the nanowires used in the currrent experiments they fall into the short wire regime. So, to be able to simulate correctly the results of the previously done experiments or make predictions for the later experiments which might again be done with short wires the results should be obtained in the short wire limit. In the short wire limit, the Majorana modes are not completely separated. Majoranas at the two ends overlap and there is a finite energy associated with the overlap. When an external magnetic field is applied, the effective length of the wire decreases, which further increases the overlap. As a result, in the experiments we may see Majorana oscillations with shorter time period. While, the effect of disorder may be more pronounced in the shorter wires and the topological phase may be more easily destroyed.

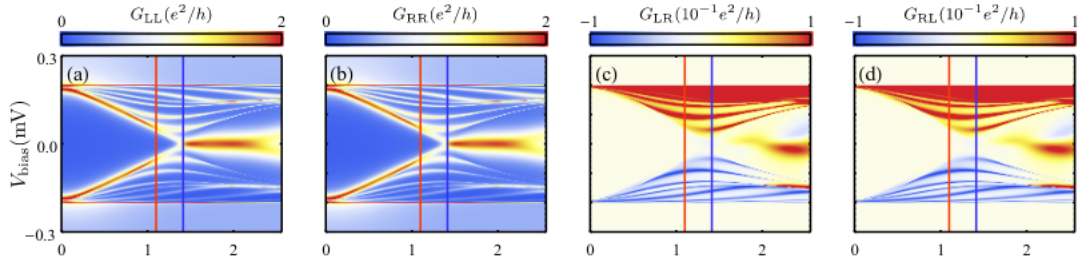

Figure 6.32: [source:Haining Pan(2020)]

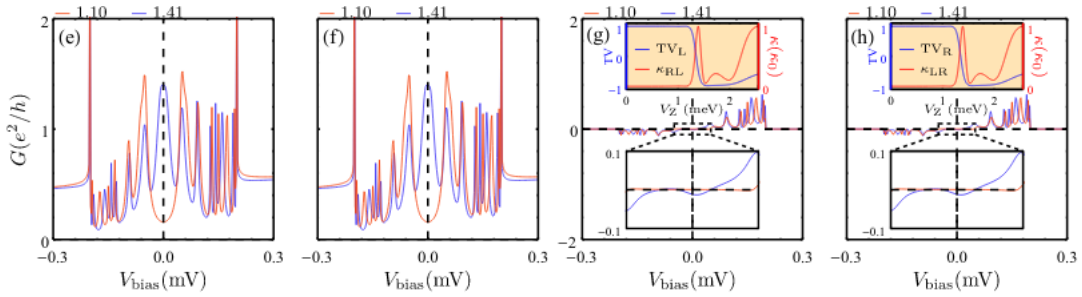

Figure 6.33: [source:Haining Pan(2020)]

Above plots have been obtained in the pristine short wire limit.

There are a few important features incumbent only in short wire:
1. Majorana oscillations have a smaller period: This happens due to overlapping Majorana modes.
2. Nonlocal conductance gap is not as small as in the longer wires.
3. TV starts rising at higher magnetic fields this implies that the topological phase is not properly defined at higher fields.
4. Thermal conductance shows a peak at TQPT and then drops to zero but starts growing again at the higher field.

All the above features are due to overlapping Majorana modes, the effect which becomes pronounced due to shorter length wire.

6.16 Short nanowire with superconducting gap collapse

In the hamiltonian, when we write the superconducting term there is an associated constant which we call superconducting bulk gap denoted by Δ_0. This, however, does not remain constant in the presence of varying magnetic field and tends to be suppressed as the magnetic field is increased, and eventually collapses. Due to collapse of the superconducting gap topological phase ceases to exist. The superconducting gap closure is modeled by the following formula:
$\Delta(V_z) = \sqrt{1-(V_z/V_c)}$. V_c is the critical value of the zeeman field at which the bulk gap closure happens. The V_c has been set at such a value that it lies above the topological gap. In this way, we observe how the plots compared to the pristine case change only quantitatively, while all the qualitative features remain same. Since the bulk gap closure happens after TQPT, the visible features of separate topological phases in the data remain intact.

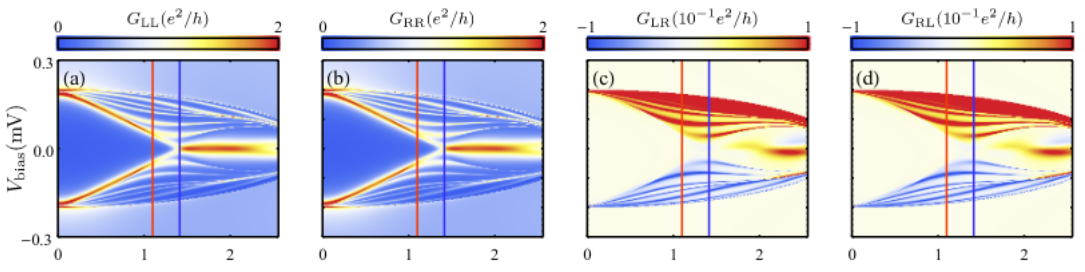

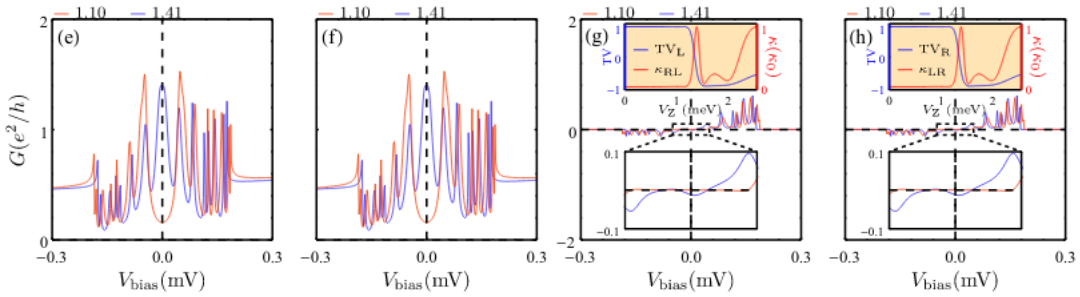

Figure 6.34: [source:Haining Pan(2020)]

Conductance vs bias plots near the zero bias in Figs (g) and (h) are same as the pristine short wire case. The collapse of SC gap is also visible in the nonlocal conductance. There is a gap closure and reopoening at the TQPT, however, another gap closure happens towards the point of superconducting gap collapse.

6.17 Short nanowire with strong disorder

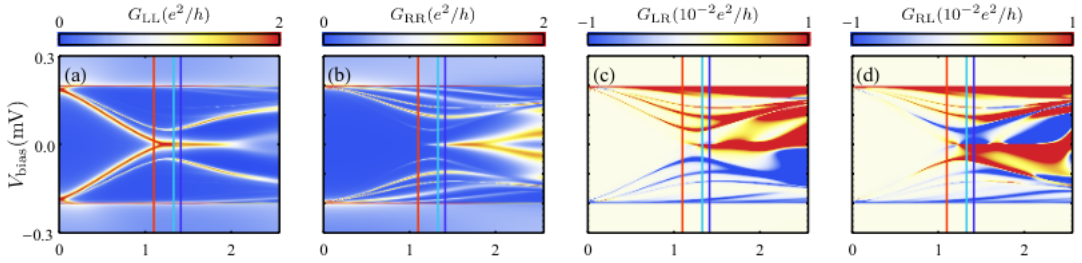

Figure 6.35: [source:Haining Pan(2020)]

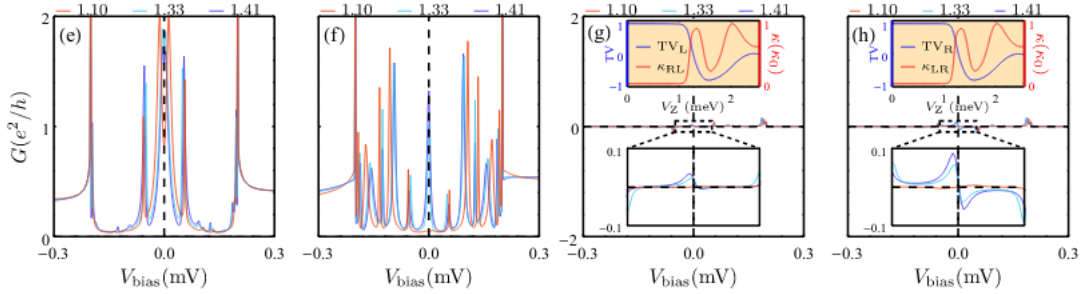

Figure 6.36: [source:Haining Pan(2020)]

We expect for the strong disorder case that topology must be ill defined. This is because, in the shorter wires, topology is more fragile than the long wires due to overalapping Majorana modes. The results infact confirm our expectation. There is a trivial ZBCP while the topological ZBCP is completely destryed. In nonlocal conductance measurement in Figs (c) and (d) there is a gap closing but no gap reopening. Thermal conductance rises to a peak at a certain V_z but oscillates rapidly after that. TV never drops to zero. This confirms our expectation that the topology must be ill-defined. And, in the experiments, the fact that nonlocal conductance gap does not open after closing and the abrupt oscillations of thermal conductance may be used to confirm that we are dealing with a strong disorder case.

6.18 Short nanowire with superconducting gap collapse and strong disorder

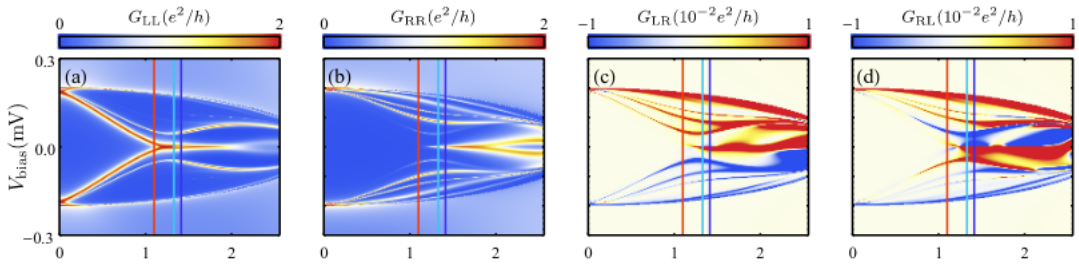

Figure 6.37: [source:Haining Pan(2020)]

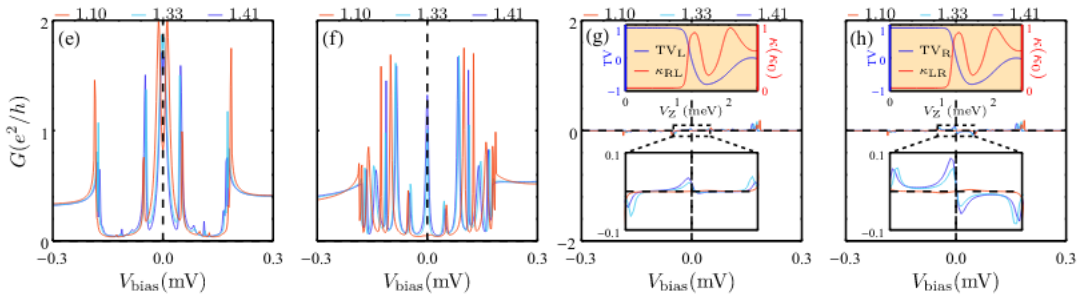

Figure 6.38: [source:Haining Pan(2020)]

Lastly, the results for short wire and strong disorder case are presented. The experiments to detect Majorana modes have so far been performed in this regime only. The results indicate that clearly defined topological phases cease to exist in this regime. Thermal conductance shows oscillations after TV shows a dip. TV does not flip to -1 completely. Such results clearly indicate that the topology is not well defined.

Chapter 7

Summary and Conclusion

We started from Quantum Hall Effect in a 2DEG and studied and obtained the topological edge states using kwant. We then studied how we can obtain these edge states without the application of an external magnetic field. This type of device is called Chern insulator and formed a part of the Nobel Prize winning work of Duncane Haldane. We then saw how we can realize a Chern insulator with Graphene and the model was called Haldane model. A Chern insulator lacks time reversal symmetry, but if we combine two Chern insulators with the edge states of opposite chirality the system we obtained was time reversal symmetric and was called Quantum spin hall insulator or a 2D Topological insulator. We studied that the edge states for such a device are protected from scattering due to time reversal symmetry. Then, we asked if it is possible to obtain a 3D topological insulator. We realised such a system by stacking together 2d topological insulators in three dimensions. We then studied various experimental techniques by which the surface states of a 3D topological insulator can be observed experimentally.

Next, we studied how we can obtain Majorana fermions in a 2D quantum spin hall insulator, p-wave superconductor, or a 3D topological insulator. Then, we saw how we can realize Majorana fermions at the ends of a 1D-Kitaev chain, and studied step by step method to extend this model to be realizable in semiconductor-superconductor heterostructures. We reviewed the experimental and theoretical progress that has taken place in the field since the model was proposed first by Jay D Sau et al in 2010. we observed that there are several theoretically expected behaviours like quantized zero bias peak, and Majorana oscillations which are not observed experimentally. Theorists have tried to explain the deviations in the experiments by including some extra parameters which may be present in the experiments but were not there in the original theory. But, we observe there is no common consensus among the theorists and the theoretical papers by Sharma et al and Haining Pan et al suggest that no Majorana fermion has ever been observed in the experiments and all the results which are there are due to impurity and disorder. They showed that similar results can appear in the current experimental conditions even if the system is not in the topological regime.

At any rate, the field suffers from many doubts and fears and the experimental techniques need to improve a lot to provide a reliable data. Meanwhile, there have been theoretical papers as well which suggest to perform braiding operations for quantum computation using quasi-majorana modes which are partially separated Majorana modes in the trivial regime of the system.

Bibliography

1. Hall, E. H. “On a New Action of the Magnet on Electric Currents.” American Journal of Mathematics, vol. 2, no. 3, 1879, pp. 287–292.
2. Ando, T., Matsumoto, Y., Uemura, Y. (1975). Theory of Hall Effect in a Two-Dimensional Electron System. Journal of the Physical Society of Japan, 39(2), 279–288.
3. Wakabayashi, J., Kawaji, S. (1978). Hall Effect in Silicon MOS Inversion Layers under Strong Magnetic Fields. Journal of the Physical Society of Japan, 44(6), 1839–1849.
4. Novoselov, K. S., Jiang, Z., Zhang, Y., Morozov, S. V., Stormer, H. L., Zeitler, U., ... Geim, A. K. (2007). Room-Temperature Quantum Hall Effect in Graphene. Science, 315(5817), 1379–1379.
5. K. v. Klitzing, G. Dorda, and M. Pepper Phys. Rev. Lett. 45, 494 – 11 August 1980
6. Prange, R. E. (1990). Introduction. Graduate Texts in Contemporary Physics, 1–35.
7. Suddards, M. E., Baumgartner, A., Henini, M., Mellor, C. J. (2012). Scanning capacitance imaging of compressible and incompressible quantum Hall effect edge strips. New Journal of Physics, 14(8), 083015.
8. R. E. Peierls, “On the Theory of Diamagnetism of Conduction Electrons,” Z. Phys. 80, 763 (1933).
9. Benetatos, P., Marchetti, M. C. (2002). Plasticity in current-driven vortex lattices. Physical Review B, 65(13).
10. Tomadin, A., Vignale, G., Polini, M. (2014). Corbino Disk Viscometer for 2D Quantum Electron Liquids. Physical Review Letters, 113(23).
11. Haldane, F. D. M. “Model for a Quantum Hall Effect without Landau Levels”. Phys. Rev. Lett. 61, 2015 (1988).
12. Chang, C.-Z., Zhang, J., Feng, X., Shen, J., Zhang, Z., Guo, M., ... Xue, Q.-K. (2013). Experimental Observation of the Quantum Anomalous Hall Effect in a Magnetic Topological Insulator. Science, 340(6129), 167–170.
13. Geim, A. K., Novoselov, K. S. (2007). The rise of graphene. Nature Materials, 6(3), 183–191.
14. Novoselov, K. S. (2004). Electric Field Effect in Atomically Thin Carbon Films. Science, 306(5696), 666–669.
15. It’s still all about graphene. (2011). Nature Materials, 10(1), 1–1.
16. Kharissova, Oxana Kharisov, Boris. (2008). Graphenes, One of the Hottest Areas in the Nanotechnology: Attention of Chemists is Needed. The Open Inorganic Chemistry Journal. 2. 39-49.
17. Wallace, P. R. (1947). The Band Theory of Graphite. Physical Review, 71(9), 622–634.
18. Wright, A. R. (2013). Realising Haldane’s vision for a Chern insulator in buckled lattices. Scientific Reports, 3(1).

19. F. Duncan M. Haldane, Nobel Lecture-(2016)

20. Berry, M. V. (1984). Quantal Phase Factors Accompanying Adiabatic Changes. Proceedings of the Royal Society A: Mathematical, Physical and Engineering Sciences, 392(1802), 45–57.

21. Murakawa, K., Suwa, S. (1950). Revision of the Hyperfine Structure of the Mercury Spectrum. Journal of the Physical Society of Japan, 5(6), 429–434.

22. Xiao, D., Chang, M.-C., Niu, Q. (2010). Berry phase effects on electronic properties. Reviews of Modern Physics, 82(3), 1959–2007., Dyakonov, M. I., Perel, V. I. (1971). Current-induced spin orientation of electrons in semiconductors. Physics Letters A, 35(6), 459–460.

23. Correa, J. H., Pezo, A., Figueira, M. S. (2018). Braiding of edge states in narrow zigzag graphene nanoribbons: Effects of third-neighbor hopping on transport and magnetic properties. Physical Review B, 98(4).,Konig, M., Wiedmann, S., Brune, C., Roth, A., Buhmann, H., Molenkamp, L. W., ... Zhang, S.-C. (2007). Quantum Spin Hall Insulator State in HgTe Quantum Wells. Science, 318(5851), 766–770.

24. Shen, S.-Q. (2012). Topological Insulators. Springer Series in Solid-State Sciences.

25. Maciejko, J., Hughes, T. L., Zhang, S.-C. (2011). The Quantum Spin Hall Effect. Annual Review of Condensed Matter Physics, 2(1), 31–53.

26. Kane, C. L., Mele, E. J. (2005). Quantum Spin Hall Effect in Graphene. Physical Review Letters, 95(22).

27. Bernevig, B. A., Hughes, T. L., Zhang, S.-C. (2006). Quantum Spin Hall Effect and Topological Phase Transition in HgTe Quantum Wells. Science, 314(5806), 1757–1761.

28. K. Kato, Y., D. Awschalom, D. (2008). Electrical Manipulation of Spins in Nonmagnetic Semiconductors. Journal of the Physical Society of Japan, 77(3), 031006.

29. König, M., Buhmann, H., W. Molenkamp, L., Hughes, T., Liu, C.-X., Qi, X.-L., Zhang, S.-C. (2008). The Quantum Spin Hall Effect: Theory and Experiment. Journal of the Physical Society of Japan, 77(3), 031007.

30. Fu, L., Kane, C. L., Mele, E. J. (2007). Topological Insulators in Three Dimensions. Physical Review Letters, 98(10).

31. Hsieh, D., Qian, D., Wray, L., Xia, Y., Hor, Y. S., Cava, R. J., Hasan, M. Z. (2008). A topological Dirac insulator in a quantum spin Hall phase. Nature, 452(7190), 970–974.

32. Hasan Lab, Princeton, Damascelli, A., Hussain, Z., Shen, Z.-X. (2003). Angle-resolved photoemission studies of the cuprate superconductors. Reviews of Modern Physics, 75(2), 473–541.

33. Hasan Lab, Princeton

34. Hasan, M. Z., Moore, J. E. (2011). Three-Dimensional Topological Insulators. Annual Review of Condensed Matter Physics, 2(1), 55–78.

35. Li, C., Hu, L.-H., Zhou, Y., Zhang, F.-C. (2018). Selective equal spin Andreev reflection at vortex core center in magnetic semiconductor-superconductor heterostructure. Scientific Reports, 8(1).

36. Hasan, M., Lin, H., Bansil, A. (2009). Warping the cone on a Topological Insulator. Physics, 2.

37. Hart, S., Ren, H., Wagner, T., Leubner, P., Mühlbauer, M., Brüne, C., ... Yacoby, A. (2014). Induced superconductivity in the quantum spin Hall edge. Nature Physics, 10(9), 638–643.

38. Beenakker, C. W. J. (2013). Search for Majorana Fermions in Superconductors. Annual Review of Condensed Matter Physics, 4(1), 113–136.

39. Beenakker, C. W. J. (2013). Search for Majorana Fermions in Superconductors. Annual Review of Condensed Matter Physics, 4(1), 113–136.

40. Fu, L., Kane, C. L. (2008). Superconducting Proximity Effect and Majorana Fermions at the Surface of a Topological Insulator. Physical Review Letters, 100(9).

41. Sau, J. D., Tewari, S., Lutchyn, R. M., Stanescu, T. D., Das Sarma, S. (2010). Non-Abelian quantum order in spin-orbit-coupled semiconductors: Search for topological Majorana particles in solid-state systems. Physical Review B, 82(21).

42. Alicea, J. (2010). Majorana fermions in a tunable semiconductor device. Physical Review B, 81(12).

43. Sau, J. D., Lutchyn, R. M., Tewari, S., Das Sarma, S. (2010). Generic New Platform for Topological Quantum Computation Using Semiconductor Heterostructures. Physical Review Letters, 104(4).

44. Mourik, V., Zuo, K., Frolov, S. M., Plissard, S. R., Bakkers, E. P. A. M., Kouwenhoven, L. P. (2012). Signatures of Majorana Fermions in Hybrid Superconductor-Semiconductor Nanowire Devices. Science, 336(6084), 1003–1007.

45. Sharma, G., Zeng, C., Stanescu, T. D., Tewari, S. (2020). Hybridization energy oscillations of Majorana and Andreev bound states in semiconductor-superconductor nanowire heterostructures. Physical Review B, 101(24).

46. Tingyong Cheng, TYChen Group

47. Lin, C.-H., Sau, J. D., Das Sarma, S. (2012). Zero-bias conductance peak in Majorana wires made of semiconductor/superconductor hybrid structures. Physical Review B, 86(22).

48. Datta, S. (2005). Quantum Transport: Atom to Transistor. Cambridge: Cambridge University Press.

49. Gül, Ö., Zhang, H., Bommer, J. D. S., de Moor, M. W. A., Car, D., Plissard, S. R., ... Kouwenhoven, L. P. (2018). Ballistic Majorana nanowire devices. Nature Nanotechnology, 13(3), 192–197.

50. Liu, C.-X., Sau, J. D., Stanescu, T. D., Das Sarma, S. (2017). Andreev bound states versus Majorana bound states in quantum dot-nanowire-superconductor hybrid structures: Trivial versus topological zero-bias conductance peaks. Physical Review B, 96(7).

51. Cao, Z., H. Zhang, H. Lü, W. He, H. Lu and X. Xie. "Decays of Majorana or Andreev Oscillations Induced by Steplike Spin-Orbit Coupling." Physical review letters 122 14 (2019): 147701 .

52. Pan, Haining Sau, Jay Das Sarma, Sankar. (2021). Three-terminal nonlocal conductance in Majorana nanowires: Distinguishing topological and trivial in realistic systems with disorder and inhomogeneous potential. Physical Review B. 103. 10.1103/PhysRevB.103.014513.